

Institute of Experimental and Clinical Pharmacology and Toxicology
(Director: Prof. Dr. T. Eschenhagen)
University Medical Center Hamburg-Eppendorf

The role of cardiac myosin binding protein C and its phosphorylation in the regulation of cardiac contraction

Doctoral thesis

Submitted to the Department of Chemistry
Faculty of Mathematics, Informatics and Natural Sciences
University of Hamburg

In fulfillment of the requirements for the degree Doctor of Natural Sciences (Dr. rer. nat.)

by Lutz Pohlmann

Hamburg 2008

1st reviewer: Prof. Dr. M. Korth

2nd reviewer: Prof. Dr. T. Eschenhagen

Date of the Disputation: May 09, 2008

Table of Contents

1	Introduction	1
1.1	Excitation-contraction coupling and the regulation of cardiac contraction	1
1.2	β -Adrenergic modulation of contraction	5
1.3	Cardiac myosin binding protein C (cMyBP-C)	6
1.4	Familial Hypertrophic Cardiomyopathy	10
1.5	Objectives	13
2	Material and Methods	14
2.1	Targeted cMyBP-C knock-out mouse (KO)	14
2.2	Isolation of intact adult mouse ventricular myocytes	14
2.3	IonOptix measurements and analysis	16
2.3.1	Experimental set-up	17
2.3.2	The principle of measuring sarcomere length	17
2.3.3	Calibration of length measurements	19
2.3.4	Simultaneous recording of intracellular Ca^{2+} transients with Fura-2	19
2.3.5	Calibration of Ca^{2+} levels	24
2.4	Work performing heart in the Langendorff mode	25
2.5	Isometric contractility of left atrial tissue	25
2.5.1	Response of left atrial tissue to external Ca^{2+}	25
2.5.2	Response of left atrial tissue to isoprenaline	26
2.6	SDS-PAGE and Western Blot	26
2.6.1	Organ extraction	26
2.6.2	Protein preparation	26
2.6.3	SDS-PAGE/Western Blot	27
2.6.4	Immunostaining	27
2.7	Separation of myosin heavy chain (MHC)-isoforms	28
2.8	β -Adrenergic receptor binding assay	29
2.9	Statistical analysis	30
3	Results	31
3.1	Establishment of contractility measurements in single intact adult mouse ventricular myocytes	31
3.1.1	Evaluation of conditions for the IonOptix measurements	31
3.1.2	Effect of voltage	32
3.1.3	Effect of stimulation frequency	33
3.1.4	Effect of different extracellular Ca^{2+} concentrations	35
3.1.5	Measurements in the presence or absence of Fura-2	38

3.1.6	Summary	40
3.2	The role of cMyBP-C in sarcomere contraction	40
3.2.1	Myocyte hypertrophy contributes to ventricular hypertrophy in KO mice ...	40
3.2.2	Impaired contractile properties of isolated ventricular KO myocytes	42
3.2.3	Compensatory changes in protein expression in KO ventricles.....	46
3.2.4	Inhibition of actin-myosin interaction	48
3.2.5	Impaired Ca^{2+} transients and relation between sarcomere length and cytosolic Ca^{2+} in KO myocytes.....	51
3.2.6	Isometric contractions of KO left atria	55
3.2.7	Summary	56
3.3	β -Adrenergic response in the cMyBP-C KO model.....	57
3.3.1	Response to β -adrenergic stimulation in Langendorff perfused hearts.....	57
3.3.2	Response to β -adrenergic stimulation in ventricular myocytes	58
3.3.3	Isometric tension in left atria	62
3.3.4	β -Adrenergic receptor binding.....	64
3.3.5	L-type Ca^{2+} current.....	66
3.3.6	Summary	67
4	Discussion.....	68
4.1	Evaluation of the IonOptix measurements	69
4.1.1	Effect of voltage	69
4.1.2	Effect of stimulation frequency	69
4.1.3	Effect of extracellular Ca^{2+} and the influence of Fura-2 buffering	71
4.2	The role of cMyBP-C in cardiac contractility	72
4.2.1	Reduced diastolic sarcomere length in KO	72
4.2.2	Altered Ca^{2+} sensitivity in KO.....	74
4.2.3	Compensatory changes in KO	76
4.2.4	Contractile behavior in HET myocytes	77
4.3	The role of cMyBP-C phosphorylation: β -Adrenergic response in the KO	78
4.4	General conclusions	81
5	Summary	83
6	References.....	86
7	Appendix	95
7.1	List of abbreviations	95
7.2	List of chemicals	97
7.3	List of antibodies	99
7.4	List of laboratory consumables	100
7.5	List of laboratory equipment.....	101

7.6	Chemicals with indication of risk phrases and safety precautions	103
7.6.1	Indication of particular risks.....	103
7.6.1	Indication of safety precautions.....	105
7.7.	Publications and congress participations	108
7.8	Curriculum vitae	110
7.9	Affirmation	111
8	Acknowledgement.....	112

1 Introduction

The task of the heart is to maintain the circulation of blood over a life-time period. To achieve this, a steady cycle of contraction and relaxation of the heart's atria and ventricles is necessary. The rhythm of the heart is first of all autonomously controlled. An excitation signal is generated by few cells in the sino-atrial node and this action potential is forwarded to the working myocardium leading to a concerted contraction of all myocytes. This ensures a basic rhythm of about 70 heart beats per minute in human. In addition to this, several mechanisms exist, which are able to modify rate and force of contraction in order to adapt to the varying needs of the organism. These mechanisms include the Frank-Starling mechanism of force, the positive force-frequency relationship and the regulation by the autonomous nervous system.

1.1 Excitation-contraction coupling and the regulation of cardiac contraction

Excitation-contraction coupling describes the process which enables the chambers of the heart to contract and relax (for reviews see Bers, 2002; Kobayashi and Solaro, 2005). A central role in this process is played by Ca^{2+} ions (Figure 1.1). In a relaxed cardiac myocyte the concentration of Ca^{2+} is extremely low (10^{-7} M compared to $1\text{-}2 \times 10^{-3}$ M in the extracellular space). Upon membrane depolarization by the cardiac action potential, L-type Ca^{2+} channels (or dihydropyridine receptors (DHPR), since they can be blocked by this class of drugs) are activated leading to an influx of Ca^{2+} . Ca^{2+} then binds to the ryanodine receptor (RyR), which is another Ca^{2+} channel in the membrane of the sarcoplasmic reticulum (SR), the analogue of the endoplasmic reticulum in muscle cells. The SR is the Ca^{2+} store of the myocytes and it contains Ca^{2+} at a millimolar level bound to the protein calsequestrin. Activation of the RyR by elevation of the intracellular Ca^{2+} concentration triggers the release of further Ca^{2+} from the SR and this provides a global increase of Ca^{2+} in the myocyte. This process of Ca^{2+} triggering its own release is called calcium-induced calcium release (CICR) and leads to an increase of intracellular Ca^{2+} up to 10^{-5} M. Such a level of Ca^{2+} is able to activate the myofilaments and initiate contraction.

The myofilaments consist of thin and thick filaments which, in striated muscle, are highly regularly arranged, forming the striated sarcomere pattern. The interaction between thin and thick filaments leads to cross-bridge binding, which is the basis for force generation and shortening of the sarcomeres (Figure 1.2). Each thick filament is a polymer of

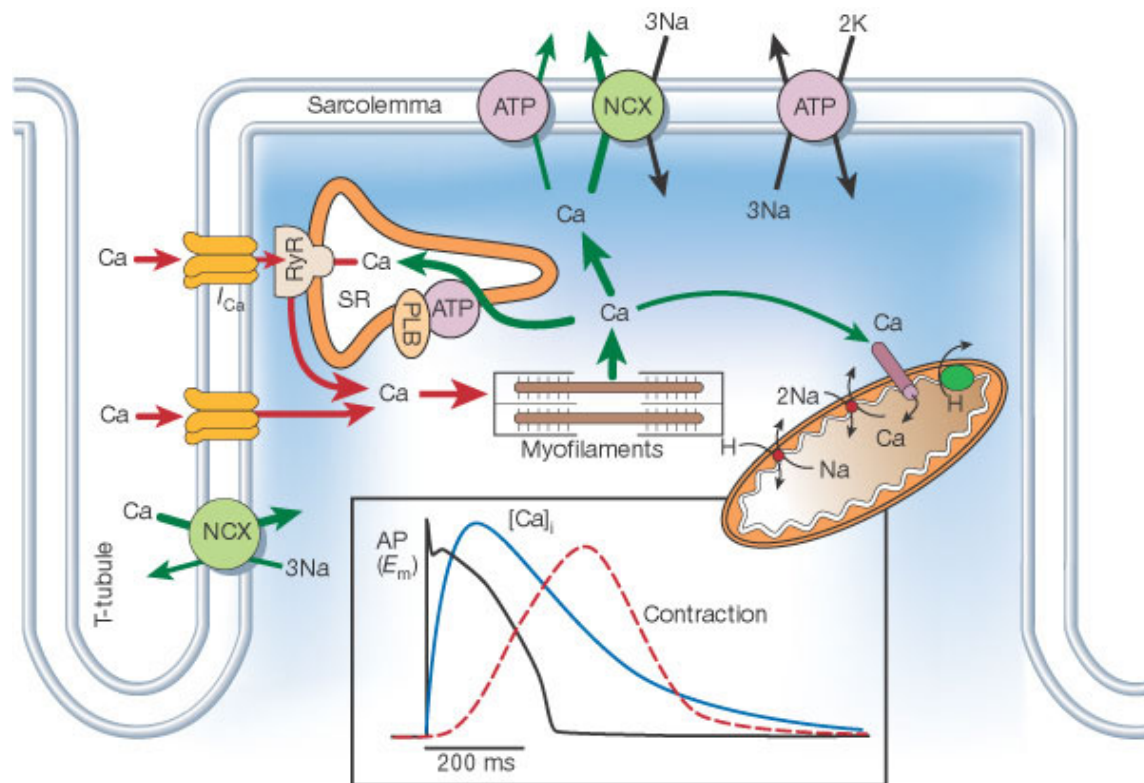


Figure 1.1 Ca^{2+} transport in ventricular myocytes. Mechanisms that increase the intracellular Ca^{2+} concentration are delineated by red arrows; mechanisms that remove Ca^{2+} from the cytosol are delineated by green arrows. The inset shows the time courses of an action potential (AP), intracellular Ca^{2+} transient ($[\text{Ca}]_i$) and contraction (measured in a rabbit ventricular myocyte). I_{Ca} , inward Ca^{2+} current; NCX, $\text{Na}^{+}/\text{Ca}^{2+}$ exchanger; PLB, phospholamban; ATP, ATPase; RyR, ryanodine receptor; SR, sarco-endoplasmic reticulum (from Bers, 2002).

several hundred myosin molecules. Myosin consists of two heavy chains (myosin heavy chain, MHC) and four light chains (two essential light chains, ELC, and two regulatory light chains, RLC). The C-terminal parts of the heavy chains form the thick filament backbone, also referred to as light meromyosin (LMM) or simply the rod-portion of myosin. The N-terminal part of each heavy chain and two light chains form the so-called myosin head or myosin subfragment-1 (S1), which contains ATPase activity and which is able to bind to actin, thus forming the cross-bridge. The paired S1 regions project outward from the filament rod at regular intervals of 14.3 nm. LMM and S1 are connected by the lever arm or myosin subfragment-2 (S2). The thin filaments are anchored in the Z-disc and mainly consist of actin, which is polymerized to a two-stranded helical structure (F-actin). Alongside the F-actin runs the tropomyosin (Tm), an extended dimeric molecule spanning seven actin monomers. In a regular pattern the troponin complex, a heterotrimer of troponin C (Tn-C), troponin I (Tn-I) and troponin T (Tn-T), is situated on the thin filament, interacting with both actin and tropomyosin. Together with tropomyosin,

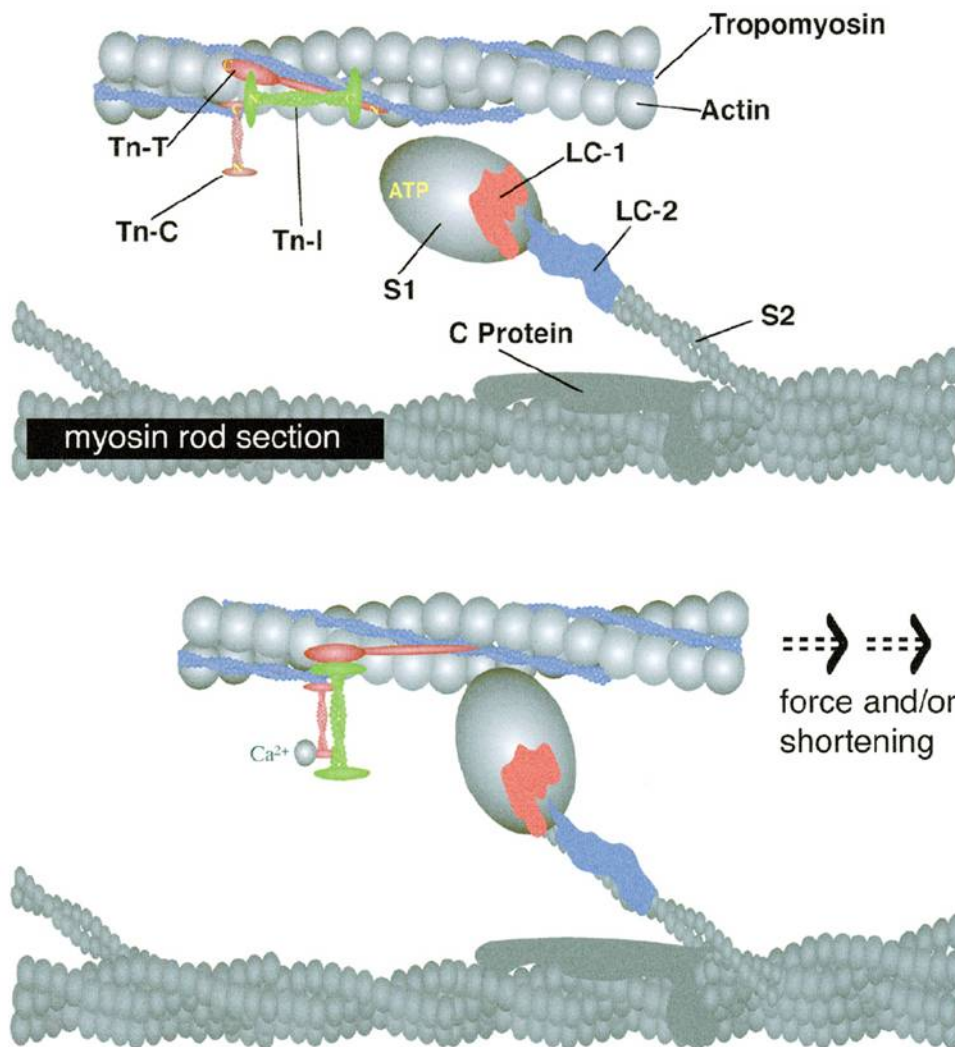


Figure 1.2 Sarcomere structure. The major proteins involved in contractile activation and regulation are shown in diastole (relaxed state of the sarcomere; top panel) and in systole (during cross-bridge formation; bottom panel). The thin filament is composed of actin, tropomyosin, and the hetero-trimer troponin (composed of the troponins Tn-T, Tn-C, and Tn-I). The thick filament is composed of myosin, an asymmetric dimer composed of a globular head portion (S1), a hinged stalk region (S2) and a rod section. The S1 portion is associated with two hetero-dimers, light-chain 1 and 2 (LC-1; LC-2) and contains both the ATP hydrolysis domain and the actin binding domain. The myosin rod section is also associated with the myosin binding protein C (C Protein) (from de Tombe, 2003).

the troponins regulate the interaction of actin with myosin. In the relaxed state of the sarcomere, binding of actin to the myosin head is blocked by Tn-I and tropomyosin. Troponin C contains a low-affinity binding site for Ca^{2+} , and binding of Ca^{2+} to this site induces a conformational shift, which in succession leads to the binding of Tn-C to Tn-I, thus releasing the actin-Tn-I binding. This shift also induces movement of tropomyosin so that the binding sites for myosin on actin are exposed and cross-bridges can form. The formation of strong bound cross-bridges induces further movement of Tm and

spreads the activation further along the thin filament. The myosin head contains ATPase activity and upon hydrolysis of ATP the myosin head domain (S1) interacting with actin undergoes an angular rotation, thus making the power stroke that moves the thick filament. Dissociation of ADP induces the actomyosin complex to return to the relaxed state. During a single twitch, each myosin head probably repeats this so-called cross-bridge cycle several times.

To stop cross-bridge cycling, the intracellular Ca^{2+} concentration has to be lowered. This is mainly achieved by two mechanisms. Ca^{2+} can be extruded out of the cell by a $\text{Na}^+/\text{Ca}^{2+}$ -exchanger (NCX1) or transported back into the SR via an ATP-dependent pump (sarco-endoplasmic reticulum Ca^{2+} ATPase, SERCA). SERCA is under the control of a small regulatory protein, phospholamban (PLB), which when bound to SERCA reduces its activity. SERCA is the main protein involved in lowering intracellular Ca^{2+} concentration in a way that it removes in human about 70% and in small rodents even 90% of the released Ca^{2+} . In heart failure, however, SERCA contributes only just to 50% to the extrusion of Ca^{2+} outside the myocyte. It is important in this context to note that both systems, SERCA and NCX, have to be well balanced, because imbalance in one or the other direction would cause the cell either to lose Ca^{2+} or to get overloaded with Ca^{2+} .

Another important component of the sarcomere is the giant protein titin, which forms a filament that is anchored in the Z-disc and reaches out into the M-line region, thus spanning a half sarcomere. Titin contains several extensible regions in its I-band region which work like a molecular spring providing on the one hand the restoring force after contraction when the cell is shortened over its slack length, and on the other hand the passive force, which represents the resistance of the myocyte when it is stretched (Granzier and Labeit, 2004). Further, titin seems to play a role in stabilizing the thick filament during contraction and in the development of the sarcomeres.

In order to adequately respond to the demands of the organism, several mechanisms exist to modulate force and rates of force development and relaxation. Among these are the mechanism of stretch activation, which results in increased force in response to stretch (Frank-Starling mechanism), and the positive force-frequency relationship. Both mechanisms increase contractile force in response to stretch and stimulation frequency, respectively. Yet, the most important mechanism in regulating the heart's response to increased demands is the activation of β -adrenergic receptors.

1.2 β -Adrenergic modulation of contraction

The autonomous nervous system controls heart function via adrenoceptors (sympathetic nervous system) and muscarinic acetylcholine receptors (parasympathetic nervous system; Brodde and Michel, 1999). In this context, the stimulation of frequency and force of contraction by adrenaline and noradrenaline via β -adrenergic receptors plays the most important role. Most β -adrenergic receptors in the heart (about 70%) belong to the β_1 -subtype, and only a minority (about 30%) is of the β_2 -subtype. The existence of β_3 -adrenergic receptors in the heart has been reported, yet their distinct function remains unclear (Gauthier et al., 2000; Heubach et al., 2002). Stimulation of β -adrenergic receptors in the heart increases the force of contraction (positive inotropic effect), frequency (positive chronotropic), rate of contraction (positive klotropic) and rate of relaxation (positive lusitropic). β -Adrenergic receptors couple to guanine nucleotide-binding proteins and are therefore called G-protein coupled receptors (GPCRs). The G-

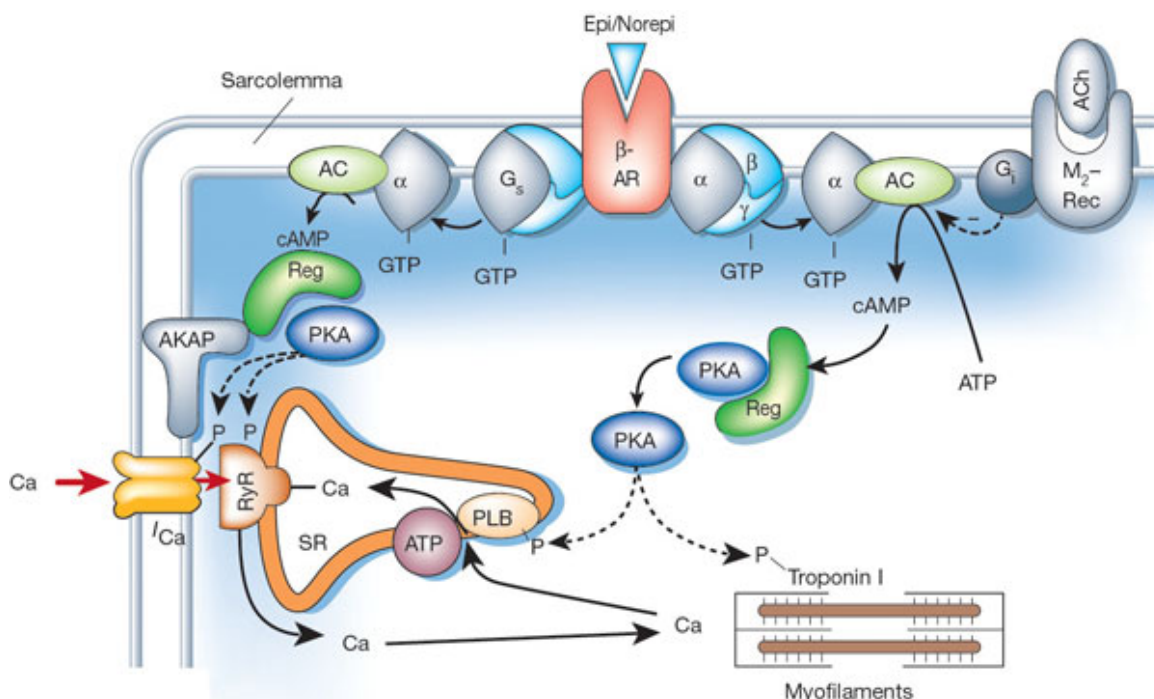


Figure 1.3 β -Adrenergic receptor activation and phosphorylation targets relevant to excitation-contraction coupling. The figure also shows the M_2 -muscarinic receptor, which is activated by acetyl-choline and via an inhibitory G-protein inhibits cAMP formation. β -AR, β -adrenergic receptor; Epi/Norepi, Adrenaline/Noradrenaline; G_s , stimulating G-protein; AC, adenylyl cyclase; M_2 -Rec, M_2 -muscarinic receptor; ACh, acetyl-choline; G_i , inhibitory G-protein; PKA, cAMP-dependent protein kinase; AKAP, A kinase anchoring protein; PLB, phospholamban; Reg, PKA regulatory subunit; SR, sarcoplasmic reticulum (from Bers, 2002).

proteins consist of three subunits ($G\alpha$, $G\beta$, $G\gamma$) and are activated upon ligand binding to the receptor. Upon activation, the $G\alpha$ -subunit hydrolyses GTP and dissociates from the $G\beta\gamma$ -subunits. In the case of the β_1 -adrenergic receptor the $G\alpha$ is a stimulating G-protein ($G\alpha_s$), which activates the adenylyl cyclase. The adenylyl cyclase generates cyclic adenosine mono-phosphate (cAMP), which is a second messenger and activates the cAMP-dependent protein kinase (PKA). PKA phosphorylates several proteins involved in excitation-contraction coupling, and thus conveys effects leading to enhanced cardiac performance (Figure 1.3).

Phosphorylation of the L-type Ca^{2+} -channel (DHPR) and ryanodine receptor (RyR) increases the intracellular Ca^{2+} rise and this increases force of contraction. Phosphorylation of cardiac myofilaments decreases the Ca^{2+} sensitivity of the thin filament, enabling Ca^{2+} to dissociate quicker from TnC and thus hastening relaxation. Phosphorylation of PLB relieves its inhibition on SERCA, so that Ca^{2+} reuptake into the SR is hastened. Another protein phosphorylated after β -adrenergic receptor stimulation is cardiac myosin binding protein C, yet its participation in the β -adrenergic effect is still a subject of debate (for further details see 1.3). An overshoot of β -adrenergic activation is prevented by phosphodiesterases (PDE) which constantly degrade the second messenger cAMP.

In heart failure the β -adrenergic system is chronically activated, yet cardiac function is impaired. The density especially of β_1 -adrenergic receptors is decreased. Many studies have therefore proven the beneficial effect of β -adrenergic receptor blockers in the treatment of patients with heart failure (Bristow, 2000).

1.3. Cardiac myosin binding protein C (cMyBP-C)

Myosin binding protein C (MyBP-C, C-protein) is a sarcomeric protein of about 128-137 kDa size, which is associated with the thick filaments in striated muscles (for reviews see Winegrad, 1999; Flashman et al., 2004; Carrier, 2007). It was first identified in the early 1970s as a contamination in myosin preparations (Starr and Offer, 1971; Offer et al., 1973) and is located in the cross-bridge containing C-zones of the A-band (Craig and Offer, 1976; Figure 1.4 A and B). There it is arranged in 7-9 transversal stripes, with a distance of 43 nm between the stripes (Rome et al., 1973; Bennett et al., 1986). Three isoforms of MyBP-C exist: slow skeletal, fast skeletal and cardiac, each encoded by a

separate gene. While the two skeletal isoforms can be co-expressed in skeletal muscle, the cardiac isoform (cMyBP-C) is exclusively expressed in the heart with never one of the skeletal isoforms present during development (Gautel et al., 1998; Fougousse et al., 1998). All three MyBP-C proteins share a common core structure of ten globular domains (termed C1 – C10 from the N- to the C-terminus). Seven are immunoglobulin I-like domains (IgI) and three are fibronectin type III domains (FnIII). Between the domains C1 and C2 a linker exists, which is highly conserved and therefore termed the MyBP-C motif (Figure 1.4 C). cMyBP-C comprises three particularities compared to the two skeletal isoforms: an additional IgI-like domain at the N-terminus (termed C0), a 28 amino acid insertion within domain C5 and an amino acid insertion (LAGGGRRIS) within the C1-C2 linker (MyBP-C motif). Further, only cMyBP-C can be phosphorylated (Hartzell and Titus, 1982; Hartzell and Glass, 1984; Gautel et al., 1995). Three serine residues, all

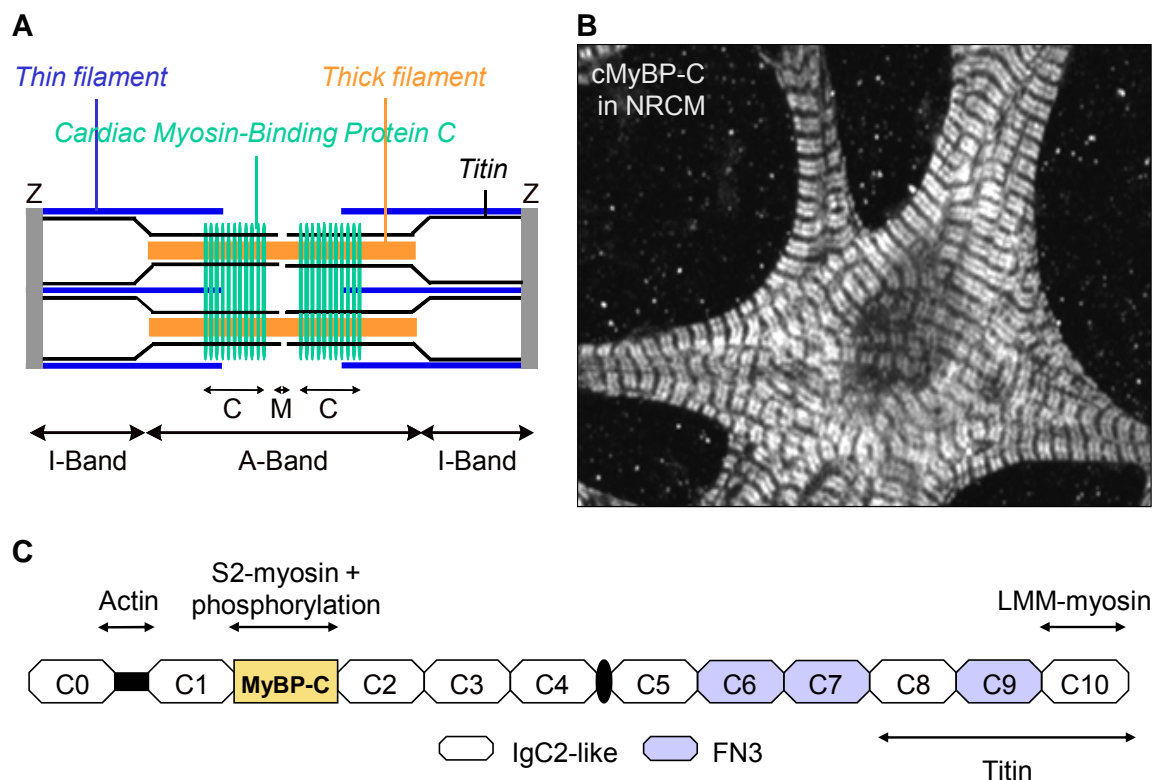


Figure 1.4 cMyBP-C in the sarcomere. (A) Schematic structure of the sarcomere delimited by the Z-lines (grey), the thick filament (orange), the thin filament (blue), the titin filament (black) and cMyBP-C (green), which is arrayed transversely in the C-zones of the A-band of the sarcomere surrounding the M-band. (B) Typical doublets of cMyBP-C in neonatal rat cardiac myocytes (NRCM), recognized by a specific antibody directed against the domains C0-C1. (C) Schematic structure of cMyBP-C, composed of immunoglobulin domains (white), fibronectin domains (blue) and a specific MyBP-C motif (yellow). The localization of the domains involved in binding to other proteins is indicated (from Carrier, 2007).

present in the conserved MyBP-C motif, are subject to phosphorylation and are termed phosphorylation sites A (Ser276 in human and Ser273 in mice, respectively), B (Ser285 in human and Ser282 in mice, respectively) and C (Ser304 in human and Ser302 in mice, respectively). Phosphorylation occurs in response to β -adrenergic agonists by cAMP-dependent protein kinase A (PKA); site B, however, is also phosphorylated by an endogenous Ca^{2+} /calmodulin-dependent kinase (CaMKII). The phosphorylation of site B, which is the serine of the cardiac specific insertion, is the pre-requisite before sites A and C become available for phosphorylation (McClellan et al., 2001).

MyBP-C interacts with several other components of the sarcomere and in the cardiac isoform some of these interactions are modified upon phosphorylation. Thus, both a structural and a regulatory role have been attributed to MyBP-C. With its C-terminal domains (C7 – C10) MyBP-C binds to the light meromyosin (LMM), which forms the thick filament backbone, and to titin. These interactions are believed to play a critical role in the formation and stabilization of the sarcomere structure. Titin, due to its spanning a half-sarcomere, is the structural ruler in myofibrillogenesis (Whiting et al., 1989). Its interacting zone with MyBP-C dictates the position of the latter in the sarcomere. From this position MyBP-C likely promotes the polymerization of myosin into thick filaments: In vitro polymerization of myosin yielded elongated fibers with a uniform diameter and great compactness only in the presence of MyBP-C (Koretz, 1979; Davis, 1988). However, the role of MyBP-C in the formation of sarcomeres seems to be more modulatory rather than essential, since myofibrils of shorter length and less uniform diameter could be generated in vitro also in the absence of MyBP-C, and murine knock-out models of cMyBP-C all exhibited an intact, striated sarcomere pattern (Harris et al., 2002; Carrier et al., 2004).

The dephosphorylated form of MyBP-C binds to the S2 subfragment of myosin, the so-called lever arm domain, which connects the myosin head to the thick filament backbone (Starr and Offer, 1978). This binding site is located in the MyBP-C motif where the phosphorylation sites are present in the cardiac isoform. When cMyBP-C is phosphorylated, the interaction with S2 myosin is released and residues between the domains C0 and C1 bind to actin (Gruen et al., 1999; Squire et al., 2003; Kulikovskaya et al., 2003). This allows the myosin heads to take a position more favorable for actin binding (Weisberg and Winegrad, 1996). cMyBP-C is therefore generally believed to act like a brake on the myosin heads, representing an internal load during contraction. Phosphorylation of cMyBP-C, just like its extraction, has been shown to remove this constraint and increase Ca^{2+} sensitivity of force, force of contraction and the velocity of

force development (Kunst et al., 2000; Calaghan et al., 2000; Stelzer et al., 2006a; Stelzer et al., 2006b; Stelzer et al., 2006c; Stelzer et al., 2007b). These results suggest that cMyBP-C phosphorylation (induced by intracellular Ca^{2+} levels via Ca^{2+} /calmodulin-dependent kinase or by β -adrenergic stimulation via PKA) modulates the interaction between the myosin heads and actin and is therefore a sarcomeric regulator of cardiac contraction. Recent studies demonstrated that the functional alterations in cardiac pathologies, such as atrial fibrillation, heart failure and ischemia, were associated with a decreased amount of phosphorylated cMyBP-C and data obtained with transgenic mice expressing constitutively phosphorylated cMyBP-C suggest that cMyBP-C phosphorylation is cardioprotective (El-Armouche et al., 2006; El-Armouche et al., 2007; de Tombe, 2006; Sadayappan et al., 2006).

The arrangement of MyBP-C in the sarcomere is still not fully resolved and in the recent years two major models have been hypothesized for the incorporation of MyBP-C into the thick filament. One proposed arrangement of MyBP-C as a trimeric collar around the thick filament backbone (Moolman-Smook et al., 2002; Figure 1.5). This model was based on the finding of an internal interaction in the MyBP-C molecule between domains C5 and C8. Via this interaction three molecules of MyBP-C can form a collar around the

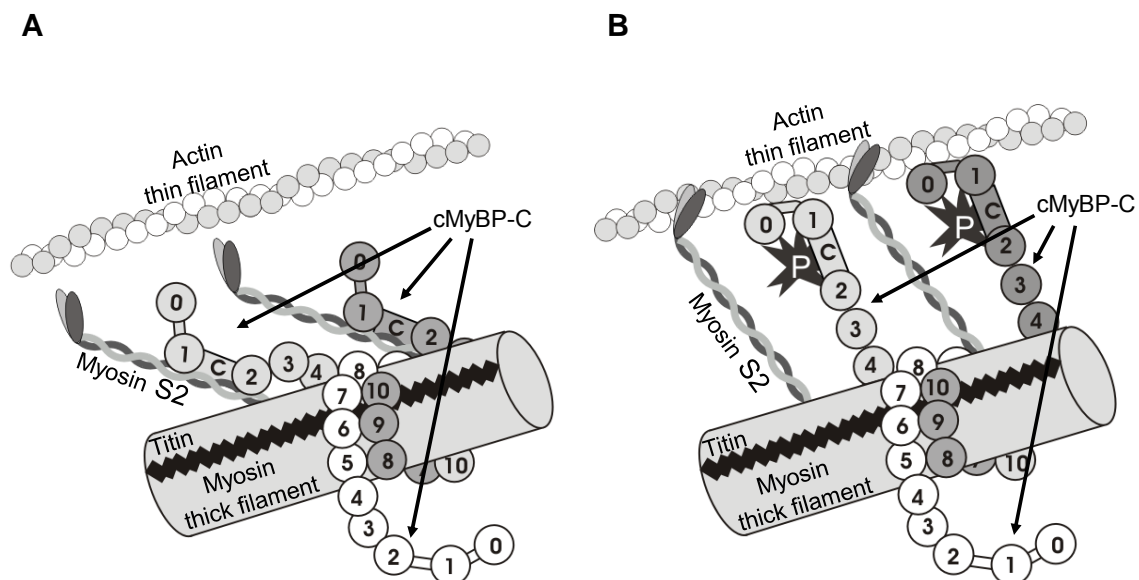


Figure 1.5 The trimeric collar model of cMyBP-C between the thin and thick filaments of the sarcomere. (A) When cMyBP-C is not phosphorylated, it interacts with the S2 subfragment of myosin via the MyBP-C motif located between domains C1-C2. (B) After phosphorylation, cMyBP-C does not interact with the S2 subfragment but with actin. Numbers indicate the different domains of cMyBP-C; C, MyBP-C motif; P, phosphorylation of cMyBP-C (from Carrier, 2007).

myosin rod with their C-terminal domains (C5-C10). The N-terminal domains reach out into the interfilament space and are so enabled to bind to the lever arm (S2) domain of myosin and, after phosphorylation, to actin. An alternative model, however, regarded the formation of a collar quite unlikely and proposed arrangement of MyBP-C axially along the thick filament (Squire et al., 2003). This model took into account that domains C8-C10 are involved in titin binding, but could not explain the C5:C8 interaction within the MyBP-C molecule.

Interest in cardiac MyBP-C has intensified since the discovery that the encoding gene is one of the most frequently affected in the development of familial hypertrophic cardiomyopathy, an inherited disease of the sarcomere.

1.4 Familial hypertrophic cardiomyopathy

Familial hypertrophic cardiomyopathy (FHC) is the genetic form of hypertrophic cardiomyopathy (HCM). HCM, in contrast to dilated cardiomyopathy (DCM), which is associated with eccentric enlargement of the heart, is characterized by left ventricular hypertrophy, which, in addition, is asymmetric with main involvement of the interventricular septum. Histology shows myocyte hypertrophy, myocardial disarray and fibrosis. FHC is an autosomal dominant disease with a prevalence of 1:500 in the Caucasian population. Patients can stay asymptomatic for a long time. Systolic function is normally preserved, but diastolic function is impaired. In most cases FHC is a relatively benign disease, with an annual mortality of less than 1%. Yet, severe cases occur, which are either associated with special mutations or with more than one mutation. Additionally, FHC presents an increased risk for arrhythmias and sudden cardiac death. Actually, FHC is the most common cause of sudden cardiac death in young adults and competitive athletes (for reviews on FHC see Richard et al., 2006; Alcalai et al., 2008).

FHC displays a broad genetic heterogeneity, which may be one reason for the clinical variability in degree of hypertrophy, age of onset, and severity of symptoms. In about 60% of the affected patients the disease-causing mutation could be detected and until today more than 450 mutations in at least 13 different genes have been identified, all of them encoding sarcomere- and myofilament-related proteins (Table 1.1). The first mutations were identified in the genes encoding for β -myosin heavy chain (β -MHC), α -tropomyosin, and troponin T, leading to the classification of FHC as a disease of the

Table 1.1 *Causative genes in FHC.*

Encoded protein	Gene symbol	Chromosome locus	Sarcomere component	No. of cases	Percentage of all cases
β -Myosin heavy chain	<i>MYH7</i>	14q12	Thick filament	212	44
Myosin binding protein C	<i>MYBPC3</i>	11p11.2	Thick filament	165	35
Troponin T	<i>TNNT2</i>	1q32	Thin filament	33	7
Troponin I	<i>TNNI3</i>	19q13.4	Thin filament	27	5
α -Tropomyosin	<i>TPM1</i>	15q22.1	Thin filament	12	2.5
Regulatory myosin light chain	<i>MYL2</i>	12q24.3	Thick filament	10	2
Essential myosin light chain	<i>MYL3</i>	3p21	Thick filament	5	1
Actin	<i>ACTC1</i>	15q14	Thin filament	7	1
Titin	<i>TTN</i>	2q31	Thick filament/ Z-disc	2	<1
Muscle LIM protein	<i>CSRP3</i>	11p15.1	Z-disc	3	<1

(Some genes where only one mutation was identified were not included; from Alcalai et al., 2008).

sarcomere (Geisterfer-Lowrance et al., 1990; Thierfelder et al., 1994). cMyBP-C was the fourth gene identified (Bonne et al., 1995; Watkins et al., 1995), and together with β -MHC, it is the most affected gene with a prevalence of 30-40% of all mutations.

Most mutations found in FHC are missense mutations that cause amino acid exchange and lead to mutated full length proteins. These mutated proteins are able to incorporate into the sarcomere, and there they can act as so-called poison polypeptides. Poison polypeptides exert a dominant negative effect on the function and/or assembly of the sarcomere, thus impairing sarcomere function. Yet, it is also possible that a mutation leads to a gain of function of a protein. This could result in an enhanced cardiac performance with high energy consumption leading in the long term to energy depletion (Keller et al., 2004; Crilley et al., 2003).

In cMyBP-C, however, the majority of mutations are not missense mutations. Here, more frequently single base pair insertions and deletions occur, leading to a frameshift with a premature termination codon. This is predicted to produce C-terminal truncated proteins. Truncated proteins, however, could not be detected in the tissue of affected patients, leading to the assumption that only one allele remains functional and occasionally fails to produce enough new protein, a mechanism called haploinsufficiency.

Taken together, the mechanisms by which mutations in cMyBP-C and other proteins involved in FHC lead to impaired sarcomere structure and function are complex and remain still not fully understood. This is why during the recent years several genetically engineered mouse models have been created to assess consequences of FHC-causing mutations. The genetic approaches consisted of either transgenesis or gene targeting. While transgenesis adds a foreign DNA sequence to the genome and leads to overexpression of a protein, gene targeting aims at replacing the endogenous gene with a modified one (for details see Dalloz et al., 2001). Concerning cMyBP-C, until today, seven mouse models have been published in the context of FHC. Yang et al. (1998, 1999) developed two transgenic mouse lines which overexpress a C-terminal truncated cMyBP-C missing either both the myosin and titin binding domains or only the myosin binding domain. A third transgenic mouse line was developed by this group which overexpresses a cMyBP-C mutant without phosphorylation domain (Yang et al., 2001). Gene targeting was used to create a knock-in model for a truncated cMyBP-C in which the titin and myosin binding domains were replaced by a novel amino acid sequence (McConnell et al., 1999). In this model, mice homozygous for the mutation express less than 10% of the truncated protein (McConnell et al., 2001). In a second knock-in mouse model an N-terminal region of cMyBP-C was deleted (Witt et al., 2001). Finally, two knock-out mouse models of cMyBP-C were created by gene targeting: Harris et al. (2002) developed a functional knock-out by replacing exons 3 to 10 by a neomycin resistance gene. Although these mice accumulated mutant mRNA, no protein was expressed. The knock-out model of Carrier et al. (2004) was based upon deletion of exons 1 and 2 including the transcription initiation site. Consequently, no mRNA for cMyBP-C was synthesized, representing a transcriptional knock-out. Both knock-out models display similar features of hypertrophy and dilation with functional impairment in the homozygous state, yet only the transcriptional knock-out model also displayed a phenotype of mild hypertrophy in the heterozygous mice at older age (10 – 11 months).

None of the genetically engineered models of FHC exactly mimics the phenotype of affected patients and discrepancies exist between similar models (e.g. in the targeted

cMyBP-C knock-out models). Yet, they display each typical features of FHC, morphological, histological, or functional, that can be correlated with clinical data and allow conclusions about mechanisms involved in the pathology. For example, the Arg403Gln mutation in a α -MHC targeted mouse model displayed a severe phenotype of hypertrophy and cardiac dysfunction already in the heterozygous state whereas the homozygous animals died soon after birth. In contrast, the phenotypes of cMyBP-C models in the heterozygous state are often very mild, if at all present, and show hypertrophy without functional deficits (McConnell et al., 2001). This is in agreement with the often described benign prognosis of patients with cMyBP-C mutations in contrast to the severe outcome in β -MHC affected patients. Finally, the fact that the homozygous state in many of the cMyBP-C models leads to a more severe phenotype reflects what is observed in human FHC, where patients who carry two mutated alleles (homozygotes, double heterozygotes and compound heterozygotes) are stronger affected than corresponding patients with only a single mutation.

1.5 Objectives

The aim of the present work was to determine the role of cMyBP-C in the regulation of cardiac contraction with a special focus on the importance of phosphorylation of cMyBP-C in this regulation. Particularly, the following questions were asked:

- (1) Do cardiac myocytes and muscle preparations from targeted cMyBP-C knock-out mice (which do not express cMyBP-C and develop cardiac hypertrophy) exhibit altered cardiac function?
- (2) Do cardiac myocytes and muscle preparations from targeted cMyBP-C knock-out mice correctly respond to β -adrenergic stimulation?

The main experimental procedure consisted of functional analysis in isolated intact ventricular myocytes. For this, a method to analyze the contractile behavior and the intracellular Ca^{2+} transients of these freely suspended myocytes was established in the Institute of Experimental and Clinical Pharmacology. Further functional analysis was performed in isolated cardiac muscles (from left atria) under loaded conditions. Expression analyses (proteins, β -adrenergic receptors) were performed on ventricular homogenates.

2 Material and Methods

2.1 Targeted cMyBP-C knock-out mouse (KO)

The cMyBP-C knock-out mice (cMyBP-C null mice, KO) had been generated previously as described in Carrier et al. (2004). In this model the transcription initiation site and the exons 1 – 2 of the *MYBPC3* gene were replaced by a neomycin resistance gene. This inactivates transcription of the cMyBP-C gene and results in absence of both cMyBP-C mRNA and protein. In the homozygous state, with two null alleles, the mice exhibited a phenotype of left ventricular hypertrophy with dilation of the ventricles, a decreased fractional shortening at three months of age (measured by echocardiography) and an impaired relaxation at nine months of age (assessed by hemodynamic measurements). In the heterozygous state, with only one inactivated allele, the mice developed at the age of 10 – 11 months left ventricular hypertrophy, which, in contrast to the homozygous animals, was asymmetric mainly involving the interventricular septum. Therefore, heterozygous mice display a key feature of familial hypertrophic cardiomyopathy (FHC).

2.2 Isolation of intact adult mouse ventricular myocytes

Intact ventricular myocytes were isolated from the adult mouse heart by perfusion of the heart with recombinant collagenases according to the method of O'Connell et al. (2003). The mice were injected intraperitoneally with heparine (0.05 ml of 10,000 IU/ml stock solution =500 IU) about 5-10 min prior to the experimental protocol to avoid blood clotting in the coronary vessels during the following procedure. The mice were anesthetized with CO₂ and then killed by decapitation or cervical dislocation. The thorax was opened and the aorta was cut about 2 mm from its entry into the heart. Then the heart was quickly excised and the aorta was slid onto a cannula with two fine curve-tip forceps and tied with a thread. The cannulated heart was mounted on a temperature-controlled perfusion system (Figures 2.1 and 2.2) and perfused for 8 min with a Ca²⁺-free perfusion buffer (in mM: 113 NaCl, 4.7 KCl, 0.6 KH₂PO₄, 0.6 Na₂HPO₄, 1.2 MgSO₄, 12 NaHCO₃, 10 KHCO₃, 30 taurine, 5.5 glucose, 10 2,3-butanedione monoxime (BDM), 10 4-(2-hydroxyethyl)-1-piperazineethanesulfonic acid (HEPES), pH 7.46) before switching to the digestion buffer containing in addition 0.1 mg/ml of recombinant collagenases/proteases (Liberase Blendzyme 3, Roche Diagnostics) and 12.5 µM CaCl₂. The perfusion was performed with a constant flow rate of 3 ml/min and the temperature

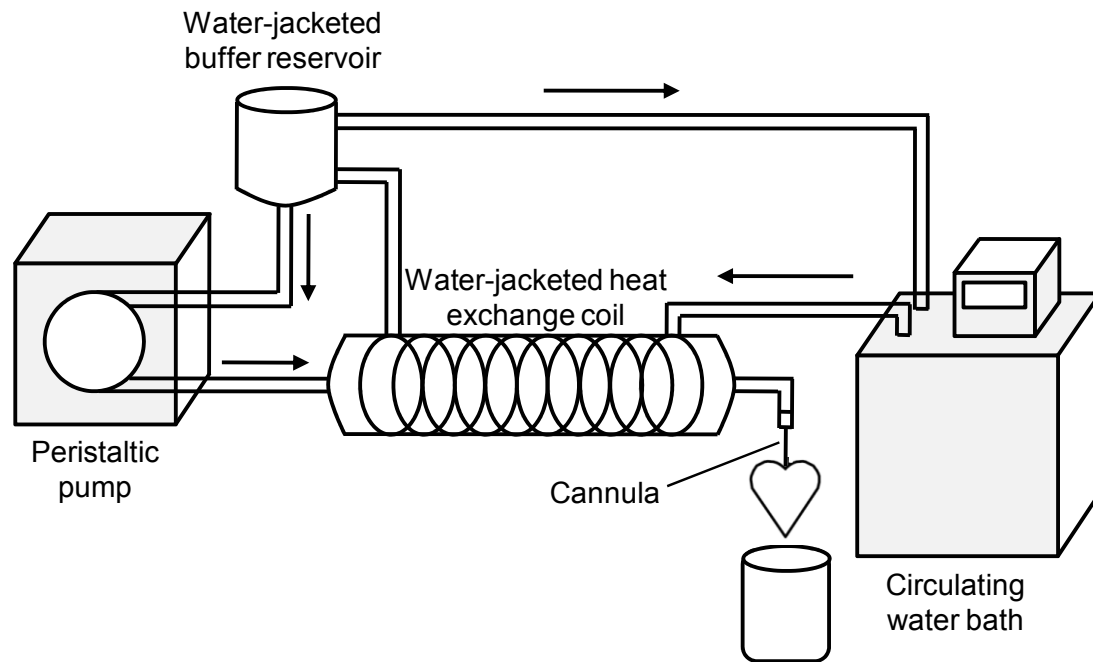


Figure 2.1 Schematic depiction of the perfusion system for the isolation of adult mouse ventricular myocytes.

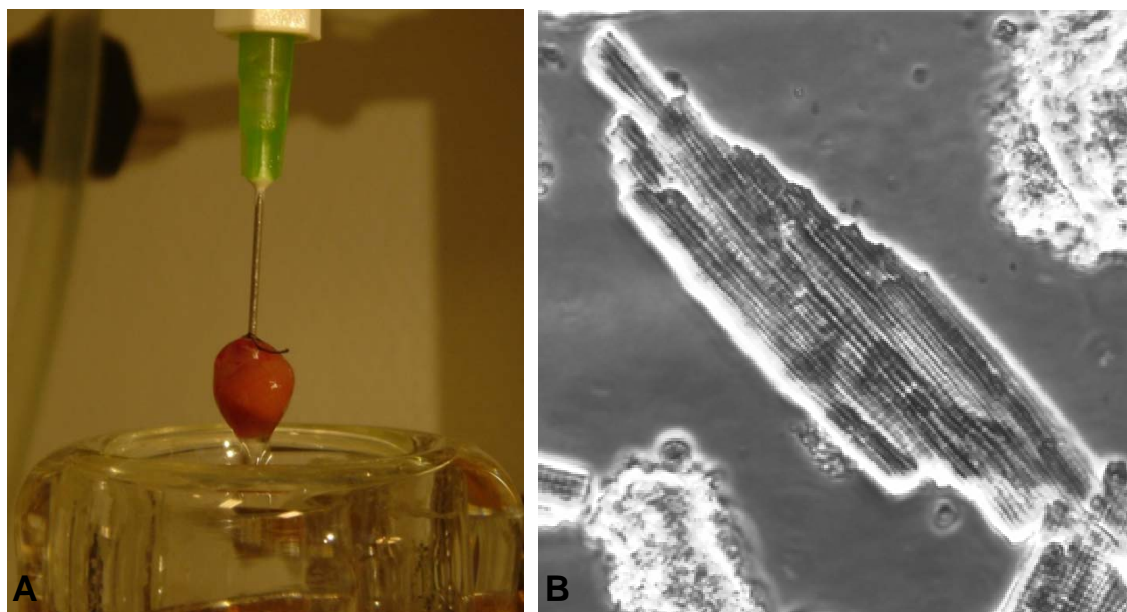


Figure 2.2 Adult mouse heart during perfusion (A) and an isolated ventricular myocyte from the adult mouse heart (B).

of the water bath was adjusted in a way that the solutions had a temperature of 37 °C when reaching the cannula.

After 8 to 10 min of digestion the ventricles were cut off, placed in digestion buffer and the tissue was dissociated using forceps. Further enzyme activity was inhibited by addition of 5% fetal bovine serum. Debris was sedimented by gravity and the

supernatant, containing the intact cardiac myocytes, was centrifuged (1 min at 180 x g). The pellet was resuspended in fresh buffer and Ca^{2+} was slowly reintroduced by adding CaCl_2 , increasing the Ca^{2+} concentration gradually from 12.5 μM to 62 μM , to 112 μM , to 212 μM , to 500 μM and finally to 1 mM. The myocytes were counted in a Fuchs-Rosenthal chamber (2 x 3.2 μl), and then rinsed and further diluted in the IonOptix buffer (in mM: 135 NaCl, 4.7 KCl, 0.6 KH_2PO_4 , 0.6 Na_2HPO_4 , 1.2 MgSO_4 , 1.25 CaCl_2 , 20 glucose, 10 HEPES, pH 7.46).

2.3 IonOptix measurements and analysis

The contractile properties of the isolated ventricular myocytes were determined with the IonOptix system (IonOptix Corporation, Milton, MA, USA). This is a multi-component system, which is able to record simultaneously the sarcomere length shortening and intracellular Ca^{2+} transients of electrically stimulated myocytes (Figure 2.3). In addition,

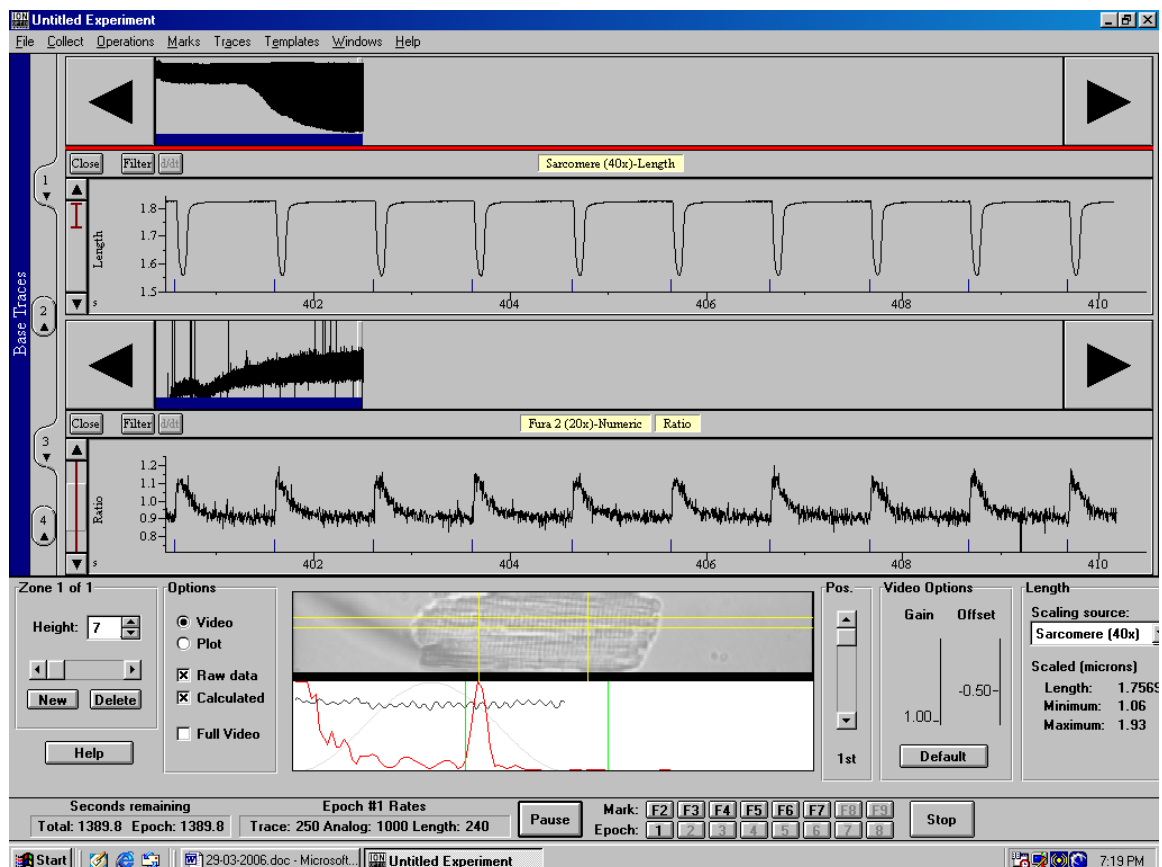


Figure 2.3 Monitor of the SarcLen Acquisition program during the simultaneous measurement of sarcomere length and intracellular Ca^{2+} transient in a ventricular myocyte paced with a frequency of 1 Hz. The camera picture of the myocyte allows acquisition of sarcomere length, whereas simultaneously fluorescent light from the Ca^{2+} sensitive dye Fura-2 is measured with a photomultiplier tube.

the system was used to determine the cell length and cell width of isolated ventricular myocytes.

2.3.1 Experimental set-up

The myocytes were diluted in IonOptix buffer to a final concentration of about 15,000 – 20,000 so-called rod-shaped myocytes per ml. Four hundred μ l of the myocyte suspension was pipetted into a cell perfusion chamber (Cell MicroControls, Norfolk, VA, USA) and mounted on the stage of an inverted microscope (Nikon Eclipse TS 100). A stimulation assay consisting of two platinum iridium electrodes allowed electric stimulation of the myocytes with a field stimulator (MyoPacer, IonOptix Corporation, Milton, MA, USA). Myocytes were paced with a frequency of 1 Hz at 10 V and with 4 ms impulse duration. The cell chamber was perfused using a drop-sensor controlled flow controller (cFlow 8 Channel Flow Controller, Cell MicroControls, Norfolk, VA, USA) to fill the chamber and a peristaltic pump (Gilson Inc., Middleton, WI, USA) to aspirate the solution. The flow rate was set to 0.5 ml/min. The criteria for using a myocyte for a measurement were: i) rod-shaped with a clear striated sarcomere pattern, ii) no visible membrane damages or membrane blebs, iii) no hypercontractile zones or spontaneous contractions and iv) a stable contraction amplitude. All experiments were performed at room temperature.

2.3.2 The principle of measuring sarcomere length

In skeletal and heart muscle the thin and thick filaments show a characteristic organization, which, due to their different optical properties, is observed under the light-microscope as a cross-striated pattern of alternating dark and light bands. When analyzing the optical density in a series of sarcomeres, this results in a sinusoidal curve with the wavelength of the sine representing the sarcomere length. This density trace was recorded by the IonOptix MyoCam™ (IonOptix Corporation, Milton, MA, USA) and then transformed by the IonWizard sarcomere length acquisition software into a signal of sarcomere length by applying a Fast Fourier Transform (FFT). The program recorded and saved sarcomere length as a function of time including also the stimulation marks which were necessary for the analysis. The camera sampled images with a frequency of 240 Hz which was quick enough to monitor cell contraction. The analysis was performed with the IonWizard 5.0 software. In each experiment 20 – 30 contractions were averaged

and from this average sarcomere length recording (Figure 2.4) the program calculated different parameters:

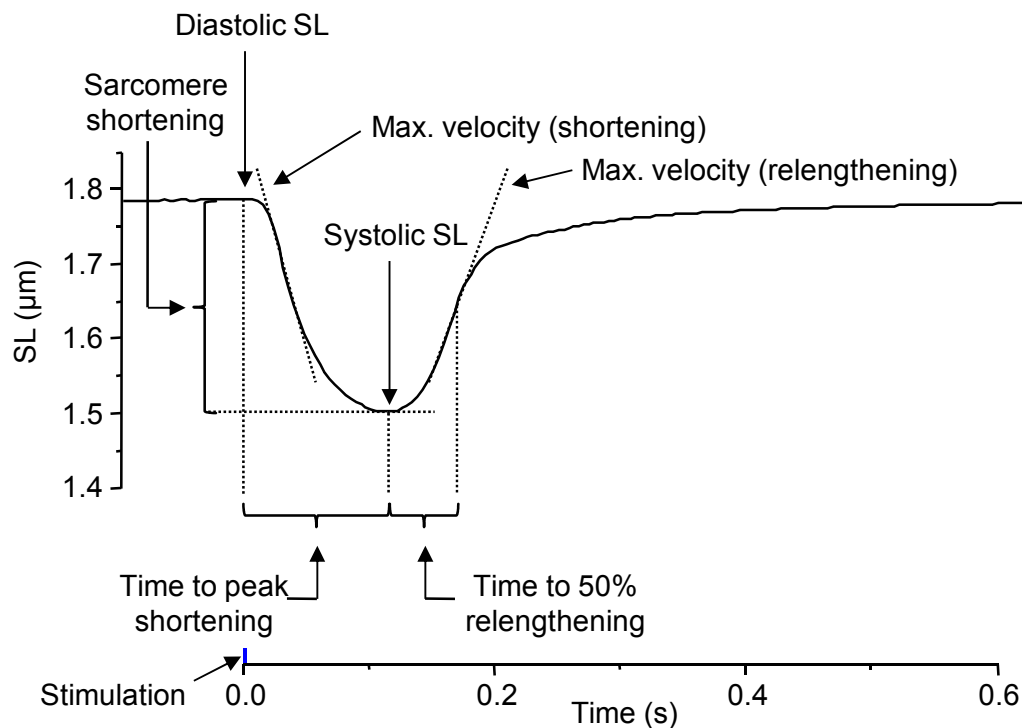


Figure 2.4 Averaged sarcomere length (SL) recording and analysis.

Diastolic sarcomere length:	The pre-stimulation baseline value of sarcomere length
Systolic sarcomere length:	The value of the sarcomere length transient at its maximal deflection from baseline
% Sarcomere shortening:	Shortening amplitude expressed as % of diastolic sarcomere length
Shortening velocity:	The minimum of the first derivative of the sarcomere length transient i.e. the steepest slope of the deflection phase of the sarcomere length recording. Since the sarcomere length declines during the shortening phase, values of shortening velocities are always negative with the most negative value representing the highest velocity.

Time to peak shortening:	Time for the transient to reach peak sarcomere length during the deflection phase of the transient
Relengthening velocity:	The maximum of the first derivative of the sarcomere length transient i.e. the steepest slope of the recovery phase of the sarcomere length recording
Time to 50% relengthening:	Time for the transient to return 50% of the peak sarcomere length during the recovery phase of the transient

2.3.3 Calibration of length measurements

The length measurements were calibrated using a stage micrometer with a defined scale. Like this, the number of pixels/ μm of the image from the IonOptix Myocym™ could be determined and entered as a fixed parameter in the software. Besides acquiring sarcomere length with the SarcLen Acquisition program, cell dimensions (cell length and cell width) were measured with the SoftEdge Acquisition program.

2.3.4 Simultaneous recording of intracellular Ca^{2+} transients with Fura-2

To record intracellular Ca^{2+} transients the myocytes were loaded with the fluorescent Ca^{2+} chelator Fura-2 (Figure 2.5). Fura-2 is specific for Ca^{2+} ions and fluoresces after excitation with UV light. The excitation wavelength is dependent on whether it binds to Ca^{2+} or not. In the Ca^{2+} -bound state the maximum in the excitation spectrum lies at 340 nm, in the Ca^{2+} -free state it shifts towards 380 nm. Thus Fura-2 is a ratiometric Ca^{2+} indicator, i.e. the ratio of fluorescence intensity at 340 and 380 nm excitation reflects the Ca^{2+} concentration.

Figure 2.6 shows how the peak fluorescence shifts from 380 nm to 340 nm when the concentration of free Ca^{2+} increases. Buffers with the exactly adjusted Ca^{2+} concentrations were obtained from the Fura-2 Calcium Imaging Buffer Kit (Molecular Probes).

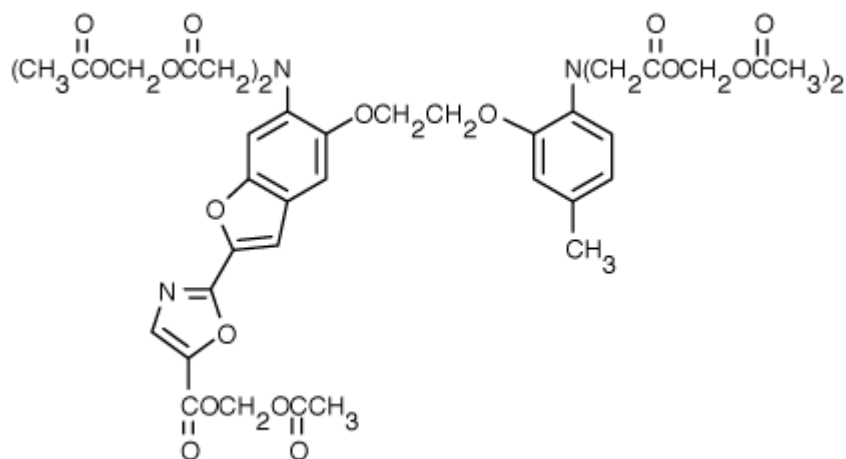


Figure 2.5 Fura-2 acetoxymethyl ester

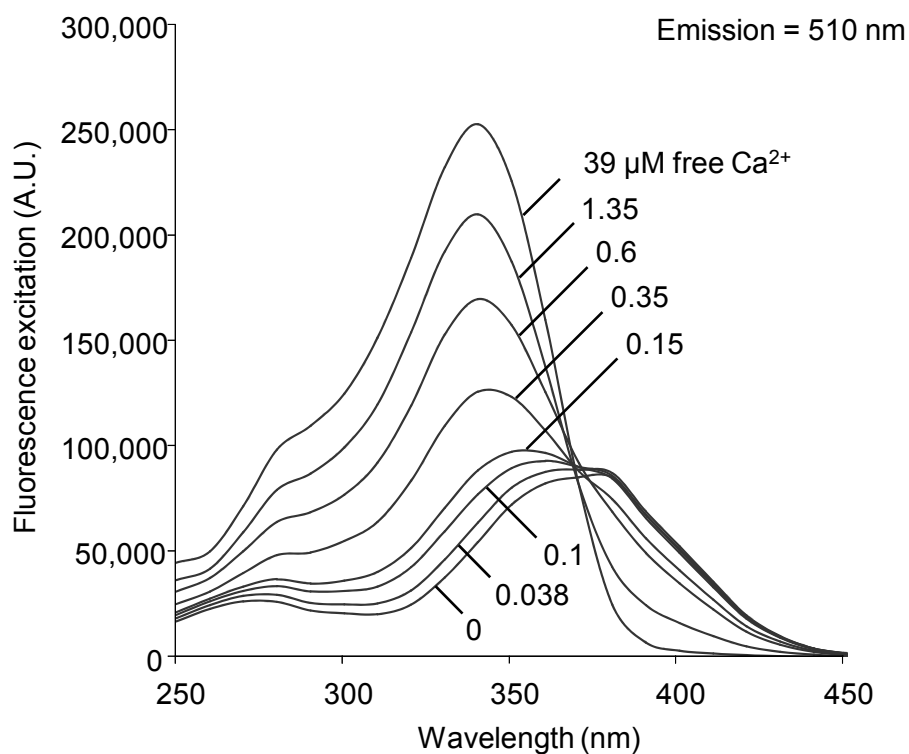


Figure 2.6 Fluorescence spectra of Fura-2. The emission of fluorescence from Fura-2 after excitation was recorded in eight calibrating solutions with different Ca^{2+} concentrations (0 – 39 μM).

Since Fura-2 as a salt cannot permeate cell membranes, the cell permeant, Ca^{2+} -insensitive acetoxymethyl ester of Fura-2 (Fura-2 AM) was used. After penetrating inside the myocytes, the lipophilic blocking groups are cleaved by non-specific esterases and Fura-2 is thus enabled to bind Ca^{2+} . Like this the Ca^{2+} -sensitive form of Fura-2 is

accumulated inside the myocytes. Myocytes were incubated for 15 min at room temperature, rinsed and incubated for another 15 min before starting the measurement.

Alternate excitation with 340 and 380 nm UV light at a high rate was achieved with the IonOptix HyperSwitch Dual Excitation Light Source (IonOptix Corporation, Milton, MA, USA). The light from a 75 W Xenon arc bulb was formed into a converging beam and focused on a high-speed galvanometer driven mirror. This mirror directed the now diverging light to one of two collecting lenses. One path was sent straight into a dichroic cube where it encountered an emission filter and then passed through the dichroic mirror towards a liquid light guide to the microscope. In the second path the light was steered into the dichroic cube at a 90 degree angle where it encountered a second emission filter and was then reflected by the dichroic mirror towards the liquid light guide. Thus, two light beams with either 340 nm or 380 nm were alternatively sent to the myocyte chamber on the microscope (Figure 2.7).

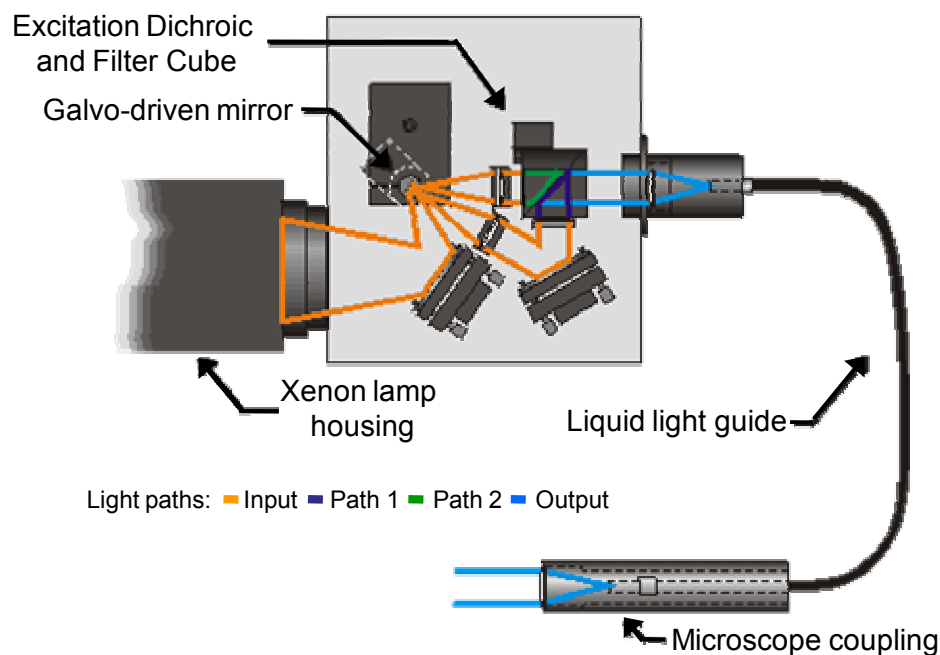
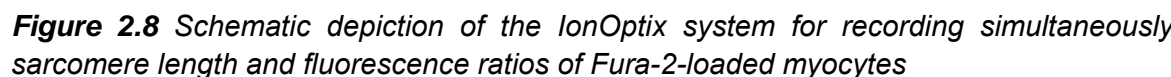


Figure 2.7 IonOptix HyperSwitch Dual Excitation Light Source

The excitation light reached the Fura-2-loaded myocytes through the objective with a frequency of 250 wavelength pairs per second which guaranteed an adequate time resolution to depict the intracellular Ca^{2+} transients.

The emitted fluorescence light from the microscope (green light path in Figure 2.8) was reflected by a dichroic mirror into a photo multiplier tube (PMT) which generated a little



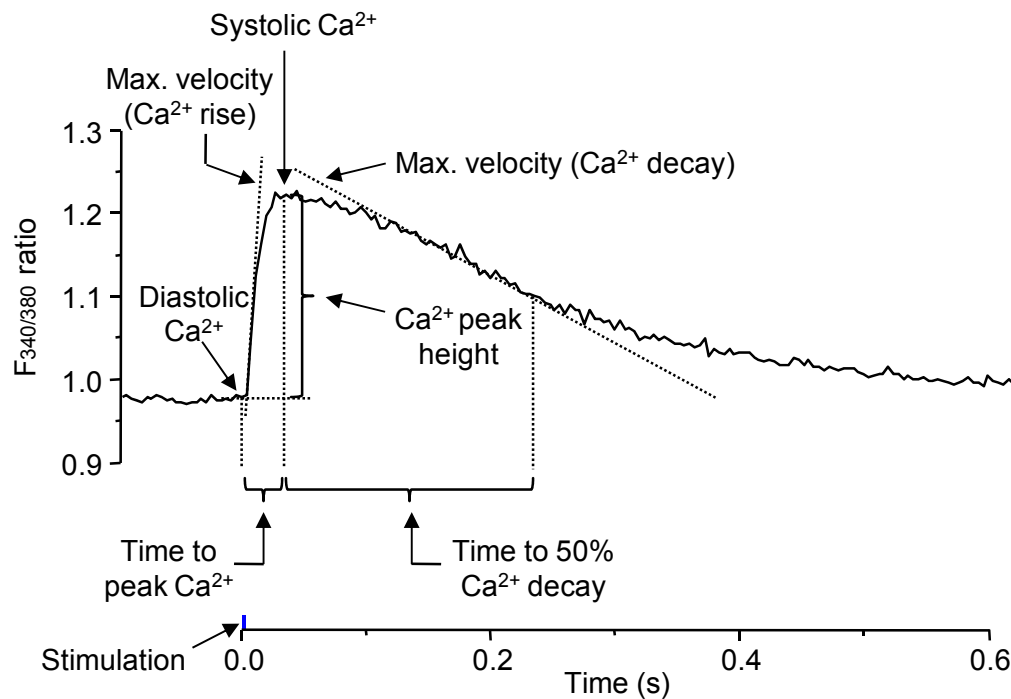


Figure 2.9 Averaged Ca^{2+} transient and transient analysis

Diastolic Ca^{2+} concentration: The pre-stimulation baseline value of the fluorescence ratio

Systolic Ca^{2+} concentration: The value of the fluorescence ratio of the Ca^{2+} transient at its maximal deflection from baseline

% Ca^{2+} peak height: Peak amplitude expressed as % of diastolic fluorescence ratio

Maximal velocity of Ca^{2+} rise: The maximum of the first derivative of the Ca^{2+} transient i.e. the steepest slope of the rising phase of the Ca^{2+} transient

Time to peak Ca^{2+} : Time for the Ca^{2+} transient to reach peak fluorescence ratio during the rising phase of the transient

Minimal velocity of Ca^{2+} decay: The minimum of the first derivative of the Ca^{2+} transient i.e. the steepest slope of the recovery phase of the Ca^{2+} transient. Since the decay has a negative slope all the

values of velocity in this phase are negative with the most negative value representing the highest velocity.

Time to 50% Ca^{2+} decay: Time for the Ca^{2+} transient to return 50% of the peak fluorescence ratio during the recovery phase of the transient

2.3.5 Validation of the Ca^{2+} measurements with Fura-2

The F340/380 ratio of Fura-2, which represents the ratio between Ca^{2+} -bound Fura-2 and Ca^{2+} -free Fura-2, is independent of the actual concentration of Fura-2 inside the myocyte and therefore directly correlates with the intracellular Ca^{2+} concentration. This proportionality was validated in our system using calibrating solutions containing 50 μM Fura-2 salt and different Ca^{2+} concentrations from 0 – 39 μM (Figure 2.10). The F340/380 ratio was found to be directly proportional to the concentration of free Ca^{2+} thus showing the capability of the IonOptix system to monitor Ca^{2+} concentrations that are found inside myocytes. However, it is difficult to use this graph for the conversion of the F340/380 ratios into values of the actual Ca^{2+} concentration inside cardiac myocytes, since the experimental conditions applied above hardly reflect the conditions in intact ventricular myocytes. Temperature, viscosity, pH value, and ionic strength can all influence the dissociation constant (K_d) of Fura-2, and consequently the F340/380 ratio.

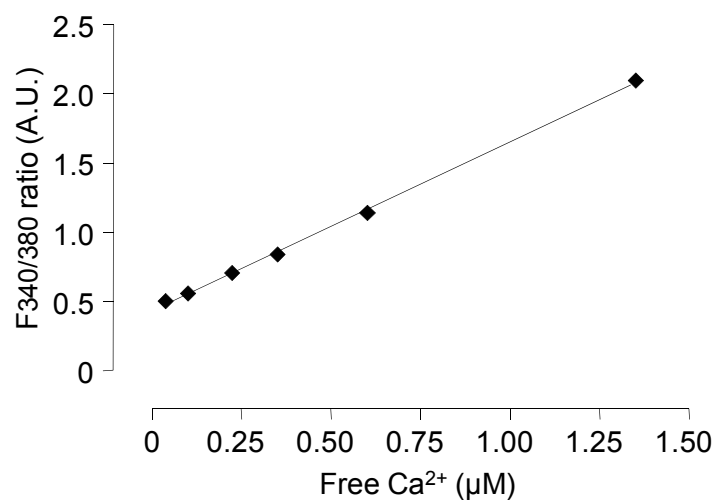


Figure 2.10 Ca^{2+} response of F340/380 ratio. Fura-2 fluorescence was measured with the IonOptix system in calibrating solutions of different concentrations of free Ca^{2+} (Fura-2 Calcium Imaging Calibration Kit, Molecular Probes, Eugene, OR, USA).

Therefore, to avoid the complex issue of calibrating the intracellular Ca^{2+} levels, during this work, only the raw values of the F340/380 ratio are used to express intracellular Ca^{2+} concentrations.

2.4 Work-performing heart in the Langendorff mode

Hearts were excised and cannulated via the aorta in the same way as for the myocyte isolation. After cannulation the heart was mounted on a temperature-controlled (37 °C) Langendorff perfusion system and perfused with Tyrode's solution (in mM: 119.8 NaCl, 5.4 KCl, 1.8 CaCl_2 , 1.05 MgCl_2 , 0.42 NaH_2PO_4 , 22.6 NaHCO_3 , 10 glucose, 0.5 ascorbic acid, 0.05 Na_2EDTA , 5 pyruvic acid, continuously gassed with 95% O_2 + 5% CO_2) with a constant pressure of 100 mm water column. The apex of the heart was connected to a force transducer, which allowed the recording of isometric force of contraction (BMON software, Ingenieurbüro Jäckel, Hanau, Germany). The hearts were perfused until they achieved constant beating amplitude, and then the perfusion was continued for at least ten minutes with or without 1 μM isoprenaline. In the end, the hearts were shock-frozen in liquid N_2 and stored at -80 °C for further analysis.

2.5 Isometric contractility of left atrial tissue

Adult mice were anesthetized with CO_2 and killed by decapitation. The heart was quickly removed into gassed Tyrode's solution (in mM: 119.8 NaCl, 5.4 KCl, 1.8 CaCl_2 , 1.05 MgCl_2 , 0.42 NaH_2PO_4 , 22.6 NaHCO_3 , 10 glucose, 0.5 ascorbic acid, 0.05 Na_2EDTA , 5 pyruvic acid, continuously gassed with 95% O_2 + 5% CO_2) containing in addition 30 mM BDM. The left atrium was dissected from the ventricles, suspended in an organ bath filled with continuously gassed Tyrode's solution and connected to a force transducer to record isometric force of contraction. Data were recorded and evaluated by a PC based system (BMON, Ingenieurbüro Jäckel, Hanau, Germany).

2.5.1 Response of left atrial tissue to external Ca^{2+}

To evaluate the maximal force of each preparation, the muscles were stretched until no further increase in twitch force occurred. Then muscle length was adjusted to half-maximal twitch force for each muscle and the organ baths were rinsed twice with Ca^{2+} -

free Tyrode's solution, which gave a calculated external Ca^{2+} concentration of 0.002 mM. Then the external Ca^{2+} concentration was gradually increased (0.4, 0.8, 1.2, 1.6, 2.0, 2.4, 2.8, 3.2, 4.0, 4.8, 5.6 and 6.4 mM) and the effect on the force of contraction was measured.

2.5.2 Response of left atrial tissue to isoprenaline

Muscle length was adjusted to achieve maximal twitch force and the effect of increasing concentrations of isoprenaline (0.001, 0.003, 0.01, 0.03, 0.1, 0.3, 1, 3, 10 μM) on the force of contraction was measured. This experiment was performed by Dr. Michael Grimm (Hamburg).

2.6 SDS-PAGE, Western blot

2.6.1 Organ extraction

Adult mice were anesthetized with CO_2 , weighed and killed by decapitation. The heart was quickly removed and rinsed in isotonic NaCl solution. After removal of atria and remnant vessels, the ventricles were carefully dried, weighed and shock-frozen in liquid N_2 .

2.6.2 Protein preparation

Frozen tissues were powdered in a crucible cooled with liquid N_2 and then homogenized with a polytron in 5% sodium-dodecylsulfate (SDS), 50 mM Tris-HCl, pH 7.5, 250 mM sucrose, 75 mM urea, 1 mM 1,4-dithiotreitol (DTT) at 4 °C. The non-soluble parts were separated by centrifugation at 14,000 rpm for 10 min and the supernatant was collected. The protein amount was determined according to the method of Bradford, where the absorbance in a solution of Coomassie Brilliant Blue is measured (Bradford, 1976). The protein quantity was determined with a standard curve obtained with known concentrations of albumin from bovine serum (BSA).

2.6.3 SDS-PAGE/Western blot

Separation of the proteins was performed by gel electrophoresis under reducing and denaturing conditions. Therefore 20 µg of proteins were prepared with Laemmli buffer (2% SDS, 10% glycerol, 100 mM DTT, 0.01% bromophenol blue, 10 mM Tris-HCl, pH 6.8) and loaded on a SDS containing polyacrylamide gel. The stacking gel consisted of 5% acrylamide/N,N'-methylene-bis-acrylamide (37.5:1), 125 mM Tris base, pH 6.8, 0.1% SDS, with 0.1% ammonium persulfate (APS) and 0.1% N,N,N',N'-tetramethylethylenediamine (TEMED) to start polymerization, and the separating gel consisted of 10-15% acrylamide/bisacrylamide (37.5:1), depending on the size of the analyzed proteins, 375 mM Tris base, pH 8.8, 0.1% SDS, with 0.1% APS and 0.04% TEMED to start polymerization. The electrophoresis was run for one to two hours at a constant voltage of 120 V with the electrophoresis buffer containing 25 mM Tris base, 192 mM glycine and 0.1% SDS. After the electrophoresis the proteins were transferred on either nitrocellulose or polyvinylidene fluoride (PVDF) membranes for 90 min with a constant current of 300 mA (transfer buffer containing 50 mM Tris base, 380 mM glycine, 0.1% SDS, 20% methanol). The efficiency of the transfer was checked afterwards by staining the membranes with Ponceau red.

2.6.4 Immunostaining

After rinsing with Tris buffered saline (150 mM NaCl, 100 mM Tris base, pH 7.5) + 0.1% Tween 20 (TBS-T), the membranes were saturated with 5% milk powder dissolved in TBS-T and then incubated overnight with different primary antibodies in TBS-T at 4 °C:

Primary antibodies:	Protein name	Dilution
β-MHC (mouse)	β-Myosin heavy chain	1:4000
SERCA2 (goat)	Sarco-endoplasmic reticulum Ca ²⁺ ATPase	1:100
PLB A1 (rabbit)	Phospholamban (total)	1:5000
Ser16-PLB (rabbit)	Ser16-phosphorylated phospholamban	1:5000
Thr17-PLB (mouse)	Thr17-phosphorylated phospholamban	1:5000
NCX1 (mouse)	Na ⁺ /Ca ²⁺ exchanger	1:1000
CSQ (rabbit)	Calsequestrin	1:2500

Secondary antibodies:	Dilution
Anti-mouse IgG HRP (Horseradish peroxidase conjugated)	1:5000
Anti-rabbit IgG HRP (Horseradish peroxidase conjugated)	1:10000
Anti-goat IgG HRP (Horseradish peroxidase conjugated)	1:5000

The membranes were incubated with the secondary antibodies for 1 h at room temperature and then the proteins were detected by chemiluminescence using the ECL plus detection kit (Amersham). This kit provides a substrate, which is transformed by the horseradish peroxidase into a luminescent product. The luminescence was monitored with a chemi-imager (ChemiGenius², Syngene, Cambridge, UK) and the intensities of the bands were analyzed by densitometry with the GeneTools software (Syngene, Cambridge, UK). The results presented in 3.2.3 were obtained by Irena Kröger and Dr. Karim R. Sultan (Hamburg).

2.7 Separation of myosin heavy chain (MHC)-isoforms

This analysis used a protocol which was published by Reiser and Kline (1998) and was performed on purified myosin extracted from ventricles from the adult mouse. The organ extraction was performed as described in 2.6.1. The tissue was powdered while still frozen and the powder was homogenized with a polytron in 8 M urea, 2 M thiourea, 75 mM DTT, 3% SDS, 0.004% bromophenol blue, 50 mM Tris base, pH 6.8 (Blough et al., 1996) at 4 °C. Samples were heated to 95 °C and centrifuged at 12,000 rpm. The supernatant was diluted 1:10 and 4 µl, corresponding to approximately 3 µg of protein, were loaded on a glycerol containing SDS polyacrylamide gel. Mini-gels were cast in the mini-Protean II gel system (Bio-Rad): The stacking gel was composed of 4% acrylamide/N,N'-methylene-bis-acrylamide (50:1), 5% glycerol, 70 mM Tris base, pH 6.7, 4 mM EDTA, 0.4% SDS (with 0.1% APS and 0.05% TEMED to initiate polymerization), and the separating gel was composed of 8% acrylamide/N,N'-methylene-bis-acrylamide (50:1), 5% glycerol, 200 mM Tris base, pH 8.8, 100 mM glycine, 0.4% SDS (with 0.1% APS and 0.05% TEMED to initiate polymerization). The electrophoresis was run for 30 h at 4°C with a constant voltage of 70 V. The upper electrode buffer contained 100 mM Tris base, 150 mM glycine, 0.1% SDS and 10 mM 2-mercaptoethanol and the lower electrode buffer contained 50 mM Tris base, 75 mM glycine and 0.05% SDS. After electrophoresis proteins on the gels were stained with Coomassie Brilliant Blue and the

bands for α - and β -MHC were scanned and quantified with the Image Gauge software. The experiment shown in 3.2.3 was performed by Dr. Catherine Coirault (Paris).

2.8 β -Adrenergic receptor binding assay

The amount of β -adrenergic receptors was evaluated by determining the binding of the β -adrenergic receptor-specific ligand (-)-[3 H]-CGP-12177 in homogenates of ventricles from adult mice. The organs were extracted, frozen and pulverized as described in 2.6.1 and 2.6.2. The pulverized tissue was then homogenized with a polytron at 4 °C in 50 mM Tris base, 5 mM MgCl₂. The suspension was centrifuged for 15 min with 500 x g at 4 °C. The supernatant was collected and centrifuged again for 20 min at 14,000 rpm at 4 °C. The pellet was resuspended in 50 mM Tris, 5 mM MgCl₂, and protein quantity was determined according to the Bradford method.

The binding assay was then performed in a multi-well filtration plate on a polyvinylidene fluoride (PVDF) membrane. Hundred μ g of protein sample were incubated for 90 min with the radioactively labeled β -adrenergic receptor ligand (-)-[3 H]-CGP-12177. To assess the ligand binding curve concentrations of the ligand between 12.5 pM and 3 nM were used and 3 nM was used for determination of maximal ligand binding (B_{max}). The solution, containing the non-bound radioligand, was then removed by aspiration through the PVDF membrane, leaving only the bound receptor-ligand complexes behind on the membrane. Each sample was also incubated with the radioligand in the presence of a high amount of the competitive β -adrenergic receptor antagonist nadolol (10 nM) to determine the non-specific binding. The amount of bound ligand was quantified with a liquid scintillation counter (Wallac 1409, PerkinElmer, Waltham, MA, USA). Therefore, the PVDF membranes with the receptor-ligand complexes were put into a scintillation cocktail, which contained fluorogenic substrates. These substrates were excited by the radioactivity emitted from the radioligand and the fluorescent light was counted by a photomultiplier tube.

Specific binding was then calculated by subtraction of the values for non-specific binding (assessed from the measurements in the presence of nadolol) from the values of total binding (Figure 2.11). The radioligand binding was expressed in counts per minute (CPM), which is already directly proportional to the number of receptor binding sites. With the knowledge of the efficacy of the counter, the specific radioactivity of the ligand

and the amount of protein in the assay, disintegrations per minute (DPM) and the density of binding sites in fmol/mg protein could be calculated. For the example presented in Figure 2.11, with a counting efficacy of ~60% and a radioactivity of the ligand of 1,37 TBq/mmol, this would result in a maximum of specific binding of 12 fmol/mg.

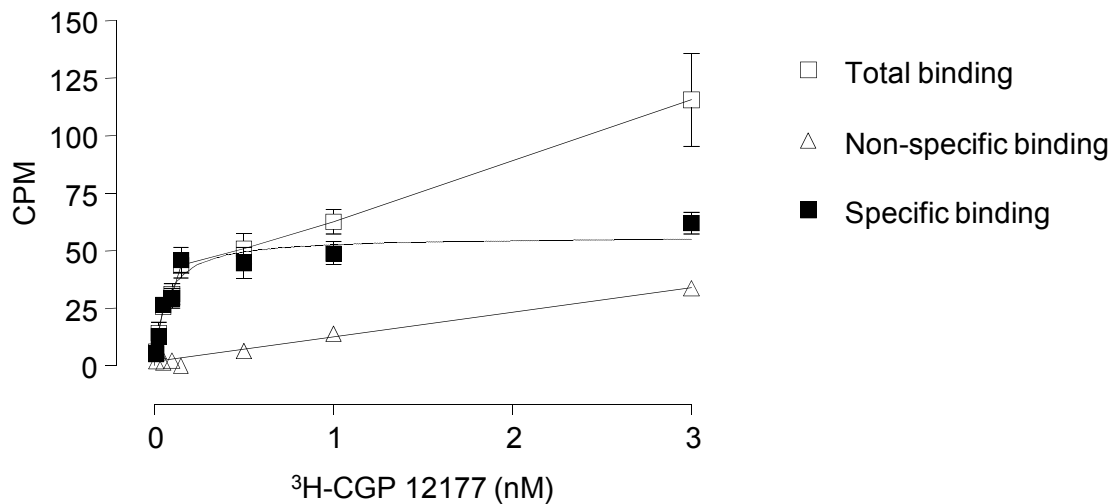


Figure 2.11 Specific β -adrenergic receptor binding. Scintillation counting gives the values for both total and non-specific binding (Non-specific binding is directly proportional to the concentration of ligand). Subtraction of the non-specific binding from the total binding results in the values for specific β -adrenergic receptor binding. The binding curve has the shape of a classical hyperbola.

2.9 Statistical analysis

The statistical analyses were performed with the GraphPad Prism 4.03 and StatView 5.0 software. When only two groups were compared, the Student t-test was used. When the measurements included two different variables (e.g. genotype and concentration), the two-way ANOVA with the Bonferroni post-hoc test was applied. Curve fit and comparison of fitting was performed with the GraphPad Prism 4.03 software. A P value of <0.05 was considered statistically significant.

3 Results

3.1 Establishment of contractility measurements in single intact adult mouse ventricular myocytes

The isolation of intact ventricular myocytes from adult mouse hearts has been started in the Institute of Experimental and Clinical Pharmacology and Toxicology only a few months prior to the beginning of my work. The procedure was established by using a protocol of O'Connell et al. (2003) and some adjustments had to be made like finding the appropriate collagenase for tissue digestion and determining the time of digestion. With the beginning of my participation the isolation of myocytes from wild-type (WT) mice was working in routine and the procedure had then to be transferred on the hypertrophied hearts of the cMyBP-C knock-out (KO) mice. Therefore, my main work during the beginning consisted in acquiring the technique of cannulating the heart. An efficient perfusion of the coronary vessels of the heart was the prerequisite for successful tissue dissociation and this could only be achieved by cannulating the extracted heart without delay (<1 min) and further by the correct positioning of the cannula exactly above the aortic valve. Also, regarding the KO hearts, their altered gross morphology represented an additional difficulty in the first attempts to isolate myocytes from KO mice. Finally, the isolation procedure yielded an average number of 300,000 – 400,000 rod-shaped myocytes per heart in WT, which represented about 20 – 30% of total myocytes. For KO hearts, however, the yield was less; here only 150,000 – 200,000 rod-shaped myocytes were obtained from one heart and it was observed that the major part of the cells was dying during the reintroduction of Ca^{2+} . This showed already that the KO myocytes were more sensitive than WT myocytes, especially with regard to high extracellular Ca^{2+} concentrations.

3.1.1 Evaluation of conditions for the IonOptix measurements

The use of the IonOptix system to monitor sarcomere length simultaneously with intracellular Ca^{2+} transients was a new method in our group and in the Institute of Experimental and Clinical Pharmacology and Toxicology. So it was necessary to determine first adequate conditions for the measurements. This was especially important with respect to the KO myocytes, since they seemed to be generally more sensitive. The influence of different voltages of stimulation, stimulation frequencies and extracellular

Ca^{2+} concentrations on the contractile behavior of the cardiomyocytes was first analyzed without pre-incubation of the myocytes with Fura-2. The quite low concentration of 0.5 mM external Ca^{2+} was used in order to conserve the KO myocytes. Later, myocytes were also loaded with Fura-2 and intracellular Ca^{2+} transients were recorded simultaneously with sarcomere shortening. Figure 3.1 shows the typical traces assessed from Fura-2 loaded myocytes in different extracellular Ca^{2+} concentrations which affect the amplitudes of shortening and of the Ca^{2+} transient.

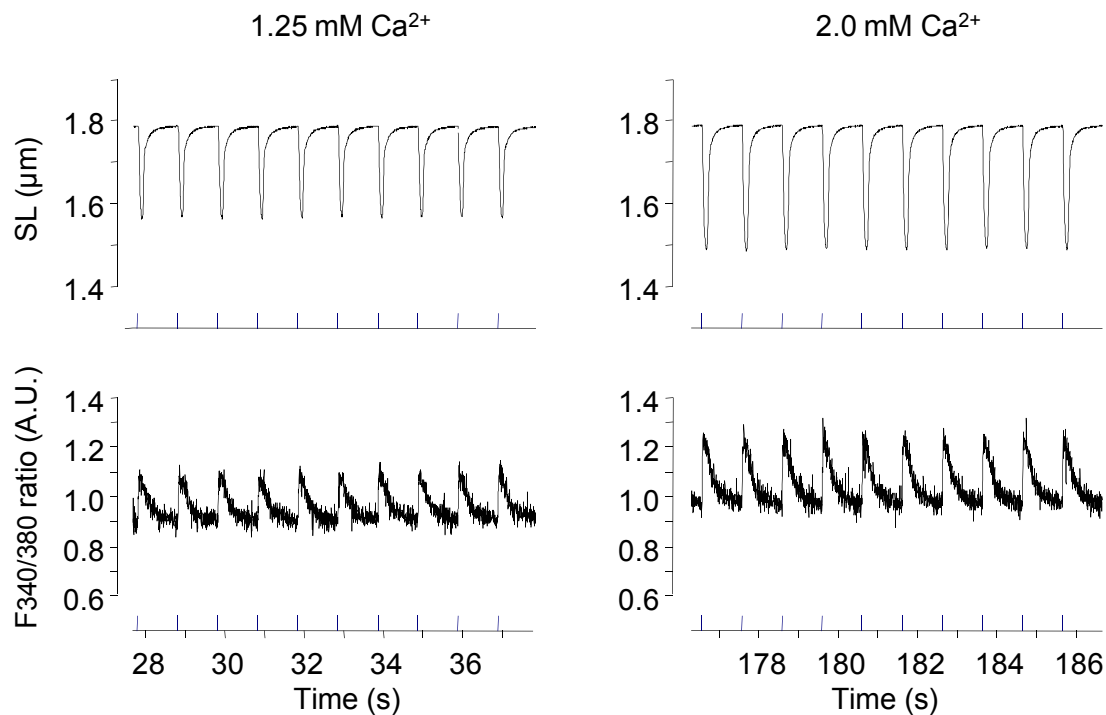


Figure 3.1 Typical traces of simultaneous recording of sarcomere length (SL) and Fura-2 fluorescence ratio (F340/380) in intact ventricular myocytes at 10 V/1 Hz-stimulation in the presence of 1.25 and 2 mM external Ca^{2+} . A change in the extracellular Ca^{2+} concentration affects both the shortening amplitude and the amplitude of the Ca^{2+} transient.

3.1.2 Effect of voltage

The effect of different voltages on the contractile behavior of WT and KO myocytes was studied in 0.5 mM external Ca^{2+} , with a stimulation frequency of 1 Hz and with voltages of 5, 10, 20 and 40 V (Figure 3.2). Neither WT nor KO myocytes contracted at 5 V, and within each group the percentage of sarcomere shortening did not change between 10, 20 and 40 V. Interestingly, at all voltages, the KO myocytes exhibited a tendency towards greater sarcomere shortening compared to WT myocytes.

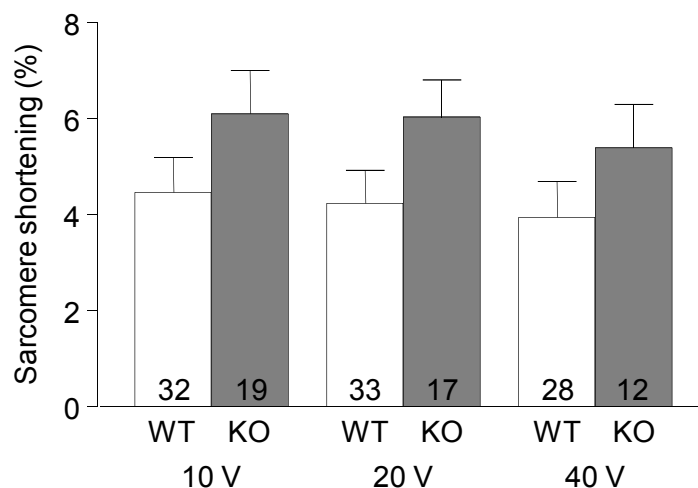


Figure 3.2 Effect of voltage on sarcomere shortening of myocytes from 30 week-old wild-type (WT) and cMyBP-C knock-out (KO) mice. Measurements were performed under 1 Hz-stimulation in 0.5 mM external Ca^{2+} . Values are mean \pm SEM. The number of myocytes is indicated in the bars.

When the kinetics of sarcomere shortening and relengthening and the times to shortening and 50% relengthening were analyzed, also no effect was seen with changes in the voltage of stimulation in either WT or KO myocytes. Yet, the comparison of WT and KO myocytes at each voltage revealed slower shortening and relengthening kinetics in KO myocytes (data not shown/cf. part 3.2).

3.1.3 Effect of stimulation frequency

Myocytes from WT and KO were stimulated at different pacing frequencies in 0.5 mM extracellular Ca^{2+} . The WT myocytes beat regularly and according to the stimulation up to 4 Hz. With higher frequencies of stimulation the myocytes were no longer able to adequately respond to the stimulation rhythm, i.e. every second beating was of smaller amplitude or completely omitted (examples are shown in Figure 3.3). In KO, this phenomenon occurred in some myocytes already at 3 Hz and was then consistently observed at 4 Hz. Therefore, analysis was only performed up to 3 Hz stimulation frequency and measurements from myocytes, which were not beating according to the stimulation rhythm, were discarded.

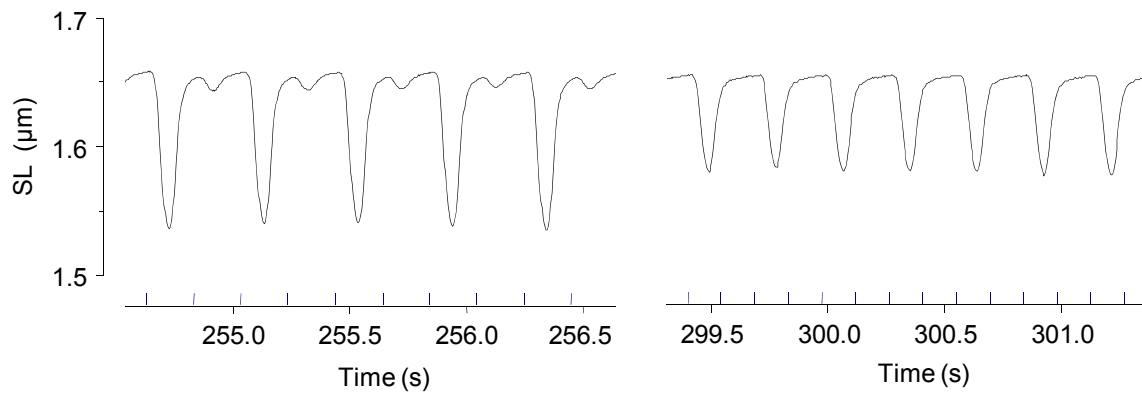


Figure 3.3 Examples of sarcomere length (SL) shortening at high frequencies. Original recordings of a wild-type (WT) myocyte stimulated with 5 Hz, 10 V (left panel) and 7 Hz, 10 V (right panel) in 0.5 mM extracellular Ca^{2+} . The blue marks represent the stimulation events.

In the range of frequencies from 0.5 up to 3 Hz, the WT myocytes were beating without alteration in sarcomere shortening (Figure 3.4). The KO myocytes, however, showed an increase in sarcomere shortening with increasing stimulation frequency. At each frequency sarcomere shortening was greater in KO myocytes than in WT myocytes, with the maximum difference in shortening between KO and WT found at 2 Hz.

Regarding the kinetic parameters, both WT and KO myocytes showed the expected acceleration of shortening and relengthening with increasing frequencies. This resulted

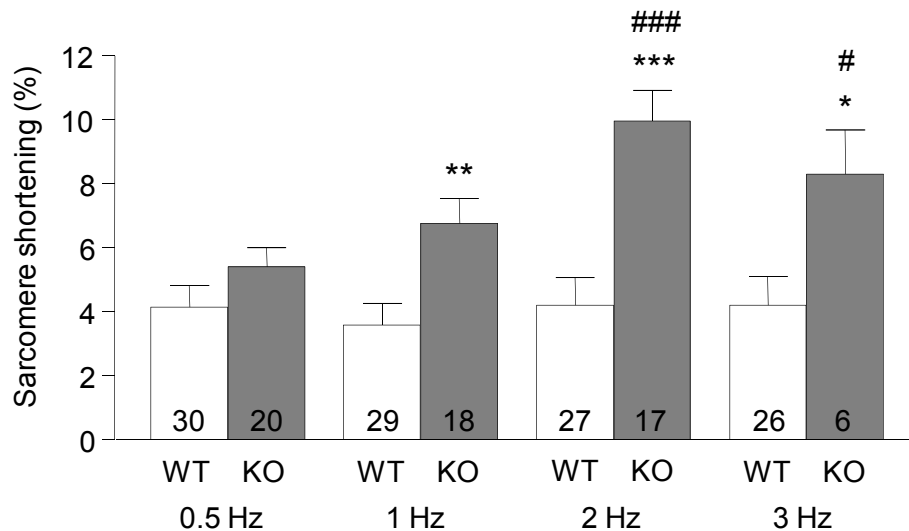


Figure 3.4 Effect of pacing frequency on sarcomere shortening of myocytes from 30 week-old wild-type (WT) and cMyBP-C knock-out (KO) mice. Measurements were performed under 10 V-stimulation in 0.5 mM external Ca^{2+} . Values are mean \pm SEM. * $P < 0.05$, ** $P < 0.01$, *** $P < 0.001$ vs. WT; # $P < 0.05$, ### $P < 0.001$ vs. 0.5 Hz, Student's *t*-test. The number of myocytes is indicated in the bars.

in shorter times to peak shortening and 50% relengthening in the higher frequencies compared to the lower frequencies (Figure 3.5). Only time to peak shortening in KO myocytes was similar in all frequencies tested. Yet, considering that in KO myocytes the shortening amplitude became greater when the stimulation frequency was increased, these similar durations of shortening indicate acceleration of shortening with increased frequencies also in KO myocytes. Furthermore, time to peak shortening in KO myocytes was longer than in WT myocytes at each tested frequency. While in the high frequencies, this may be due to the greater amplitude of shortening in KO myocytes than in WT myocytes, in the lower frequencies, where shortening amplitudes of WT and KO myocytes were similar, this indicates slower shortening of the KO myocytes.

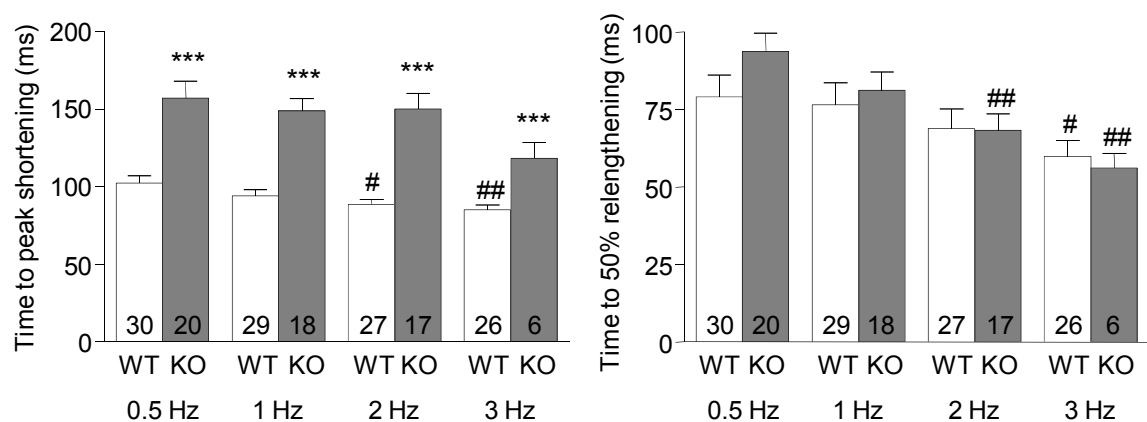


Figure 3.5 Effect of pacing frequency on the times to peak shortening and 50% relengthening in myocytes from 30 week-old wild-type (WT) and cMyBP-C knock-out (KO) mice. Measurements were performed under 10 V-stimulation in 0.5 mM external Ca^{2+} . Values are mean \pm SEM. *** $P < 0.001$ vs. WT; # $P < 0.05$, ## $P < 0.01$ vs. 0.5 Hz, Student's *t*-test. The number of myocytes is indicated in the bars.

3.1.4 Effect of different extracellular Ca^{2+} concentrations

The effect of changing extracellular Ca^{2+} concentrations on the contractile behavior was evaluated in 30 week-old WT, KO and also heterozygous knock-out (HET) myocytes. The HET mice displayed hypertrophic cardiomyopathy at 10 – 11 months of age with typical characteristics found in the human disease (Carrier et al., 2004). At the age of 30 weeks (approximately 7 months), no cardiac hypertrophy should be present in this mice. The myocytes were stimulated with 1 Hz/10 V in a buffer containing 0.5, 1, 2, 3 or 4 mM Ca^{2+} (Figure 3.6).

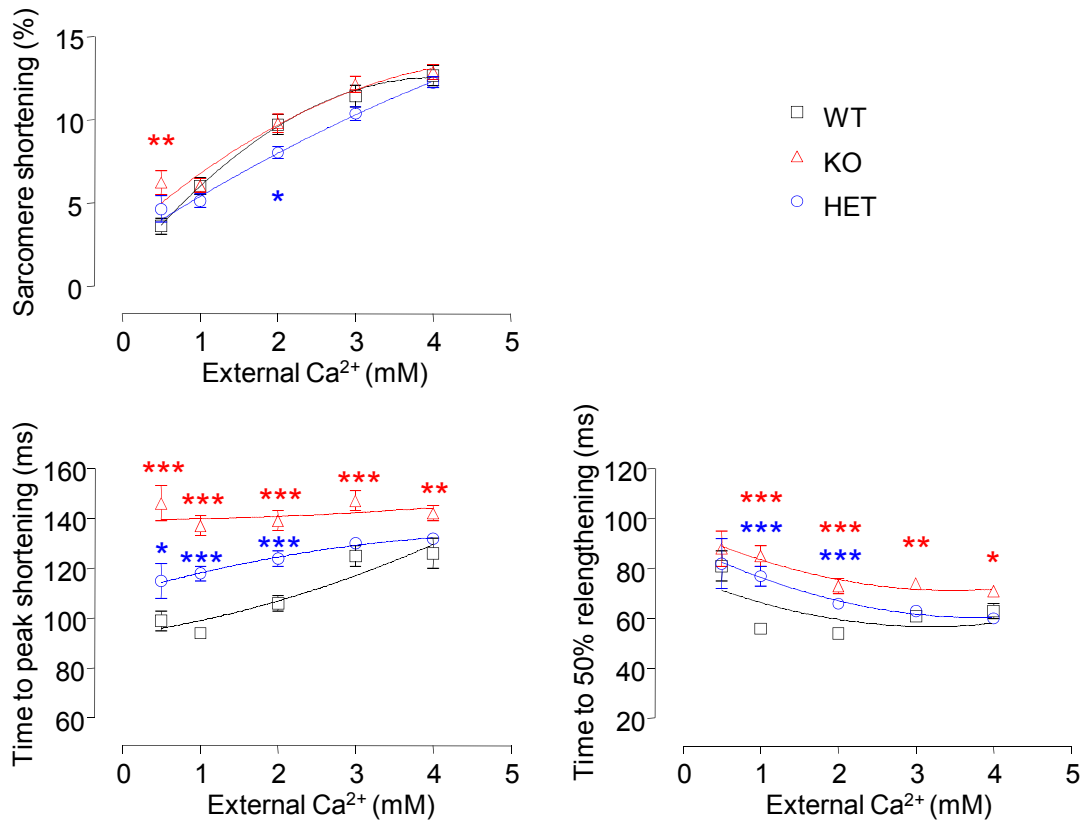


Figure 3.6 Effect of extracellular Ca^{2+} concentration on sarcomere shortening, time to peak shortening and time to 50% relengthening of myocytes from 30 week-old wild-type (WT), heterozygous *cMyBP-C* knock-out (HET) and homozygous *cMyBP-C* knock-out (KO) mice. Measurements were performed at 1 Hz/10 V-stimulation. Values are mean \pm SEM. * $P < 0.05$, ** $P < 0.01$, *** $P < 0.001$ vs. WT, Student's *t*-test. Number of myocytes: $N=26-60$ (WT), $N=22-91$ (HET), $N=28-75$ (KO). Note that the values for the different concentrations of external Ca^{2+} are not paired.

Sarcomere shortening increased in all three groups with increasing Ca^{2+} concentration. No difference was detected between WT and KO myocytes in external Ca^{2+} concentrations between 1 – 4 mM. However, in 0.5 mM external Ca^{2+} , sarcomere shortening was found to be greater in KO than in WT. In HET myocytes, sarcomere shortening tended to be smaller than WT myocytes, yet the difference was only significant in 2 mM external Ca^{2+} .

The time to peak shortening was prolonged in KO myocytes compared to WT myocytes in all concentrations of external Ca^{2+} . Similarly, time to 50% relengthening was longer in KO myocytes in 1 – 4 mM external Ca^{2+} . In HET myocytes, time to peak shortening was longer than in WT myocytes only in concentrations of external Ca^{2+} up to 2 mM and the time to 50% relengthening was longer than in WT myocytes only in 1 and 2 mM external Ca^{2+} . Interestingly, in those conditions where differences between HET and WT were

observed, the values for time to peak shortening and time to 50% relengthening in HET myocytes always were intermediate between values for WT and KO.

Since the HET mice develop their cardiac phenotype not before the age of 10 – 11 months, 60 week-old HET and WT myocytes were also analyzed (Figure 3.7). At this age no difference in sarcomere shortening and in its kinetics was found. On the other hand, both WT and HET myocytes at the age of 60 weeks displayed significant differences compared to the 30 week-old myocytes (normalized contractions are presented in Figure 3.8). Like this, differences in WT and HET in the older age may be obscured by the general impairment of contractility with age. Interestingly, when the ventricular weight to body weight ratio (VW/BW) was determined in the 60 week-old HET mice, no difference to WT could be detected (Figure 3.9). This was not consistent with the phenotype of hypertrophy previously described (Carrier et al., 2004).

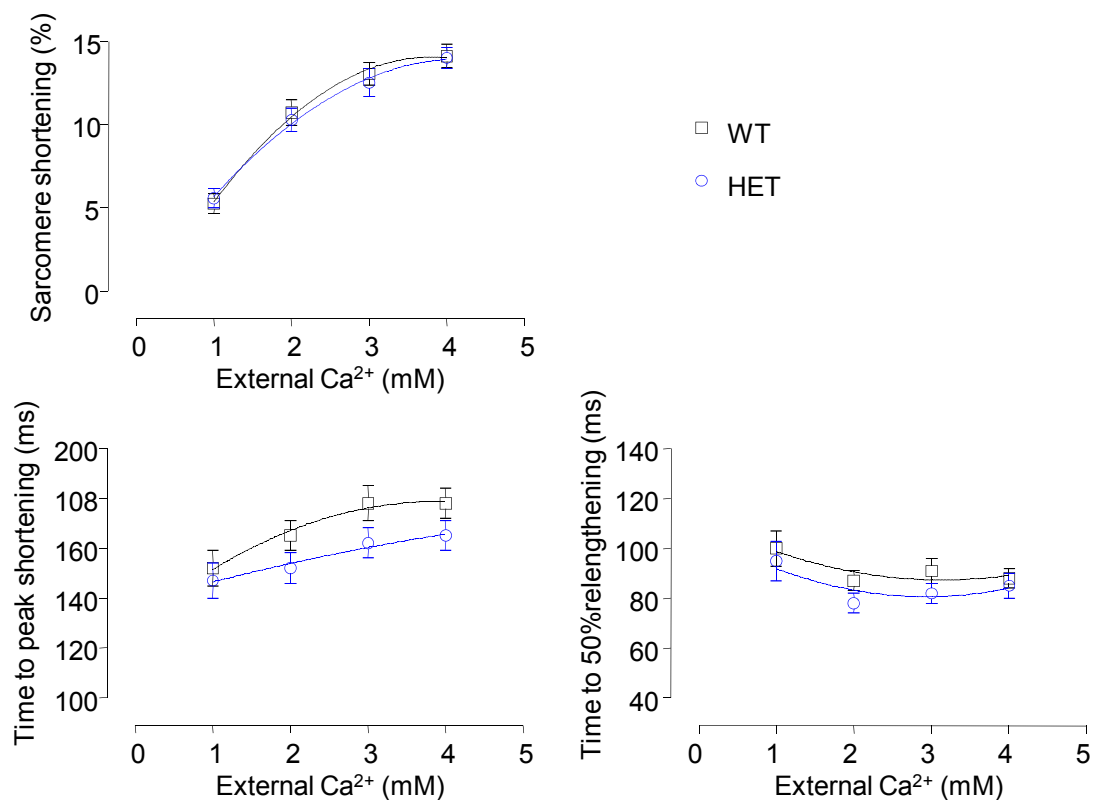


Figure 3.7 Effect of extracellular Ca^{2+} concentration on sarcomere shortening, time to peak shortening and time to 50% relengthening of myocytes from 60 week-old wild-type (WT) and heterozygous knock-out (HET) mice. Measurements were performed under 1 Hz/10 V-stimulation. Values are mean \pm SEM. Number of myocytes: N=31 (WT), N=31 (HET). Note that the values for the different concentrations of external Ca^{2+} are not paired.

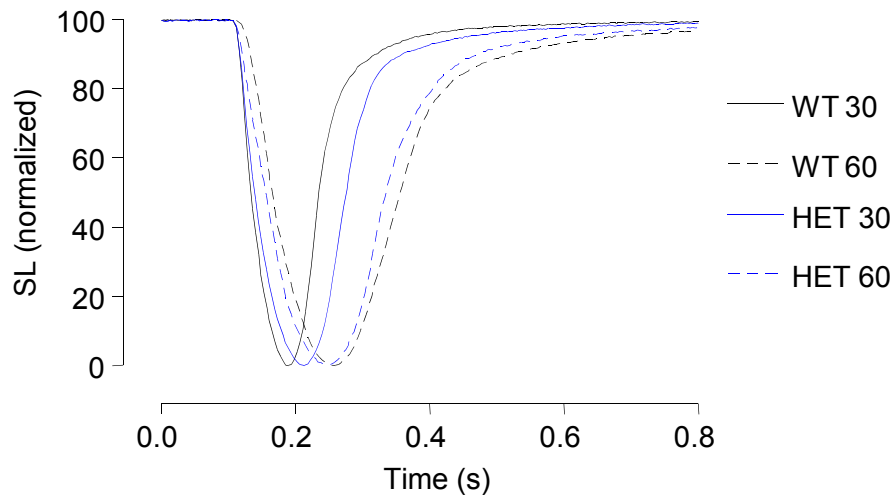


Figure 3.8 Normalized traces of sarcomere length (SL) shortening transients of myocytes from 30 and 60 week-old wild-type (WT 30 and WT 60) and heterozygous knock-out (HET 30 and HET 60) mice. Traces represent an average of 20 – 30 sarcomere shortenings.

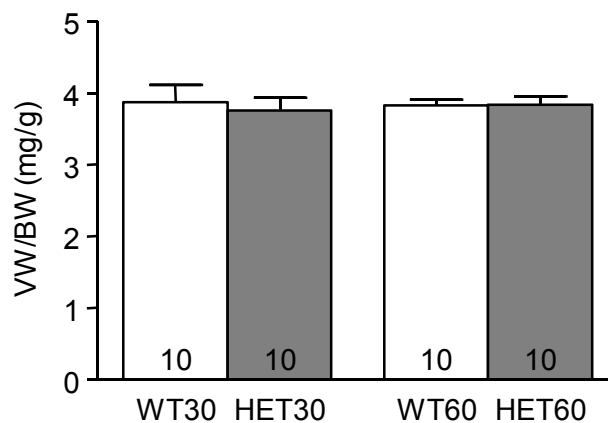


Figure 3.9 Ventricular weight to body weight ratio (VW/BW) from 30 and 60 week-old wild-type (WT30 and WT60) and heterozygous knock-out (HET30 and HET60) mice. Values are mean \pm SEM. The number of animals is indicated in the bars.

3.1.5 Measurements in the presence or absence of Fura-2

To evaluate whether the use of Fura-2 to determine intracellular Ca^{2+} affects the contractile behavior of the myocytes, measurements in the presence and absence of Fura-2 with changing extracellular Ca^{2+} concentrations in WT and KO myocytes were performed (Figure 3.10).

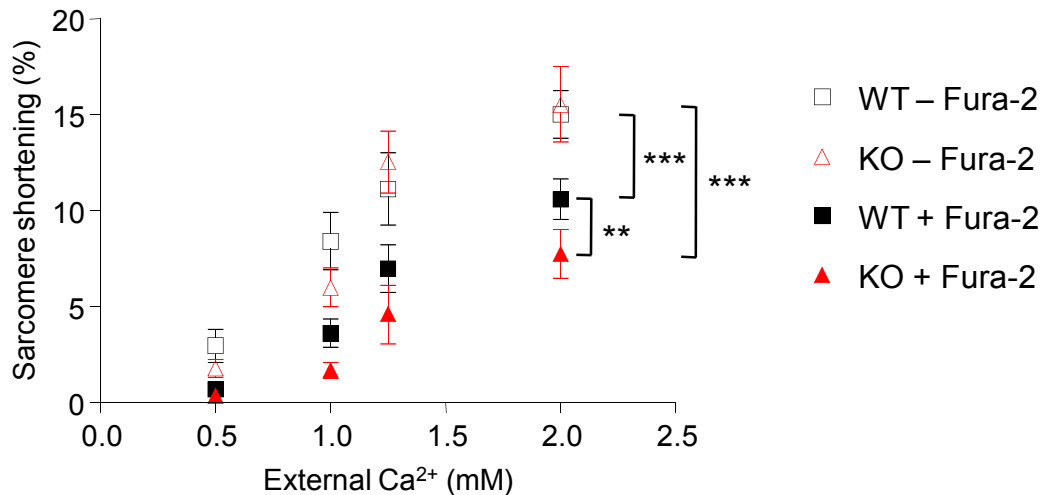


Figure 3.10 Measurements of sarcomere length shortening in 6-9 week-old wild-type (WT) and cMyBP-C knock-out (KO) myocytes either pre-incubated or not with Fura-2 (+ Fura-2 and – Fura-2, respectively) in different extracellular Ca²⁺ concentrations. Measurements were performed under 1 Hz/10 V-stimulation. Values are mean \pm SEM. ** $P < 0.01$, *** $P < 0.001$, repeated measures two-way ANOVA. Number of myocytes: $N=7$ (WT + Fura), $N=5$ (KO + Fura), $N=6$ (WT – Fura), $N=5$ (KO – Fura).

In both WT and KO myocytes pre-incubated with Fura-2, values of sarcomere shortening were lower at each concentration of extracellular Ca²⁺ when compared to the myocytes which had not been pre-incubated with Fura-2 ($P < 0.001$, two-way ANOVA). Furthermore, KO myocytes pre-incubated with Fura-2 exhibited at all concentrations of extracellular Ca²⁺ lower values of sarcomere shortening than WT ($P < 0.01$, two-way ANOVA). In contrast, in myocytes not pre-incubated with Fura-2, there was no difference in the response of the myocytes to external Ca²⁺ between WT and KO. This indicates that Fura-2 could act as a Ca²⁺ buffer. Furthermore, the results show that the KO myocytes are more affected by the Ca²⁺ buffering of Fura-2 than the WT myocytes.

Interestingly, the greater fractional sarcomere shortening observed before in KO myocytes at 0.5 mM extracellular Ca²⁺ (Figures 3.4 and 3.6) could not be reproduced in this experiment. We do not have a clear explanation for these discrepancies. However, it has to be noted that in the previous experiments sarcomere shortening was measured in several myocytes after the extracellular Ca²⁺ in the cell chamber had been adjusted to a certain concentration. In contrast, in the experiment presented above, the same myocyte was monitored while extracellular Ca²⁺ was gradually changed, thus giving paired values, however only in a small number of myocytes. Additionally, measurements presented in Figures 3.4 and 3.6 were started in the lowest concentration of extracellular Ca²⁺, whereas the experiment in Figure 3.10 started with the highest concentration. Finally, the

data in Figures 3.4 and 3.6 were obtained in the beginning of my work when the quality of the cellular preparations was not as good as later.

3.1.6 Summary

In the first attempt to measure contractile properties along with intracellular Ca^{2+} transients of intact ventricular myocytes, the impact of different parameters that can influence contraction, i.e. voltage and frequency of stimulation, extracellular Ca^{2+} concentration, and loading with the Ca^{2+} dye Fura-2, were tested in myocytes from WT, HET and KO mice. The principal findings were:

- (a) Increasing voltage of stimulation did not affect contractility of WT and KO myocytes.
- (b) Increasing the frequency of stimulation increased sarcomere shortening in KO myocytes, but not in WT myocytes.
- (c) Increasing the extracellular Ca^{2+} concentration increased sarcomere shortening and kinetics of shortening and relengthening in WT, HET, and KO myocytes. However, shortening and relengthening in HET and KO myocytes were slower compared to WT myocytes.
- (d) When myocytes were loaded with Fura-2, shortening amplitude was smaller than in myocytes without Fura-2.

Based upon the above findings, the conditions for the following experiments were chosen to be 10 V/1 Hz-stimulation and a concentration of extracellular Ca^{2+} of 1.25 mM, which resulted in a stable shortening amplitude when the myocytes were loaded with Fura-2.

3.2 The role of cMyBP-C in sarcomere contraction

3.2.1 Myocyte hypertrophy contributes to ventricular hypertrophy in KO mice

To assess the degree of hypertrophy in the cMyBP-C KO mice the VW/BW ratios were acquired from 6 and 30 week-old WT and KO mice. At both ages, VW/BW in the KO mice was higher compared to WT mice (Figure 3.11) with a stronger increase in the

30 week-old animals (44% compared to 29% in 6 weeks old mice). In both groups VW/BW was smaller in the older animals which resulted from a greater body weight at this age.

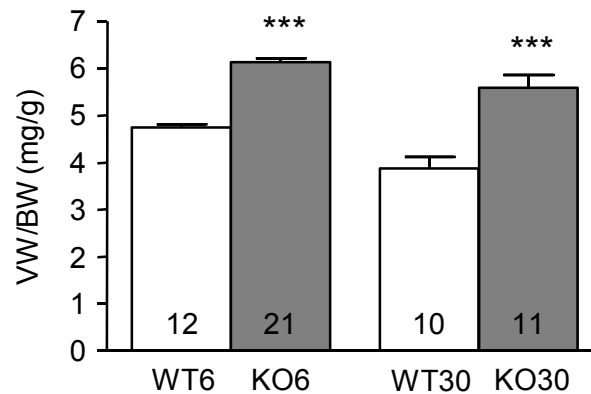


Figure 3.11 Ventricular weight to body weight ratio (VW/BW) from 6 and 30 week-old wild-type (WT6 and WT30) and homozygous cMyBP-C knock-out (KO6 and KO30) mice. Values are mean \pm SEM. *** $P < 0.001$ vs. WT, Student's *t*-test. The number of animals is indicated in the bars.

Further, the cellular dimensions of isolated adult ventricular myocytes were measured. Cell length and cell width were determined in the presence of 10 mM BDM, an inhibitor of cross-bridge cycling, which is able to fully relax the myocytes. Cell area was then calculated as the product of cell length x cell width. In 6 and 30 week-old KO mice the cardiomyocyte length was greater than in WT (+14% and +12%, respectively). In the 30 week-old KO myocytes also cell width was 22% greater, while there was no significant difference in the 6 week-old group. This lead to a 13% greater cell area in the 6 week-old and a 28% greater cell area in the 30 week-old group (Figure 3.12). This indicates that myocyte hypertrophy in KO contributes to ventricular hypertrophy.

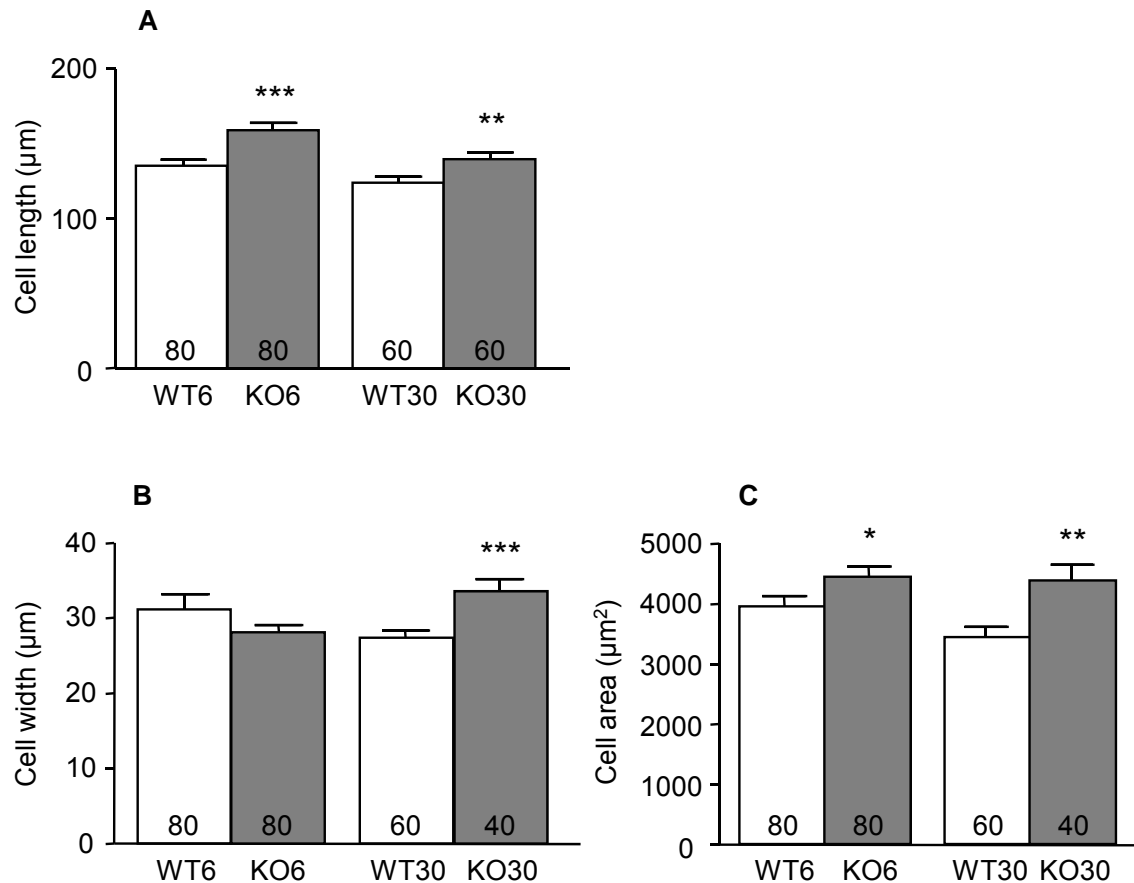


Figure 3.12 Cell dimensions of myocytes from 6 and 30 week-old wild-type (WT6 and WT30) and homozygous cMyBP-C knock-out (KO6 and KO30) mice. Measurements were performed in modified Tyrode's solution containing 0.0125 mM Ca^{2+} and 10 mM BDM. Cell length (A) and cell width (B) were acquired and cell area (C) was calculated as the product of both. Values are mean \pm SEM. * $P < 0.05$, ** $P < 0.01$, *** $P < 0.001$ vs. WT, Student's *t*-test. The number of myocytes is indicated in the bars.

3.2.2 Impaired contractile properties of isolated ventricular KO myocytes

Contractile properties of 6 week-old KO (mild hypertrophy) and 30 week-old KO (larger degree of hypertrophy) mice were assessed by recording the sarcomere length shortening and relengthening of isolated intact ventricular myocytes under 1 Hz electrical stimulation. Figure 3.13 shows the averaged contractions of representative recordings from 6 and 30 week-old WT and KO myocytes. The analysis of contractile parameters is depicted in Table 3.1.

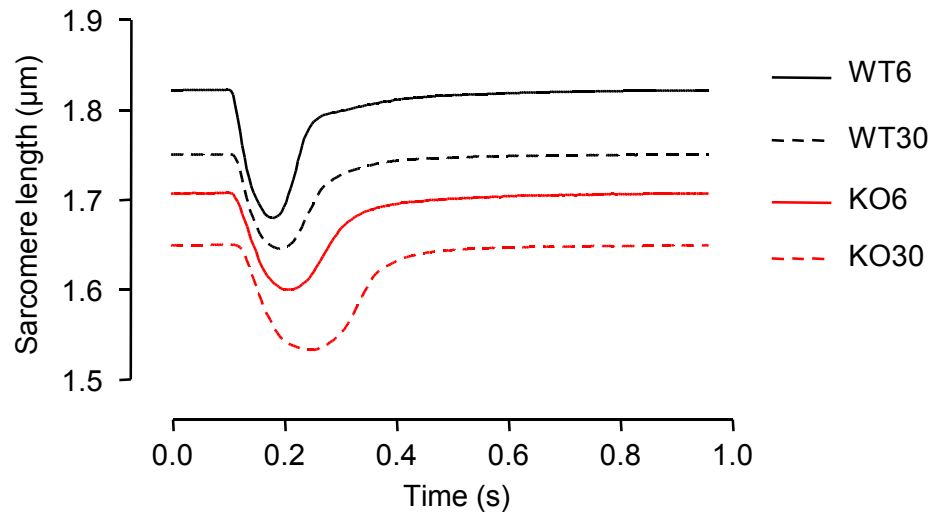


Figure 3.13 Representative examples of 20 – 30 averaged sarcomere shortenings of myocytes from 6 and 30 week-old wild-type (WT6 and WT30) and homozygous cMyBP-C knock-out (KO6 and KO30) mice. The measurements were performed under 1 Hz/10 V-stimulation in 1 – 1.25 mM external Ca^{2+} .

The diastolic sarcomere length in KO was markedly lower than in WT at both ages. In fact, the resting sarcomere length in KO was almost identical to the systolic sarcomere length in WT, meaning the sarcomere shortening in KO started from a level where it normally ended in WT. Maximal sarcomere shortening was not altered between the groups, but the kinetics of shortening and relengthening were found to be slower in KO. This phenotype worsened with age. Thus, shortening velocity in KO was 34% lower in 6 week-old and 56% lower in 30 week-old myocytes compared to WT, and relengthening velocity in KO was 33% lower in 6 week-old and 49% lower in 30 week-old myocytes compared to WT. Consequently, the times to peak shortening and 50% relengthening were prolonged in KO myocytes compared to WT (time to peak shortening +10% and +44% in 6 and 30 week-old, respectively; time to 50% relengthening +22% and +51% in 6 and 30 week-old, respectively).

Table 3.1 Sarcomere shortening in intact ventricular myocytes

	WT6	KO6	WT30	KO30
Diastolic SL, μm	1.82 \pm 0.01	1.70 \pm 0.01***	1.74 \pm 0.01	1.64 \pm 0.02***
Systolic SL, μm	1.69 \pm 0.01	1.59 \pm 0.01***	1.64 \pm 0.02	1.54 \pm 0.02***
Sarcomere shortening, %	7 \pm 1	7 \pm 1	6 \pm 1	6 \pm 1
Shortening velocity, $\mu\text{m/s}$	-2.86 \pm 0.14	-2.14 \pm 0.09***	-2.51 \pm 0.24	-1.61 \pm 0.11***
Time to peak shortening, ms	96 \pm 2	106 \pm 3**	95 \pm 2	137 \pm 5***
Relengthening velocity, $\mu\text{m/s}$	1.93 \pm 0.13	1.45 \pm 0.09***	1.68 \pm 0.18	1.13 \pm 0.10**
Time to 50% relengthening, ms	60 \pm 2	73 \pm 3***	57 \pm 3	86 \pm 4**
No. of mice/cells	17/110	24/132	9/47	15/71
Age of the mice, weeks	6.6 \pm 0.2	6.6 \pm 0.1	28.7 \pm 0.7	27.9 \pm 0.7

*Parameters of contractility were acquired in myocytes from 6 and 30 week-old wild-type (WT6 and WT30) and homozygous cMyBP-C knock-out (KO6 and KO30) mice. Measurements were performed under 1 Hz/10 V-stimulation in 1 – 1.25 mM external Ca^{2+} . Values are mean \pm SEM. ** $P < 0.01$, *** $P < 0.001$ vs. WT, Student's *t*-test.*

To investigate whether relations exist between sarcomere length and contractile behavior, correlation analyses were performed (Figure 3.14). In KO a slight negative correlation between diastolic sarcomere length and sarcomere shortening was found, whereas there was no such correlation in WT (Figure 3.14 A). No correlation existed between diastolic sarcomere length and shortening velocity. Systolic sarcomere length showed the expected negative correlation with sarcomere shortening in both groups and at both ages (Figure 3.14 B). However, the slopes were significantly less steep in KO than in WT at both ages and less steep in the older age in both WT and KO. A similar negative correlation existed between systolic sarcomere length and relengthening velocity, also with a less steep slope in KO compared to WT (Figure 3.14 C).

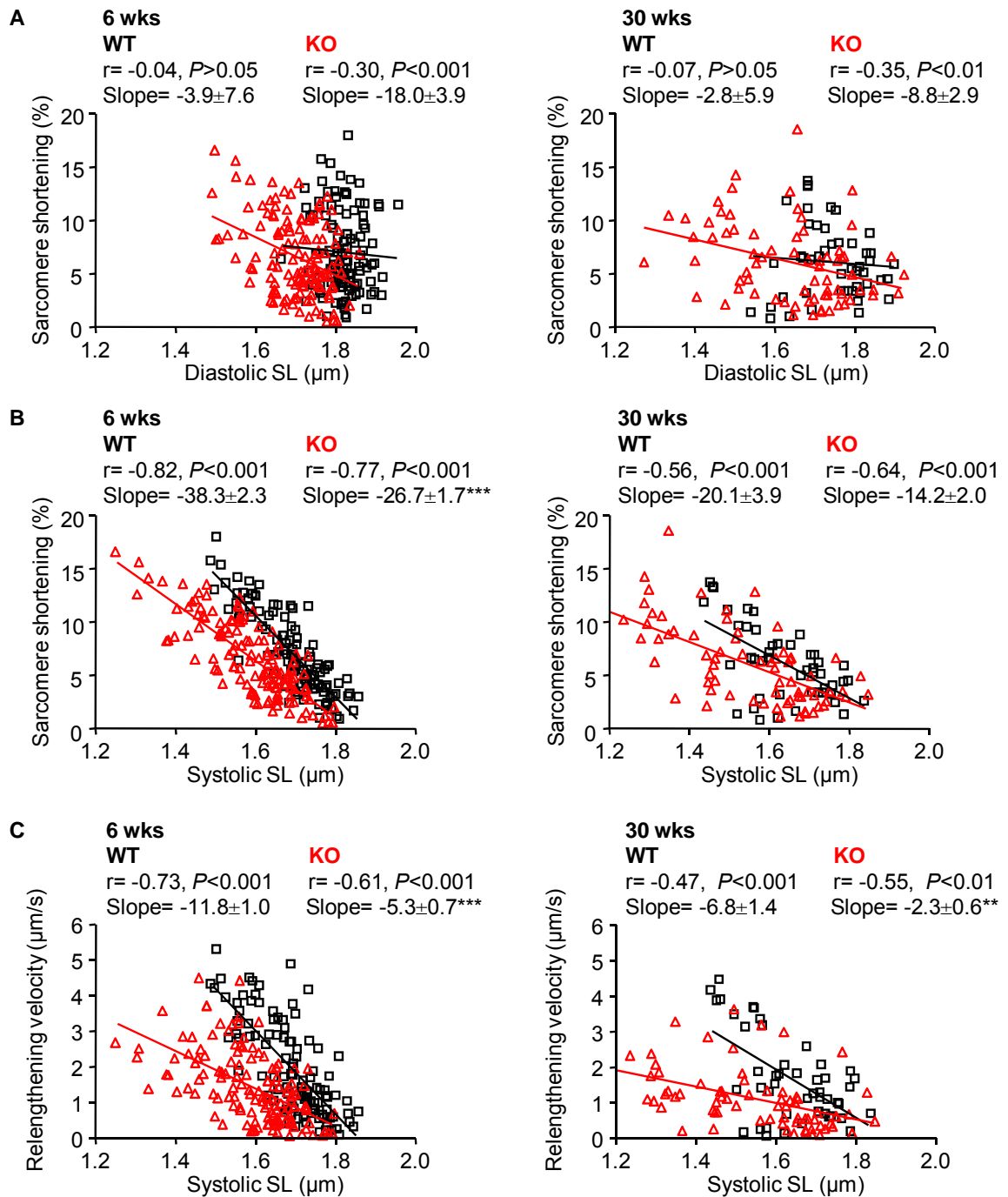


Figure 3.14 Relationship between diastolic sarcomere length and sarcomere shortening (A), systolic sarcomere length and sarcomere shortening (B) and systolic sarcomere length and relengthening velocity (C) in myocytes from 6 and 30 week-old wild-type (WT, depicted in black) and homozygous cMyBP-C knock-out (KO, depicted in red) mice. The Spearman correlation factor r and the steepness of the slopes are indicated in each panel. $^{**}P < 0.01$, $^{***}P < 0.001$ vs. WT, linear regression analysis.

3.2.3 Compensatory changes in protein expression in KO ventricles

In order to determine potential adaptations due to the ablation of cMyBP-C the amount of proteins involved in contraction and relaxation was determined. The analysis of the α - and β -MHC isoforms was performed by long-term electrophoresis in a glycerol-containing polyacrylamide gel. The results presented in Figure 3.15 were obtained by Dr. Catherine Coirault in Paris and revealed a significant shift from the α - to the β -Isoform in the KO hearts. The level of β -isoform was 5-fold higher in 6 week-old KO compared to WT ($49\pm 5\%$ vs. $9\pm 9\%$ of total MHC) and 3-fold higher in 30 week-old KO compared to WT ($20\pm 3\%$ vs. $7\pm 4\%$ of total MHC).

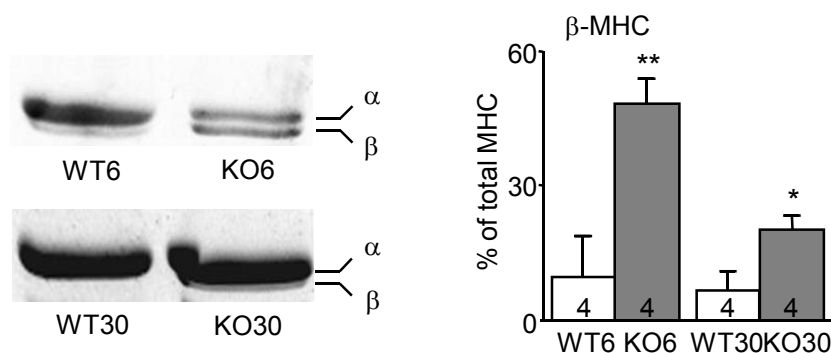


Figure 3.15 Separation of the α - and β -isoforms of myosin heavy chain (MHC) by long-term electrophoresis in a glycerol-containing polyacrylamide gel. Left panel: Representative examples obtained from samples of 6 and 30 week-old wild-type (WT6 and WT30) and homozygous cMyBP-C knock-out (KO6 and KO30) hearts. Right panel: Quantification of the amount of β -MHC as fraction of total MHC. * $P < 0.05$, ** $P < 0.01$ vs. WT, Student's *t*-test. The number of samples is indicated in the bars. The experiment was performed by Catherine Coirault (Paris).

Protein analysis by Western blot was performed on 6 and 30 week-old WT and KO ventricles by Irena Kröger and Dr. Karim R. Sultan. The analyses confirmed the higher level of the β -MHC isoform in the KO ventricles with an antibody directed specifically against the β -Isoform (Figure 3.16 A). Here the amount of β -MHC was 40-fold higher in the 6 week-old KO compared to WT and 4-fold higher in 30 week-old KO compared to WT. The amount of the cardiac-specific SERCA (SERCA2) and phospholamban (PLB) was similar in WT and KO at both ages, but a significantly higher amount of both phosphorylated isoforms of phospholamban (Ser16 and Thr17 phosphorylated) was found in the 30 week-old KO compared to WT (Figure 3.16 A). The amount of the $\text{Na}^+/\text{Ca}^{2+}$ exchanger (NCX) was 34% lower in KO than in WT (Figure 3.16 B).

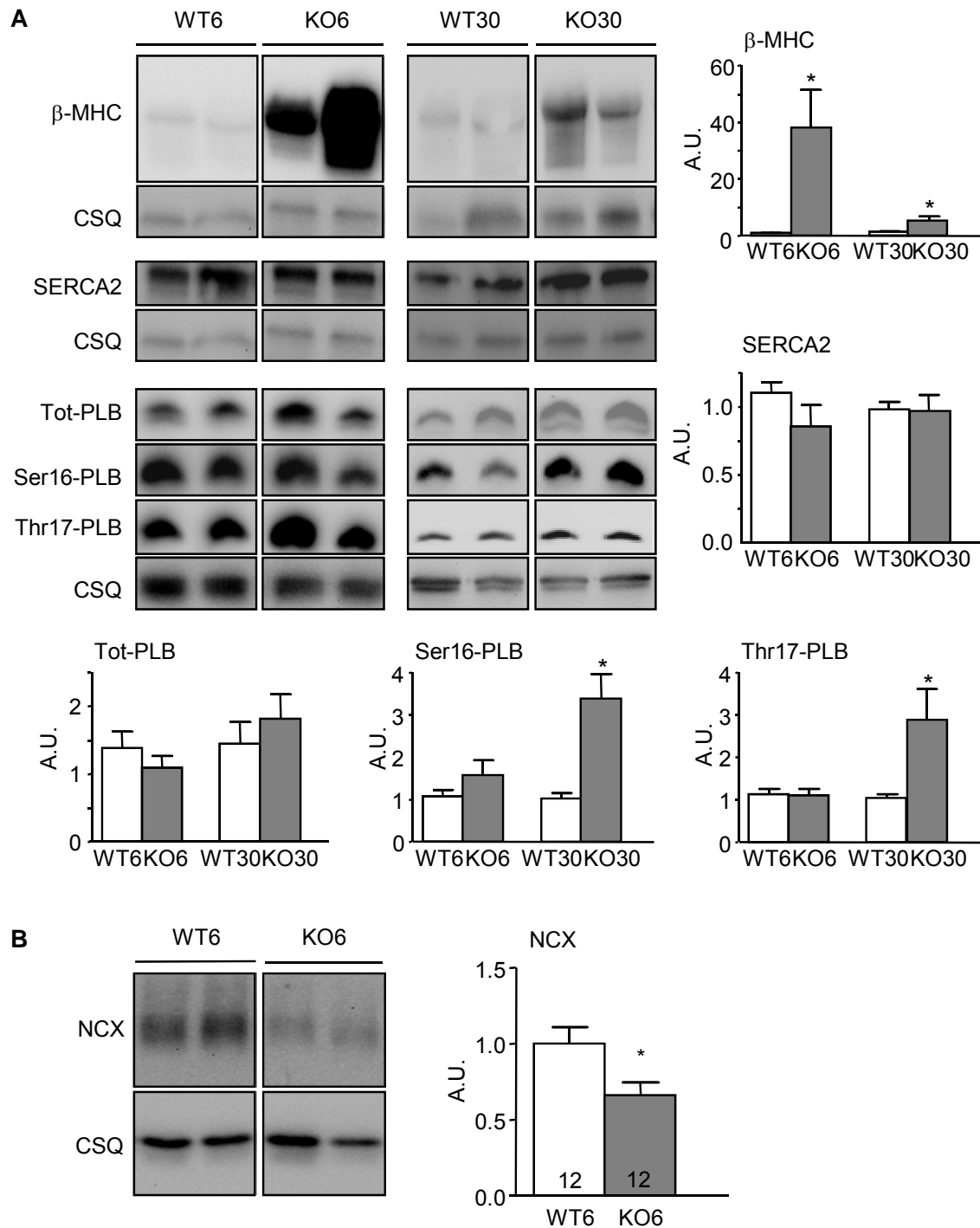


Figure 3.16 Western blot analysis of protein expression in 6 and 30 week-old wild-type (WT6 and WT30) and homozygous cMyBP-C knock-out (KO6 and KO30) hearts. **A:** Representative examples and quantification of membranes probed with antibodies directed against β -myosin heavy chain (β -MHC), sarco-endoplasmic reticulum Ca^{2+} -ATPase (SERCA2), total phospholamban (Tot-PLB), phospholamban phosphorylated at serine 16 (Ser16-PLB) and phospholamban phosphorylated at threonine 17 (Thr17-PLB). * $P < 0.05$, Student's *t*-test. $N = 6-9$. **B:** Representative examples and quantification of a membrane probed with an antibody directed against the sodium-calcium-exchanger (NCX). * $P < 0.05$, Student's *t*-test. Number of samples is indicated in the bars. The experiments were performed by Irena Kröger and Karim R. Sultan (Hamburg).

3.2.4 Inhibition of actin-myosin interaction

In paragraph 3.2.2, it was demonstrated that KO myocytes exhibited a lower diastolic sarcomere length. To investigate whether this can be attributed to active cross-bridge cycling, the effect of two inhibitors of cross-bridge cycling (BDM and blebbistatin) on the sarcomere length was investigated. First, sarcomere length was measured without electrical stimulation when the myocytes were kept either in an isotonic buffer solution with 10 mM BDM and 0.0125 mM Ca^{2+} or in a buffer solution containing 1.25 mM Ca^{2+} (Figure 3.17). In the presence of 1.25 mM Ca^{2+} the sarcomere length was lower in KO myocytes compared to WT myocytes at both ages (6 and 30 weeks). This effect was similar to what was found before when the myocytes were electrically stimulated (Figure 3.13 and Table 3.1). BDM did not change sarcomere length in WT, but increased sarcomere length in KO myocytes by 5%.

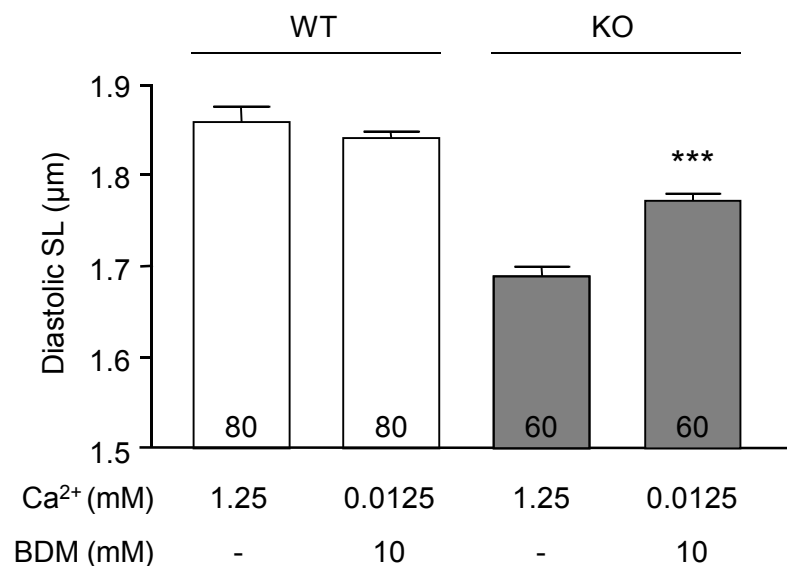


Figure 3.17 Measurement of diastolic sarcomere length (SL) in myocytes from 6 week-old wild-type (WT) and homozygous cMyBP-C knock-out (KO) mice in 1.25 mM or 0.0125 mM external Ca^{2+} in the presence or absence of 10 mM 2,3-butanedione monoxime (BDM). Values are mean \pm SEM. *** $P < 0.001$ vs. Ca^{2+} 1.25 mM, Student's *t*-test. Number of myocytes is indicated in the bars.

Next, the capacity of BDM to increase diastolic sarcomere length in KO myocytes was tested in electrically stimulated myocytes and when extracellular Ca^{2+} was completely chelated by EGTA. The complete absence of Ca^{2+} was required because in the previous experiment sarcomere length in KO still differed from WT in the presence of BDM, which may be caused by a higher intracellular Ca^{2+} level. Examples of the experimental procedure are shown in Figure 3.18 A for one WT and one KO myocyte.

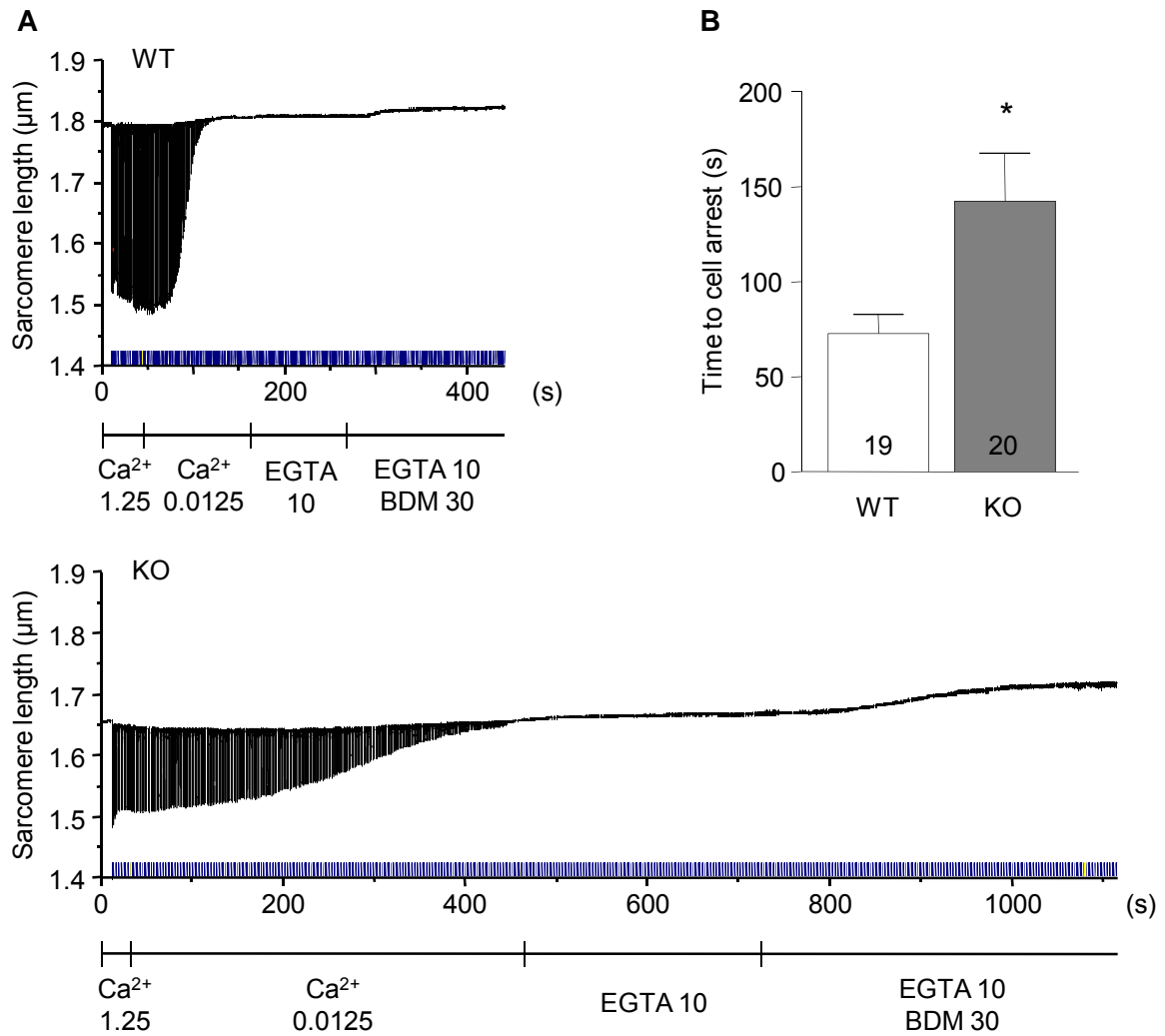


Figure 3.18 A: Sarcomere length measurements in myocytes from wild-type (WT) and homozygous *cMyBP-C* knock-out (KO) mice in the following conditions: 1.25 mM external Ca^{2+} , 0.0125 mM external Ca^{2+} , 10 mM EGTA, 10 mM EGTA + 30 mM 2,3-butanedione monoxime (BDM). Measurements were performed under continuous 1 Hz/10 V-stimulation. B: Time from the last normal twitch to cell arrest induced by lowering external Ca^{2+} concentration. Values are mean \pm SEM. * $P < 0.05$ vs. WT, Student's *t*-test. Number of myocytes is indicated in the bars.

First, the myocytes were kept in 1.25 mM external Ca^{2+} where they were regularly beating. After lowering the external Ca^{2+} concentration to 0.0125 mM beatings started to become gradually weaker until the myocyte finally stopped beating. Interestingly, the time from the last normal beating, before it became weaker, until the complete stop of beating was two-fold slower in KO than in WT myocytes (Figure 3.18 B). After cell arrest, the extracellular Ca^{2+} was completely removed with 10 mM EGTA and finally either 30 mM BDM or alternatively 10 μM blebbistatin, another inhibitor of cross-bridge cycling, was applied. Neither the lowering of external Ca^{2+} to 0.0125 mM nor the complete removal of external Ca^{2+} with EGTA changed the diastolic sarcomere length in WT or KO

myocytes (Figure 3.19). The addition of BDM or blebbistatin clearly increased diastolic sarcomere length in KO myocytes, but also a small increase in WT myocytes was observed compared to EGTA. The increase in diastolic sarcomere length in the WT, however, was only statistically significant when compared to 1.25 mM external Ca^{2+} .

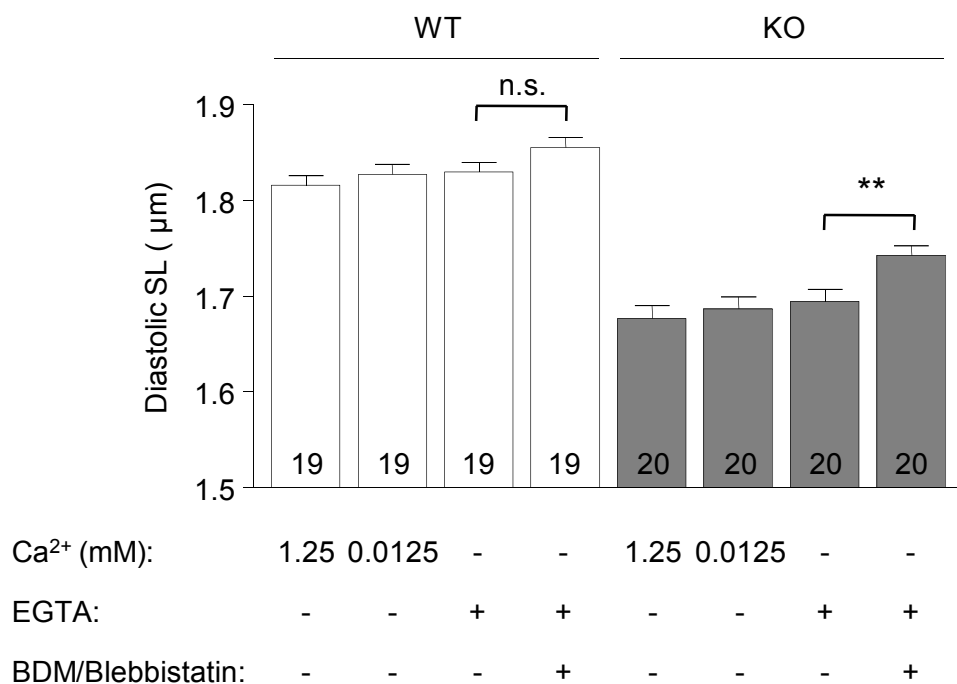


Figure 3.19 Diastolic sarcomere length in myocytes from wild-type (WT) and homozygous *cMyBP-C* knock-out (KO) mice. The conditions are indicated below the bars. Values are mean \pm SEM. ** $P < 0.01$, n.s. not significant, Student's *t*-test. Number of myocytes is indicated in the bars.

Finally, to evaluate whether a higher concentration of BDM was able to completely reverse diastolic sarcomere length in KO up to the level of WT myocytes, diastolic sarcomere length was evaluated with 10 and 100 mM BDM in the presence of 1.5 mM external Ca^{2+} (Figure 3.20). Hundred mM BDM was able to return diastolic sarcomere length in KO myocytes to the level of WT myocytes (1.80 ± 0.01 μm in KO vs. 1.81 ± 0.01 μm in WT, $P > 0.05$, Student's *t*-test).

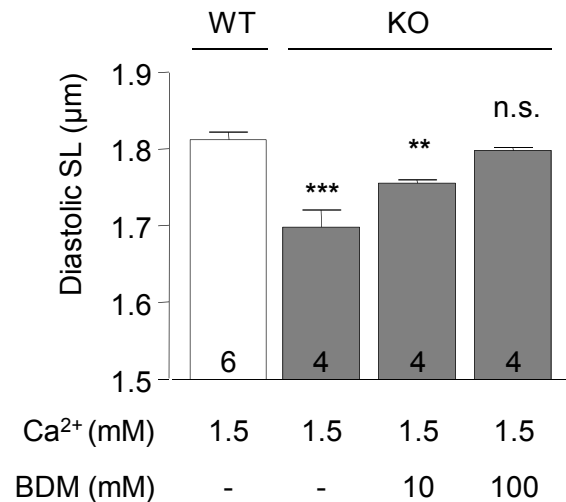


Figure 3.20 Measurement of diastolic sarcomere length in myocytes from wild-type (WT) and homozygous cMyBP-C knock-out (KO) mice in 1.5 mM external Ca²⁺ in the presence of different concentrations of 2,3-butanedione monoxime (BDM). Values are mean \pm SEM. ** $P < 0.01$, *** $P < 0.001$, n.s. not significant vs. WT, Student's *t*-test. Number of myocytes is indicated in the bars.

3.2.5 Impaired Ca²⁺ transients and relation between sarcomere length and cytosolic Ca²⁺ in KO myocytes

We then investigated whether alterations of intracellular Ca²⁺ transients are present in myocytes from 6 week-old KO mice. Therefore, sarcomere length shortening was measured simultaneously with intracellular Ca²⁺ transients. Figure 3.21 shows typical traces from a WT and a KO myocyte. The original recordings of sarcomere length and Fura-2 fluorescence ratio (on the left side of each panel) were transformed into an average trace (right side of each panel) which was then used for the analysis. The summary of the analysis is shown in Figure 3.22, and each parameter of sarcomere length shortening is matched with the corresponding parameter of the Ca²⁺ transient.

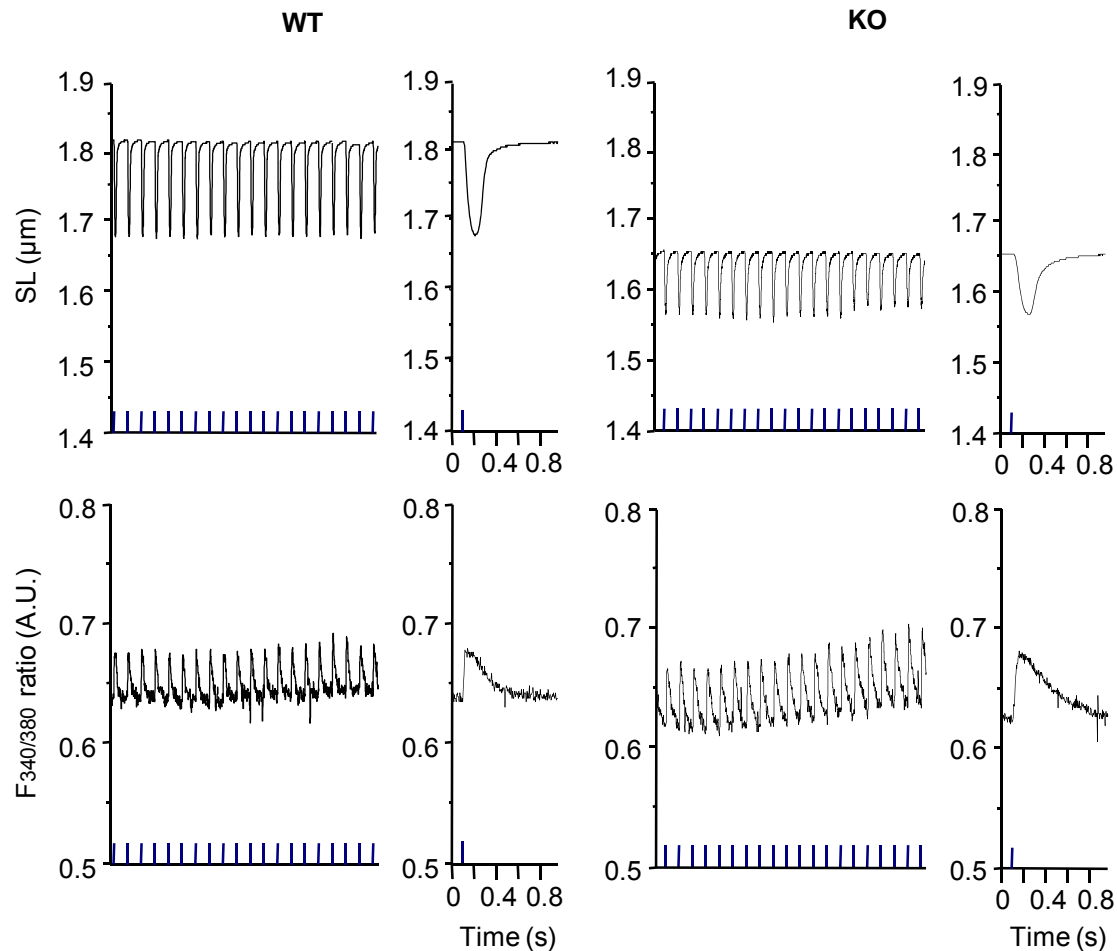


Figure 3.21 Representative recordings of sarcomere shortenings and Ca^{2+} transients in ventricular myocytes isolated from 6 week-old wild-type (WT) and homozygous *cMyBP-C* knock-out (KO) mice. Measurements were performed under 1 Hz/10 V-stimulation in 1.25 mM external Ca^{2+} .

Diastolic sarcomere length was shorter in KO than in WT, whereas the diastolic intracellular Ca^{2+} level was similar in both groups. Sarcomere shortening was similar between WT and KO and this was paralleled by similar Ca^{2+} peak amplitudes in WT and KO myocytes. In contrast, time to peak shortening in KO was 16% longer and this corresponded to a longer time to peak Ca^{2+} (+26%). Similarly, the time to 50% relengthening in KO was 39% longer than in WT and this corresponded to a longer time to 50% Ca^{2+} decay (+11%). During the further analysis of these data, the averaged transients from each of the 56 WT myocytes and 65 KO myocytes were superimposed to an averaged sarcomere length shortening curve and the corresponding Ca^{2+} transient curve (Figure 3.23). This figure visualizes nicely the findings presented above: A lower diastolic sarcomere length accompanied by a slower shortening and relengthening phase in the shortening trace of KO and a slower Ca^{2+} rise and decline in the Ca^{2+} transient of KO.

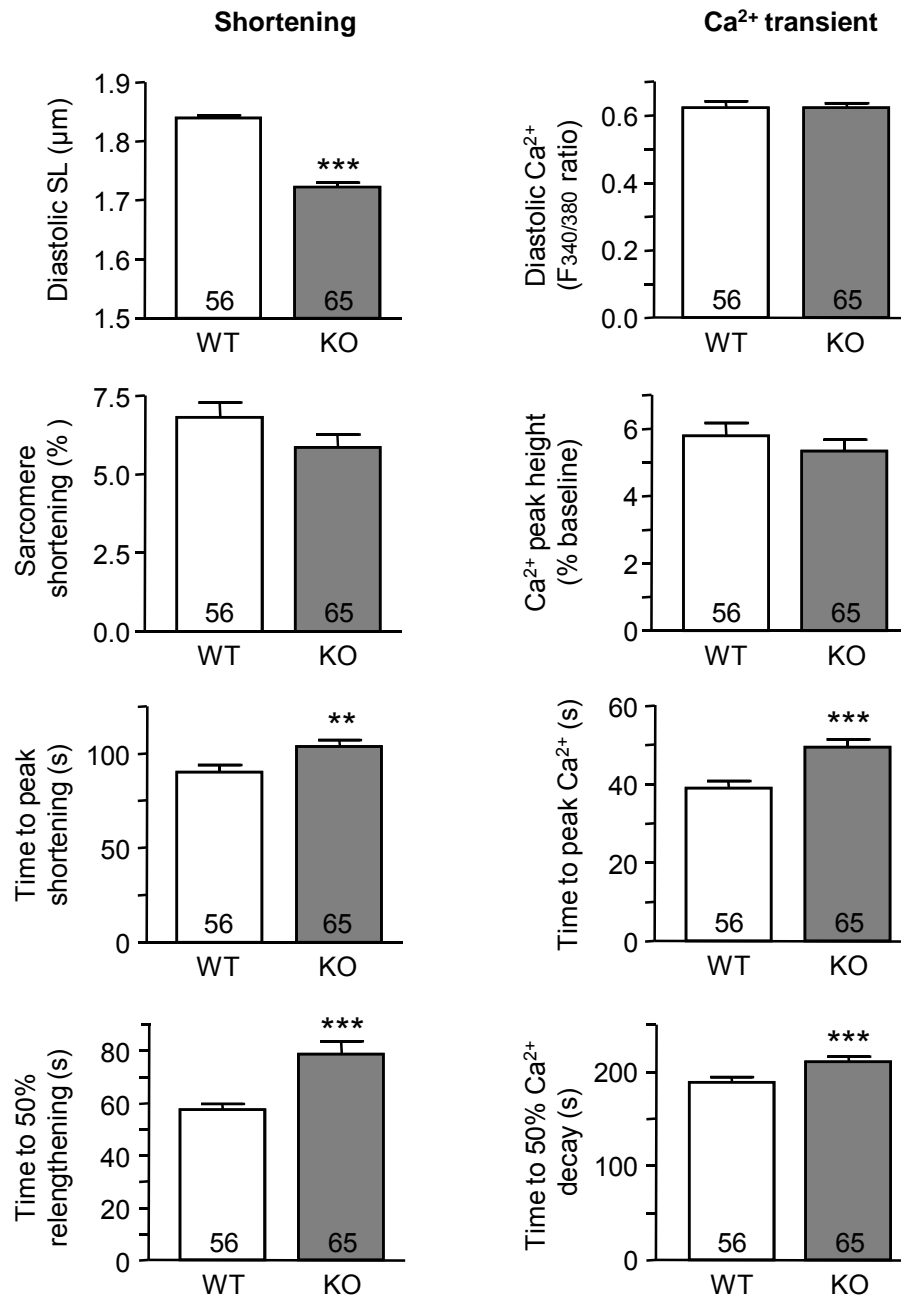


Figure 3.22 Summary of the simultaneous measurements of sarcomere shortening and Ca^{2+} transient in myocytes from 6 week-old wild-type (WT) and homozygous *cMyBP-C* knock-out (KO) mice. Measurements were performed under 1 Hz/10 V-stimulation in 1.25 mM external Ca^{2+} . The main parameters of both sarcomere shortening and Ca^{2+} transient are shown. Values are mean \pm SEM. ** $P < 0.01$, *** $P < 0.001$ vs. WT, Student's *t*-test. Number of myocytes is indicated in the bars.

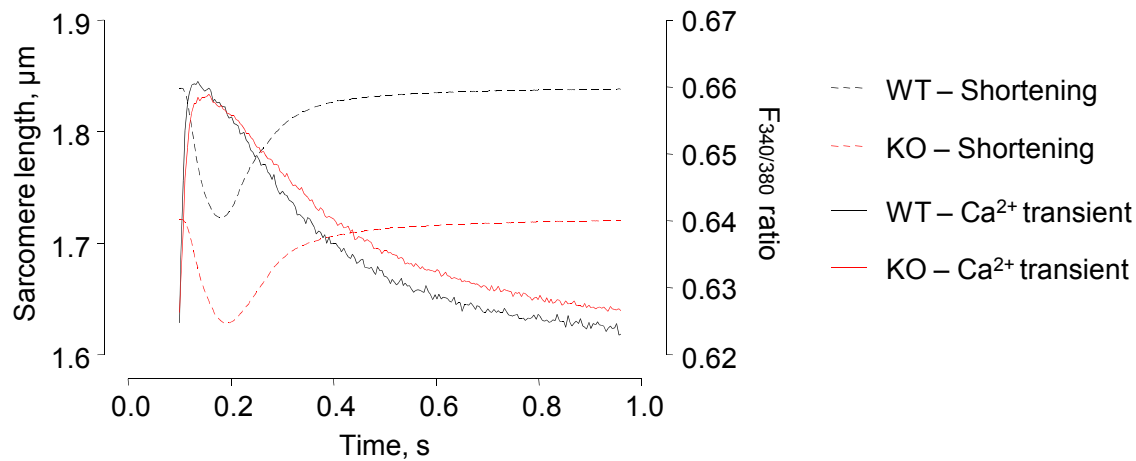


Figure 3.23 Simultaneous measurements of sarcomere length and Ca^{2+} transient in myocytes from 6 week-old wild-type (WT) and homozygous cMyBP-C knock-out (KO) mice. The graph shows the averaged sarcomere shortening and Ca^{2+} transient recordings from 56 WT and 65 KO myocytes under 1 Hz/10 V-stimulation in 1.25 mM external Ca^{2+} .

The averaged sarcomere shortening trace and Ca^{2+} transient were used to assess a phase-plane diagram of sarcomere length and F340/380 ratio for WT and KO myocytes (Figure 3.24). For each time point, the sarcomere length was plotted against the F340/380 ratio of the Ca^{2+} transient. This analysis revealed a counter-clockwise loop with the shortening proceeding upwards.

The loop for the KO myocytes showed three deviations from the WT loop: a shift to lower sarcomere length, a start of sarcomere shortening at a lower F340/380 ratio, meaning a lower intracellular Ca^{2+} concentration, and a smaller loop area. A closer analysis

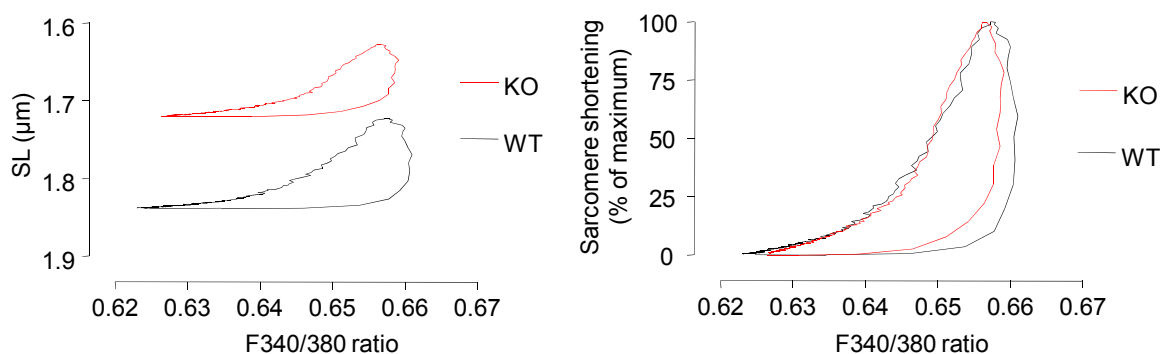


Figure 3.24 Phase plane diagram of sarcomere length (SL) and F340/380 ratio in myocytes from 6 week-old wild-type (WT) and homozygous cMyBP-C knock-out (KO) mice. The raw values (left panel) or the normalized values (right panel) of SL from the averaged SL recording (cf. Figure 3.20) were plotted against the F340/380 ratio from the averaged Ca^{2+} transient (cf. Figure 3.20) for each time point of the recording. Number of myocytes: N=56 (WT), N=65 (KO).

revealed that, at 5% and 10% of shortening peak height, the intracellular Ca^{2+} concentration was significantly lower in KO myocytes than in WT myocytes (Figure 3.25).

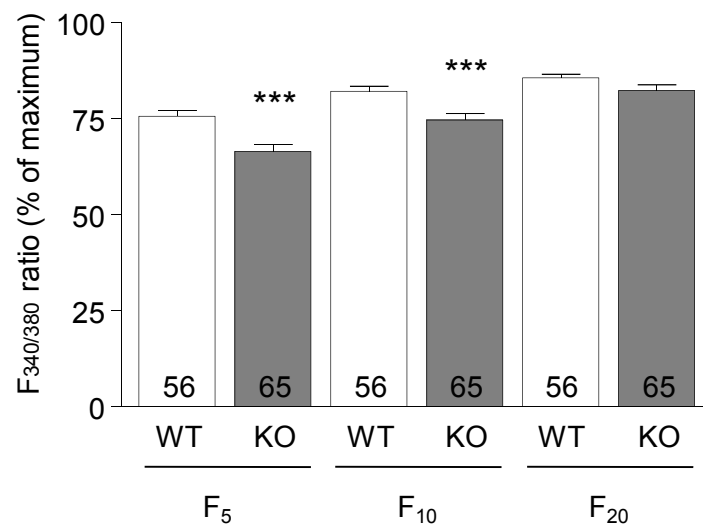


Figure 3.25 $F_{340/380}$ ratio giving 5% (F_5), 10% (F_{10}) and 20% (F_{20}) of shortening maximum in ratio in myocytes from 6 week-old wild-type (WT) and homozygous cMyBP-C knock-out (KO) mice. Values are mean \pm SEM *** $P < 0.001$ vs. WT, Student's t -test. Number of myocytes is indicated in the bars.

3.2.6 Isometric contractions of cMyBP-C KO left atria

The experiments of contractility so far were performed in freely suspended myocytes in unloaded conditions. To investigate whether changes also occur in conditions when the muscle contracts against a load, intact left atria from WT and KO mice were used. The muscles were electrically paced and challenged with different extracellular Ca^{2+} concentrations (Figure 3.26). When extracellular Ca^{2+} was removed by rinsing with Ca^{2+} -free Tyrode's solution (which gave a calculated Ca^{2+} concentration of 0.002 mM), active twitch force stopped almost immediately in WT left atria, but continued in KO at a reduced state for at least 5 min. Stepwise reintroduction of extracellular Ca^{2+} increased twitch force in both WT and KO, but revealed a significant increase in sensitivity towards external Ca^{2+} in KO (EC_{50} 1.21 \pm 0.17 mM in KO vs. 2.55 \pm 0.19 mM in WT, $P < 0.01$, two-way ANOVA). This indicates that under physiological external Ca^{2+} concentrations (~ 1.8 mM), the KO muscles contract already with more than their half-maximal force.

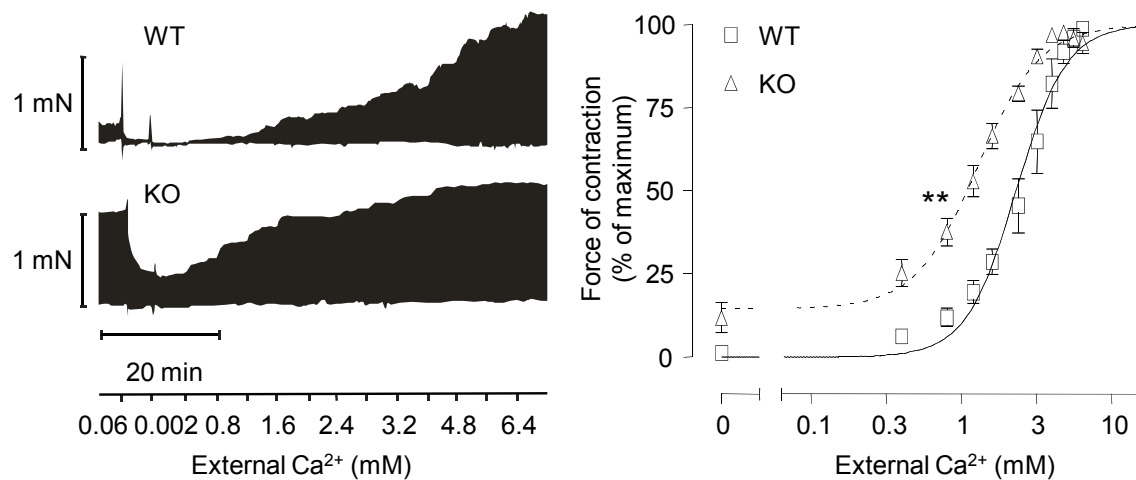


Figure 3.26 Response of isolated left atria to external Ca^{2+} . Representative recordings from wild-type (WT) and homozygous cMyBP-C knock-out (KO) atria performed at 37 °C under 1 Hz-stimulation (left panel). After equilibration of the muscles in 1.8 mM external Ca^{2+} at half-maximal tension, Ca^{2+} -free Tyrode's solution was applied (calculated Ca^{2+} concentration 0.002 mM). Ca^{2+} was then stepwise reintroduced up to a final concentration of 6.4 mM. Right panel: Relation of force and external Ca^{2+} from 4 WT and 4 KO left atria. Values are mean \pm SEM. ** $P < 0.001$, two-way ANOVA.

3.2.7 Summary

In order to evaluate the role of cMyBP-C in the sarcomere and assess its role during contraction, the KO model was investigated by performing contractility measurements in loaded and unloaded conditions. Isolated intact ventricular myocytes and intact left atria from KO and WT mice of different ages were used and the following results were obtained:

- Myocyte hypertrophy contributed to ventricular hypertrophy in KO mice.
- Diastolic sarcomere length in KO myocytes was lower than in WT and it was sensitive to BDM and blebbistatin, both inhibitors of cross-bridge cycling.
- Shortening and relengthening kinetics in KO myocytes were slower than in WT and worsened with age.
- KO hearts displayed a greater amount of β -MHC, inversely correlated with age, a greater amount of phosphorylated PLB in the old age, and a smaller amount of NCX.
- The relationship between sarcomere shortening and Fura-2 fluorescence in KO myocytes revealed signs of increased Ca^{2+} sensitivity.
- Isometrically contracting left atria from KO mice showed a higher Ca^{2+} sensitivity of force.

3.3 β -Adrenergic response in the cMyBP-C KO model

3.3.1 Response to β -adrenergic stimulation in Langendorff perfused hearts

Isolated hearts from WT and cMyBP-C KO mice were mounted on a Langendorff perfusion system and isometric force of contraction was measured before and after the addition of 1 μ M of the β -adrenergic receptor agonist isoprenaline (Figure 3.27). No change in the basal force was detected between WT and KO, and isoprenaline induced in both groups an increase in developed force. However, the force increased only by 70% in KO, whereas it increased in WT by 300%.

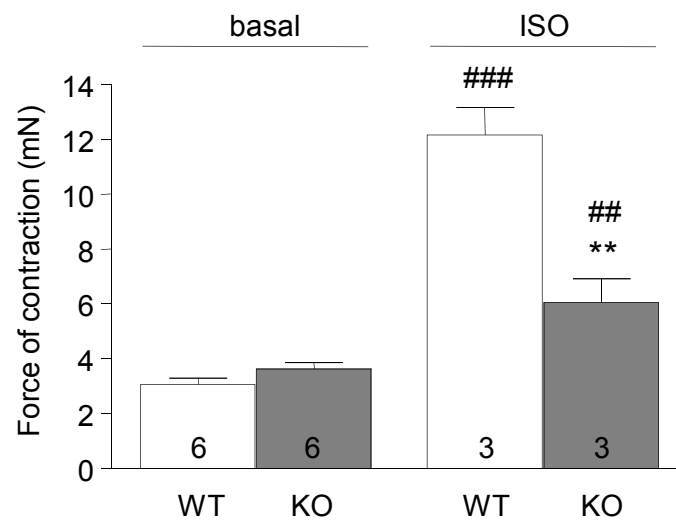


Figure 3.27 Isometric twitch tensions of isolated hearts perfused in the Langendorff mode from 6 week-old wild-type (WT) and homozygous cMyBP-C knock-out (KO) mice in the absence (basal) and presence of 1 μ M Isoprenaline (ISO). Values are mean \pm SEM. ** P <0.01 vs. WT; ## P <0.01, ### P <0.001 vs. basal, Student's t -test. The number of hearts is indicated in the bars.

3.3.2 Response to β -adrenergic stimulation in ventricular myocytes

In isolated ventricular myocytes from 6 week-old WT and KO mice sarcomere length shortening and intracellular Ca^{2+} transients were measured simultaneously in 1.25 mM external Ca^{2+} and with 10 V/1 Hz-field stimulation. From each myocyte, first, the basal contractility was measured before switching to a buffer containing the β -adrenergic receptor agonist isoprenaline in a concentration of 100 nM, which was expected to give the maximal effect. Typical examples from the measurements are shown in Figure 3.28.

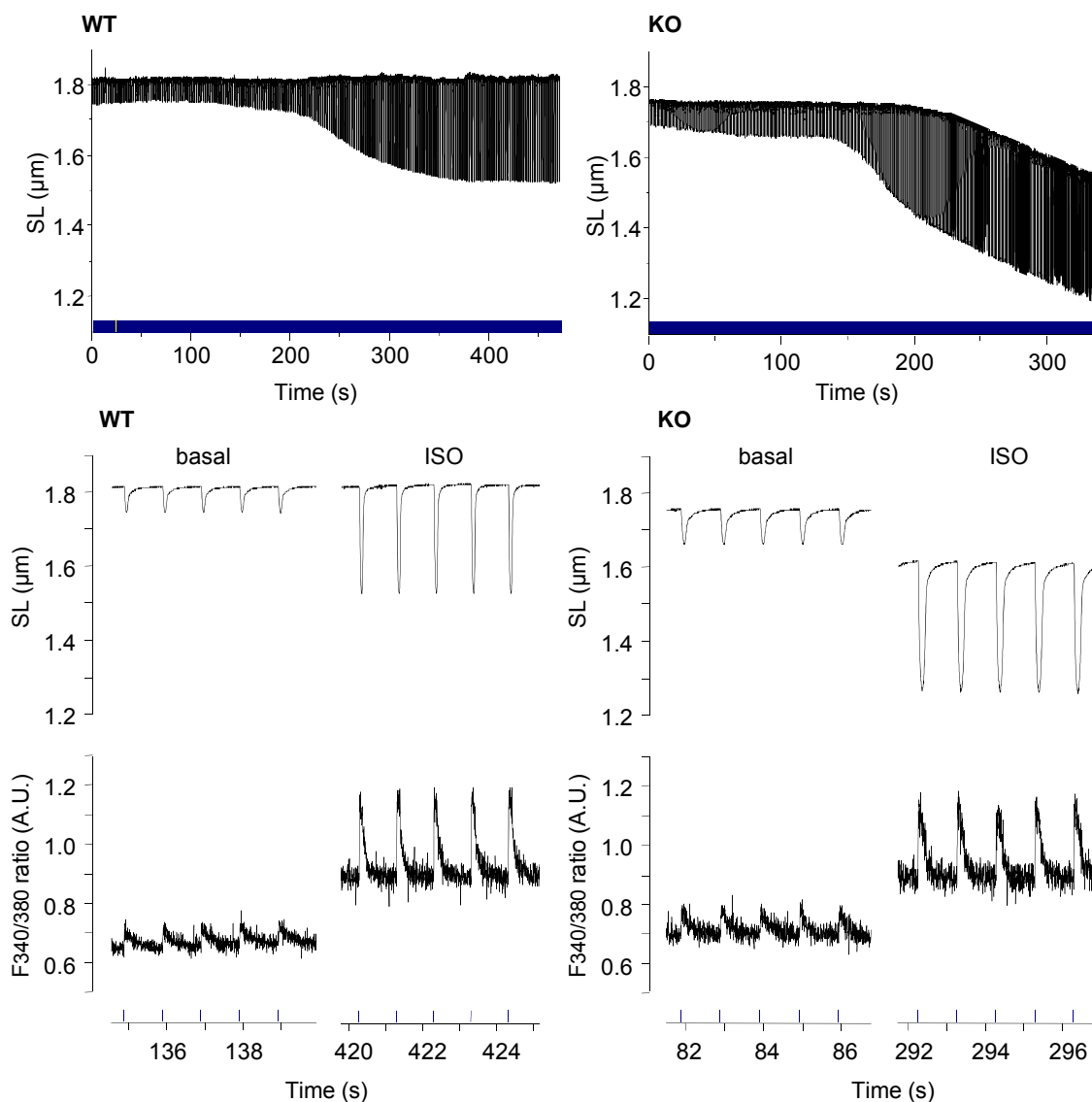


Figure 3.28 Effect of 100 nM isoprenaline (ISO) on sarcomere shortening and intracellular Ca^{2+} transient of isolated ventricular myocytes from 6 week-old wild-type (WT) and homozygous cMyBP-C knock-out (KO) mice. The upper panel represents the whole sarcomere length (SL) recording, the lower panel provides magnifications for SL and F340/380 ratio measurements to show the single twitches. Measurements were performed under 1 Hz/10 V-stimulation in 1.25 mM external Ca^{2+} .

About 2-3 minutes after the start of the perfusion with isoprenaline sarcomere shortening and intracellular Ca^{2+} transient amplitude increased gradually until they finally reached a plateau. In KO myocytes the increase in shortening amplitude was generally associated with a considerable decrease in diastolic sarcomere length, suggesting an incomplete relaxation. The summary of the analysis is presented in Figures 3.29 – 3.32.

Diastolic sarcomere length was lower in KO myocytes compared to WT at basal (Figure 3.29, left panel). Isoprenaline decreased sarcomere length in both WT and KO, yet the decrease in KO was more pronounced (-4% in KO vs. -1% in WT, $P < 0.001$, Student's *t*-test). The diastolic Ca^{2+} , which was similar in WT and KO under basal conditions, increased after the application of isoprenaline in WT and KO by 47% and 33%, respectively (Figure 3.29, right panel). Therefore, under isoprenaline stimulation, the diastolic Ca^{2+} concentration was 10% lower in KO compared to WT. When the diastolic Ca^{2+} concentration increases, diastolic sarcomere length can be expected to decrease, since more Ca^{2+} stays at the myofilaments during diastole. Interestingly, the decrease in diastolic sarcomere length after isoprenaline was greater in KO than in WT, whereas the increase in diastolic Ca^{2+} was lower.

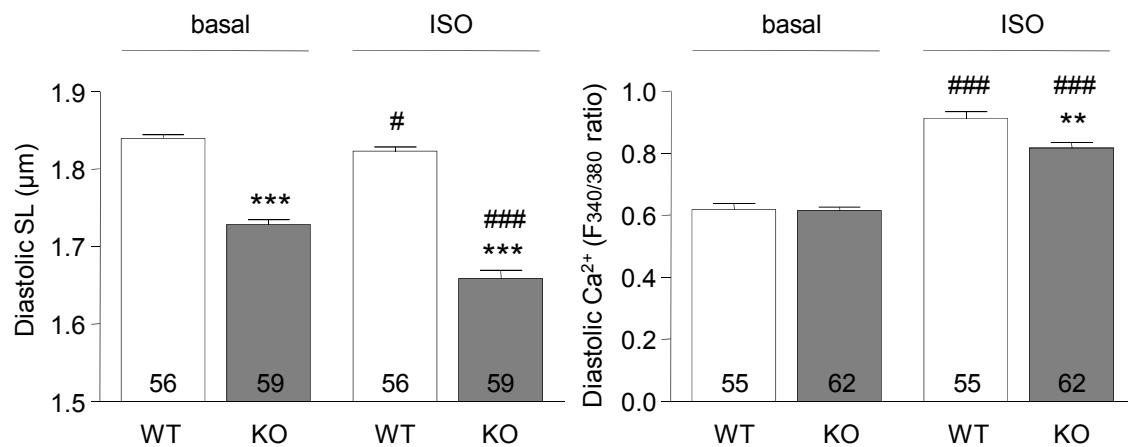


Figure 3.29 Effect of 100 nM isoprenaline (ISO) on the diastolic sarcomere length (SL) and diastolic intracellular Ca^{2+} concentration in 6 week-old wild-type (WT) and homozygous cMyBP-C knock-out (KO) myocytes. Measurements were performed under 1 Hz/10 V-stimulation in 1.25 mM external Ca^{2+} . Values are mean \pm SEM. ** $P < 0.01$, *** $P < 0.001$ vs. WT; # $P < 0.05$, ### $P < 0.001$ vs. basal, Student's *t*-test. The number of myocytes is indicated in the bars.

Fractional sarcomere length shortening and the amplitude of the intracellular Ca^{2+} transient did not differ between WT and KO under basal conditions, as was already shown before (Figure 3.22; Figure 3.30). With isoprenaline fractional sarcomere shortening increased in both WT and KO, but to a greater extent in the KO myocytes (+250% vs. +130% in WT). The amplitude of the Ca^{2+} transient, however, increased similarly in the two groups (+261% in WT vs. +266% in KO). Because the fractional sarcomere shortening increased to a greater extent in KO than in WT despite similar amplitudes of the Ca^{2+} peak, this hints at a greater Ca^{2+} sensitivity of the KO myocytes possibly brought about by isoprenaline.

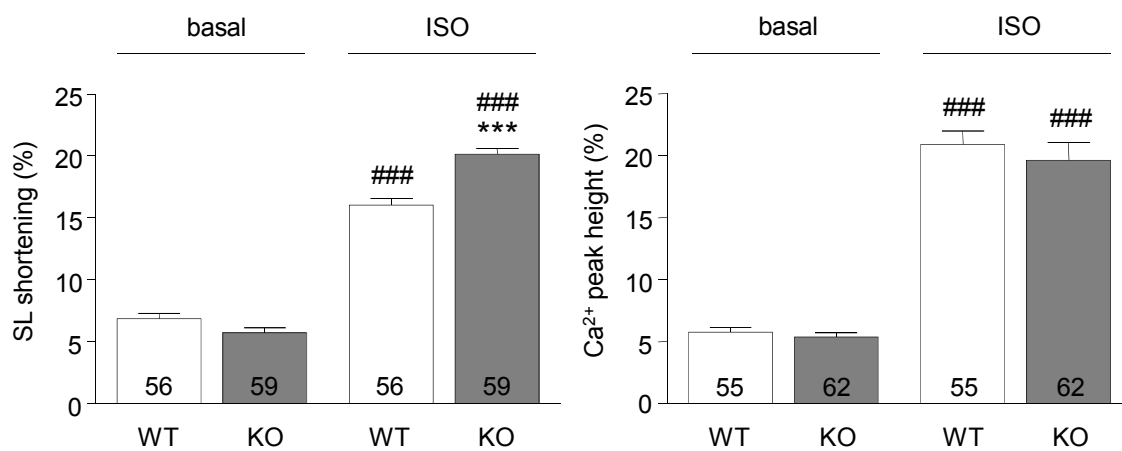


Figure 3.30 Effect of 100 nM isoprenaline (ISO) on the fractional sarcomere length (SL) shortening and Ca^{2+} peak amplitude in 6 week-old wild-type (WT) and homozygous cMyBP-C knock-out (KO) myocytes. Measurements were performed under 1 Hz/10 V-stimulation in 1.25 mM external Ca^{2+} . Values are mean \pm SEM. *** P <0.001 vs. WT, #### P <0.001 vs. basal, Student's t -test. The number of myocytes is indicated in the bars.

The kinetics of sarcomere shortening and relengthening as well as Ca^{2+} rise and Ca^{2+} decay are presented in Figure 3.31. Maximal velocity of shortening and maximal velocity of relengthening without isoprenaline were both slower in KO myocytes than in WT myocytes (-33% and -34%, respectively). Isoprenaline increased sarcomere shortening and relengthening velocities in WT by 200% and 270%, respectively, and in KO by 280% and 300%, respectively. In the presence of isoprenaline, the velocities of shortening and relengthening were still 12% and 29% lower in KO than in WT. The maximal velocities of Ca^{2+} rise and Ca^{2+} decay were similarly affected: Under basal conditions rate of Ca^{2+} rise was 31% lower in KO and there was a tendency towards a lower rate of Ca^{2+} decay. With isoprenaline, the rates of Ca^{2+} rise and decay increased by 420% and 770%, respectively, in WT and by 450% and 660%, respectively, in KO, with still 27% and 29% lower rates in KO than WT.

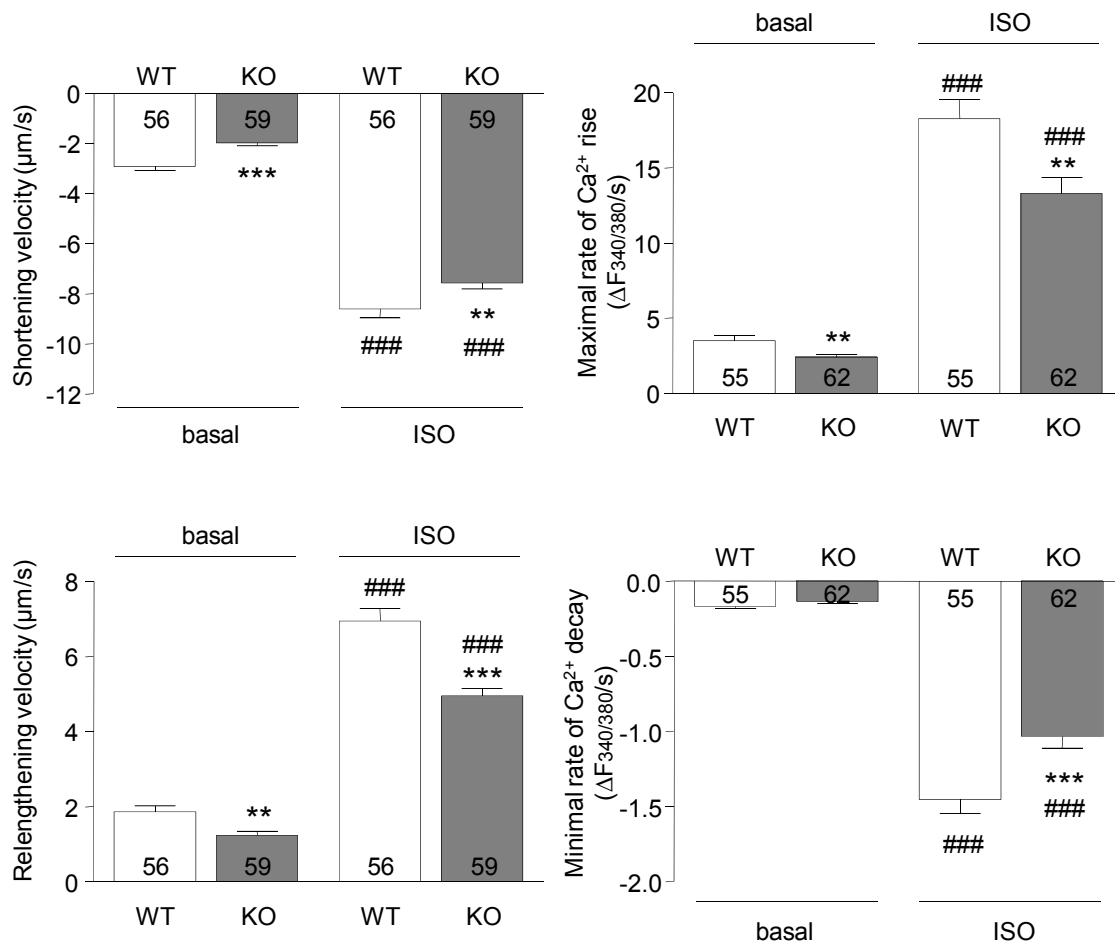


Figure 3.31 Effect of 100 nM isoprenaline (ISO) on the maximal velocities of both sarcomere shortening and relengthening and Ca²⁺ rise and Ca²⁺ decay in 6 week-old wild-type (WT) and homozygous cMyBP-C knock-out (KO) myocytes. Measurements were performed under 1 Hz/10 V-stimulation in 1.25 mM external Ca²⁺. Values are mean \pm SEM. ** $P < 0.01$, *** $P < 0.001$ vs. WT; ### $P < 0.001$ vs. basal, Student's *t*-test. The number of myocytes is indicated in the bars.

The analysis of the times to reach peak shortening and peak Ca²⁺ and 50% relengthening and 50% Ca²⁺ baseline, respectively, confirmed what was already seen in the velocities of these phases in the recordings. In all conditions KO myocytes were slower than WT, and isoprenaline application was not able to abolish this difference (Figure 3.32). In this context, it is important to note that the shortening amplitude in KO myocytes with isoprenaline was greater than in WT myocytes, which has to be taken into account when comparing differences in the WT and KO myocytes' times to peak shortening and to 50% relengthening.

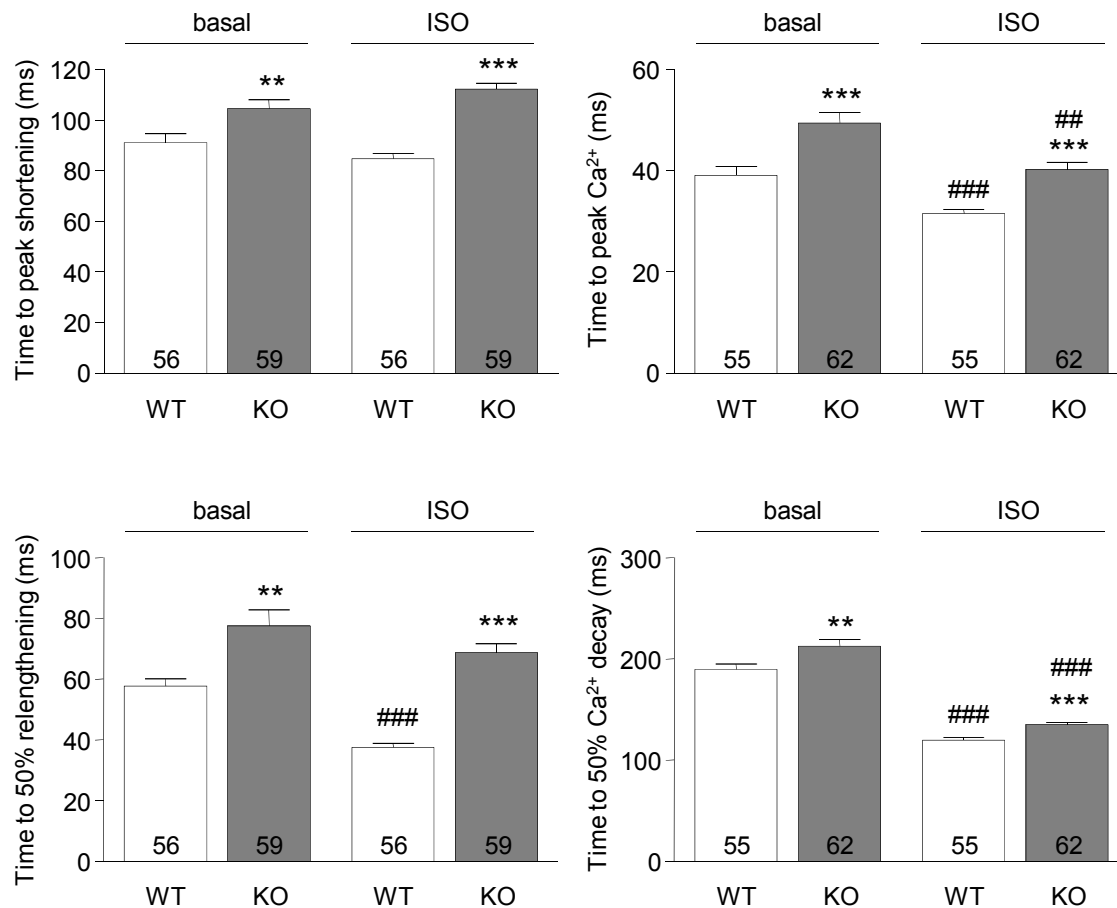


Figure 3.32 Effect of 100 nM isoprenaline (ISO) on the times to peak shortening and 50% relengthening and peak Ca^{2+} and 50% Ca^{2+} decay in 6 week-old wild-type (WT) and homozygous cMyBP-C knock-out (KO) myocytes. Measurements were performed under 1 Hz/10 V-stimulation in 1.25 mM external Ca^{2+} . Values are mean \pm SEM. ** P <0.01, *** P <0.001 vs. WT; ### P <0.01, #### P <0.001 vs. basal, Student's t -test. The number of myocytes is indicated in the bars.

3.3.4 Isometric tension atria

The effect of β -adrenergic stimulation was also assessed in isometric conditions using isolated left atria from WT and cMyBP-C KO mice. This experiment was performed by Dr. Michael Grimm. Importantly, in this experiment the atria were stretched to maximum tension, which was different than in 3.2.6, where Ca^{2+} sensitivity of force was acquired in muscles stretched to only half-maximal force. The muscles were electrically paced and the effect of increasing concentrations of the β -adrenergic agonist isoprenaline on twitch force was recorded. While performing this experiment it was observed that in the KO mice the left atria often were atrophied and showed signs of severe calcification. In the organ baths, these atria hardly developed any twitch force and did not respond to

isoprenaline stimulation (Figure 3.33). For the analysis only those left atria which responded to isoprenaline were taken into account.

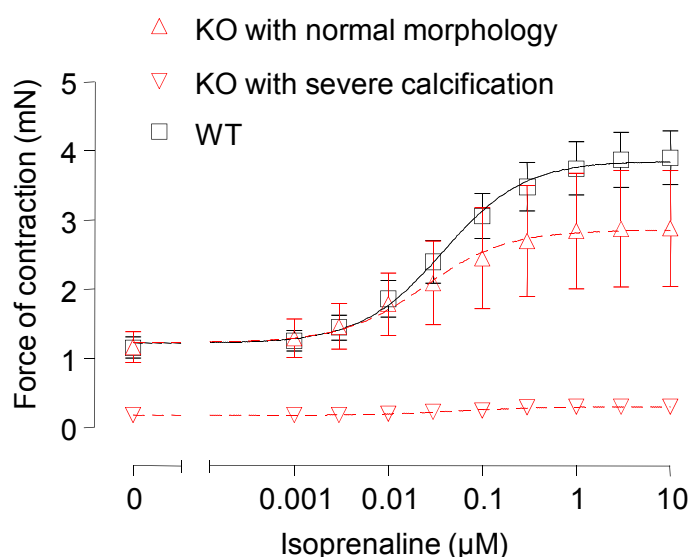


Figure 3.33 Effect of isoprenaline stimulation on the isometric force of contraction of isolated left atria from 6 week-old wild-type (WT) and cMyBP-C knock-out (KO) mice. The two different types of cMyBP-C knock-out (KO) left atria showed different contractile properties. The non-elastic and obviously calcified atria hardly developed any twitch force and did not respond to isoprenaline stimulation, whereas the atria with normal morphology and not more than very mild calcification responded adequately to isoprenaline. Muscle length was adjusted to maximal twitch force in 1.8 mM external Ca^{2+} and challenged with different concentrations of isoprenaline. Values are mean \pm SEM. $P < 0.001$, two-way ANOVA. Number of left atria: $N=5$ (KO with normal morphology), $N=4$ (KO with calcification), $N=8$ (WT). The experiment was performed by Michael Grimm (Hamburg).

Challenging left atria from WT and KO with isoprenaline gave a sigmoidal dose-response curve for both groups (Figure 3.34). EC_{50} values were not significantly different (0.042 μM for WT, 0.028 μM for KO, $P=0.9$), yet the maximal effect was lower in KO left atria (237% of basal force vs. 357% of basal force in WT, $P < 0.001$, comparison of curve fit).

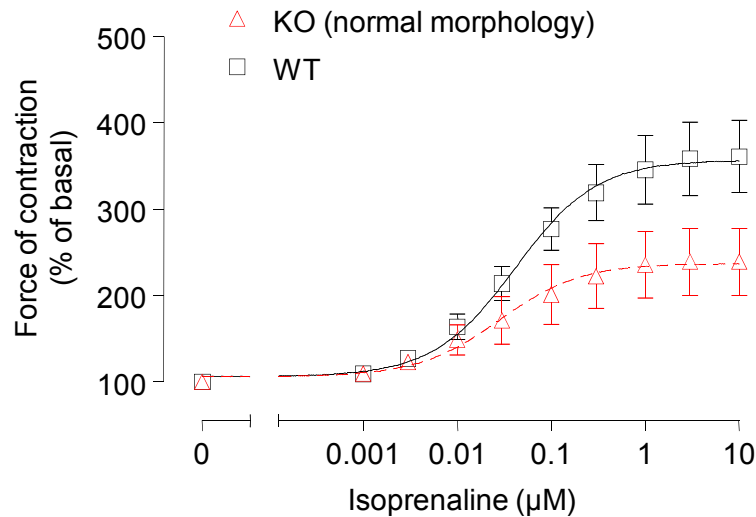


Figure 3.34 Effect of isoprenaline stimulation on the isometric force of contraction of isolated left atria from 6 week-old wild-type (WT) and cMyBP-C knock-out (KO) mice. Muscle length was adjusted to maximal twitch force in 1.8 mM external Ca^{2+} and the twitch forces obtained with different concentrations of isoprenaline were expressed as percentage of basal twitch force. Values are mean \pm SEM. $P < 0.001$, two-way ANOVA. Number of left atria: $N=8$ (WT), $N=5$ (KO). The experiment was performed by Michael Grimm (Hamburg).

3.3.3 β -Adrenergic receptor binding

Since in the presence of isoprenaline the KO myocytes displayed greater maximal shortening than WT, whereas left atria and Langendorff perfused KO hearts displayed less maximal force than WT, it seemed useful to determine the extent of binding to the β -adrenergic receptor. The content of β -adrenergic receptors in WT and KO hearts was evaluated via binding of the radioactively labeled β -adrenergic receptor ligand ^3H -CGP 12177. First, different concentrations of the ligand were used to assess the binding curves for WT and KO (Figure 3.35). The dissociation constants K_D were not different between WT and KO (0.07 ± 0.02 nM for WT vs. 0.08 ± 0.02 nM for KO, $P=0.58$), but the maximal binding B_{max} (expressed in counts per minute) was found to be significantly higher in KO (83.9 ± 4.1 vs. 56.2 ± 3.6 in WT, $P < 0.001$, comparison of curve fit).

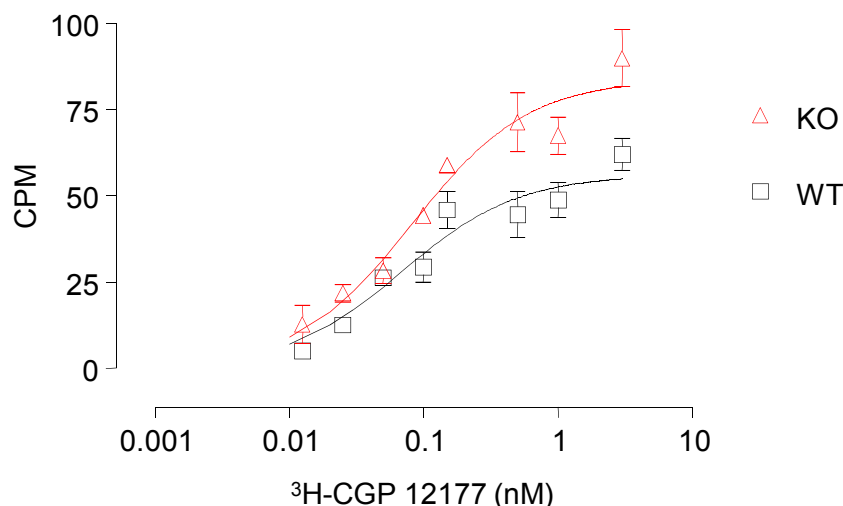


Figure 3.35 Quantification of the binding of the β -receptor ligand $^3\text{H-CGP 12177}$ in 6 week-old wild-type (WT) and cMyBP-C knock-out (KO) hearts. Saturation curves obtained from a pool of 4 WT and 4 KO hearts, respectively, with three replicates measured at each concentration of the ligand. Values are mean of the counts per minute (CPM) after ligand binding \pm SEM. Bmax was different for each curve, $P < 0.05$, comparison of curve fit.

Then, the maximal binding Bmax was assessed from eight WT and KO samples using 3 nM of the ligand, a concentration which has been proven to saturate the β -adrenergic receptors. This experiment confirmed the findings from the binding curves. β -Adrenergic receptor-binding was 33% higher in KO than in WT (Figure 3.36).

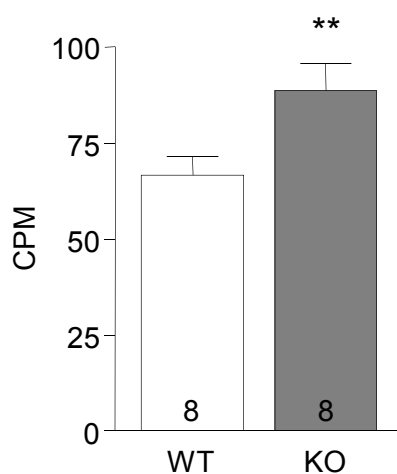


Figure 3.36 Receptor binding of the β -receptor ligand $^3\text{H-CGP 12177}$ in 6 week-old wild-type (WT) and cMyBP-C knock-out (KO) hearts. Counts per minute (CPM) obtained after saturation of the receptors with 3 nM of the ligand. Values are mean \pm SEM. $**P < 0.01$, Student's *t*-test. The number of samples is indicated in the bars.

3.3.5 L-type Ca^{2+} currents

Because the diastolic intracellular Ca^{2+} concentration after isoprenaline stimulation of intact myocytes was found to be different in KO compared to WT, the influx through the L-type Ca^{2+} channel or dihydropyridine receptor (DHPR) was investigated as one possible mechanism. This work was done in collaboration with Martin Kruse from the Institute for Neural Signal Transduction (Director: Prof. Dr. Olaf Pongs) in the Center for Molecular Neurobiology, Hamburg. Measurements on isolated WT and KO myocytes were performed using the whole cell patch clamp technique. A typical example of an L-type Ca^{2+} current obtained in the absence and presence of β -adrenergic stimulation is shown in Figure 3.37. The myocyte shown was clamped to a membrane potential of 0 V, which is the potential where maximal conductance could be expected. Since the L-type Ca^{2+} current is an inward current, the signal is proceeding downwards.

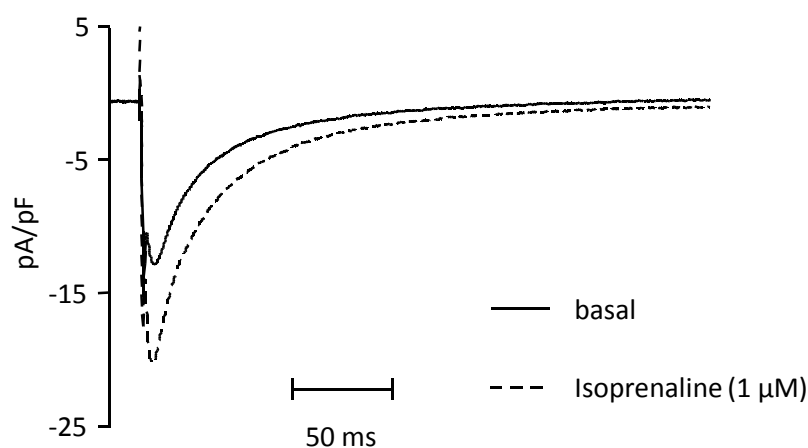


Figure 3.37 L-type Ca^{2+} current in an adult ventricular myocyte recorded with the whole cell patch clamp technique. The current was induced by clamping the myocyte to a membrane potential of 0 mV. The recorded current was normalized to cell capacitance. The baseline current and the current in the presence of 1 μM isoprenaline are shown.

The myocytes were clamped to a holding potential of -90 mV. From this pulses of 600 ms duration were applied in 10 mV-increments between -50 mV and +70 mV. Each pulse was preceded by a short pulse to -50 mV in order to inactivate the Na^{+} channels, the current of which would otherwise overlap with the Ca^{2+} current. The current-voltage relationship resulted in the expected bell-shape curve (Figure 3.38, left panel). Currents were recorded first under basal conditions and with stimulation of the myocytes with the β -adrenergic agonist isoprenaline. For the analysis of the β -adrenergic effect the currents obtained at 0 V were used (Figure 3.38, right panel). WT and KO myocytes showed no

difference in L-type Ca^{2+} currents both under basal conditions and after β -adrenergic stimulation.

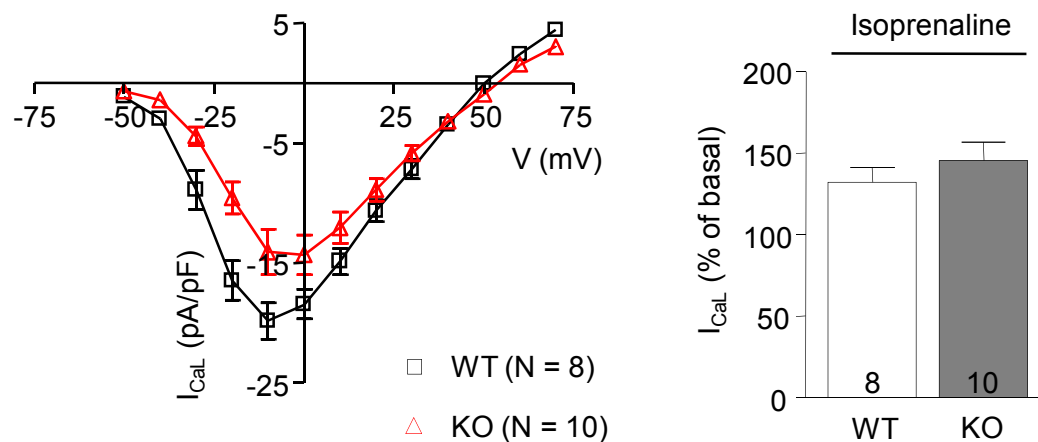


Figure 3.38 L-type Ca^{2+} current in ventricular myocytes from 6 week-old wild-type (WT) and cMyBP-C knock-out (KO) myocytes recorded with the whole-cell patch-clamp technique. Current voltage relationship measured at baseline (left panel) and effect of 1 μM isoprenaline (right panel). Values are mean \pm SEM. Number of myocytes is indicated in the bars. The experiments were performed by Martin Kruse (Institute for Neural Signal Transduction, Center for Molecular Neurobiology, Hamburg).

3.3.6 Summary

The role of cMyBP-C phosphorylation in the regulation of contraction was assessed using isoprenaline stimulation in the KO mouse model. The major results were as follow:

- Sarcomere shortening in ventricular myocytes from KO after β -adrenergic stimulation was greater than in WT, whereas the amplitude of the Ca^{2+} transient remained similar in KO and WT.
- Velocities of shortening and relengthening, and rates of Ca^{2+} rise and decline after β -adrenergic stimulation were slower in ventricular myocytes from KO compared to WT.
- Intact left atria and work performing hearts from KO mice under isometric conditions exhibited less maximal force after β -adrenergic stimulation than WT.
- The amount of β -adrenergic receptors was greater in KO than in WT hearts.
- L-type Ca^{2+} currents had similar amplitudes in WT and KO myocytes in both basal conditions and after β -adrenergic stimulation.

4 Discussion

The presence of cMyBP-C as a thick filament associated protein is known for over 30 years. Since its discovery many efforts have been undertaken to elucidate its role and precise function. A role for cMyBP-C during formation of the sarcomeres is well established. Yet, the question whether it also plays a role during the regulation of cardiac contraction is still subject of debate and remains controversial. Many studies therefore tried to assess the effects of ablation of cMyBP-C from the myocardium. This was achieved either by extracting cMyBP-C from isolated myofilaments or by using transgenic techniques to create knock-out mouse models (McConnell et al., 1999; Harris et al., 2002; Carrier et al., 2004). The results, however, varied among all these studies, e.g. Ca^{2+} sensitivity of force in the absence of cMyBP-C was either increased (Hofmann et al., 1991b; Witt et al., 2001; Palmer et al., 2004a; Cazorla et al., 2006), decreased (Harris et al., 2002) or unchanged (Palmer et al., 2004b). All experiments on the level of single cells assessing the dynamics of contraction, like Ca^{2+} sensitivity of force and velocity of tension development, have been exclusively performed in skinned myocytes or cardiac preparations, meaning only at the level of the myofilaments with the cytosolic components and an intact SR not present. Thus, this work presents the first attempt to use intact cardiac myocytes, in which all cellular mechanisms that influence contraction are preserved, to assess myocyte function on a cMyBP-C null background. The cMyBP-C knock-out mouse (KO) used in this work has been described before and displayed significant cardiac hypertrophy with dilation. As a first step, the new method of measuring sarcomere shortening and intracellular Ca^{2+} transients was evaluated and different parameters that influence contractility were tested (Results 3.1). Later, measurements to determine the role of cMyBP-C during contraction were performed in the absence (Results 3.2) and presence of cMyBP-C phosphorylation (Results 3.3). Additionally to the measurements in intact myocytes, which are freely suspended, measurements were performed under loaded conditions in intact left atria and work-performing hearts.

4.1 Evaluation of the IonOptix measurements

4.1.1 Effect of voltage

The voltage of the stimulation impulse had no influence on either shortening amplitude or the velocities of shortening and relengthening. Myocytes were not contracting until a voltage of 10 V, indicating that the minimum threshold value to initiate an action potential was lying slightly lower than this value. With higher values of voltage the fraction of myocytes that were beating did not increase, indicating that there were no differences in the excitability among the myocytes. The voltage necessary for excitation was quite high compared to the action potentials that occur *in vivo*. Such high values, however, were typically used for the field stimulation of single, isolated, and freely suspended myocytes.

4.1.2 Effect of stimulation frequency

In the living organism the variation of the beating frequency of the heart is one mechanism to adjust cardiac performance. A change in the frequency is directly correlated with a change in the developed force. In humans and most mammals the relationship between force and frequency is positive, meaning increasing frequencies induce greater force. This is attributed to the fact that with higher frequencies the duration of the repolarization phase becomes shorter so that less Ca^{2+} is extruded via NCX. This leads to an increase in SERCA activity and thus increases SR Ca^{2+} load. The higher SR Ca^{2+} load is then able to provide more Ca^{2+} during the Ca^{2+} -induced Ca^{2+} release and subsequently stronger contraction. In small rodents like mouse, however, the force-frequency relationship is often negative (Bers, 2000). This is attributed mainly to the relatively small contribution of NCX in the Ca^{2+} decline during repolarization (~7% compared to ~30% in human). But it is also important to note that mouse hearts normally display beating frequencies of ~600 beats per minute (~10 Hz). And actually, in such high frequencies the force-frequency relationship in mice was found to be positive as well (Tiemann et al., 2003).

In the present study the myocytes were not capable of maintaining such high frequencies as *in vivo*. Yet, it must be considered that recordings were obtained in 0.5 mM extracellular Ca^{2+} , which is lower than the physiological level of 1 – 2 mM, and at room temperature instead of 37°C. This expectedly slowed down kinetic processes in the cells. Thus, the fact that the myocytes could not maintain a high stimulation rhythm does not

necessarily argue for a bad quality of the isolated myocytes. On the contrary, the myocytes paced with high frequencies still beat regularly, only every second beat was of smaller amplitude or completely omitted. This might occur if the stimulus falls in the refractory phase of the action potential, when a *de novo* excitation is impossible.

The WT myocytes showed no effect of frequencies between 0.5 and 4 Hz on sarcomere shortening. Frequencies below 0.5 Hz have not been tested, which might have been necessary to see an effect in our conditions. But we consistently observed so-called post-rest potentiation in the myocytes, which means that after a resting period the first shortening after stimulation was always greater and shortening amplitude then declined until constant amplitudes were reached (Figure 4.1). This indicates that at extreme low stimulation frequencies shortening was probably greater and that a negative shortening-frequency relation was indeed present.

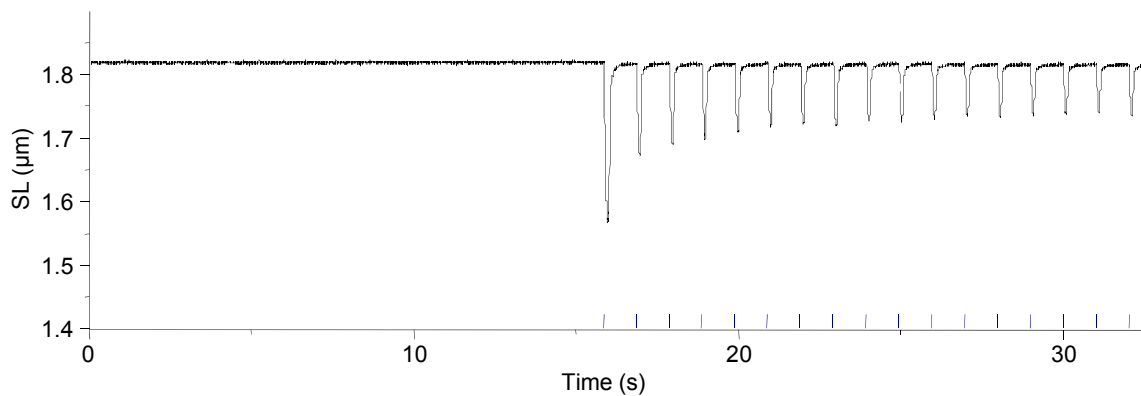


Figure 4.1 Post-rest potentiation in an intact ventricular myocyte from a 6 week-old wild-type mouse in 1.25 mM Ca^{2+} when stimulation with 10 V/1 Hz was started after a resting period of about 15 s duration.

Interestingly, in KO myocytes the relation between stimulation frequency and sarcomere shortening was positively correlated between 0.5 and 2 Hz. This argues for a greater Ca^{2+} loading of the SR, possibly due to greater SERCA activity. Since in KO NCX is lower expressed and PLB is stronger phosphorylated than in WT, it is to be expected that in KO a) SERCA participates more in removal of Ca^{2+} from the cytosol due to an increased SERCA/NCX ratio and b) SERCA is less inhibited by PLB due to higher PLB phosphorylation. Both mechanisms can account for the positive shortening-frequency relationship.

Recently, our group developed a new knock-in mouse model of cMyBP-C (KI) which carries a point mutation (G>A transition in the last nucleotide of exon 6) in the *MYBPC3*

gene. In the homozygous state these mice express only a low amount of mutant protein and they develop, similar to our KO mice, severe hypertrophy with dilation. In this model the frequency-dependence of shortening in isolated myocytes was also analyzed with stimulation frequencies from 0.25 – 3 Hz (publication in preparation). While the WT myocytes displayed the expected negative relationship, KI myocytes did not show any alterations between 0.25 and 3 Hz. Additionally, the amount of NCX, as determined by Western blot analysis, was reduced in KI, whereas no alterations in the phosphorylation of PLB were detected. SERCA activity is therefore less enhanced in KI than in KO, but this enhancement is not enough to reverse the negative shortening-frequency relationship to a positive one as it is apparently the case in the KO.

4.1.3 Effect of extracellular Ca^{2+} and the influence of Fura-2 buffering

Ca^{2+} plays a central role in excitation-contraction coupling. Therefore it is evident that the extracellular Ca^{2+} concentration has great influence on the contractile performance of the isolated cardiac myocytes. In order to determine optimal conditions for the measurements in the KO model, the influence of varying extracellular Ca^{2+} concentrations on sarcomere shortening and relengthening was examined. Elevation of the external Ca^{2+} concentration up to 4 mM was tolerated by WT, HET, and KO myocytes, and significant increases in sarcomere shortening could be measured. The initial experiments (effect of voltage and frequency), when the myocytes were not pre-incubated with Fura-2, were performed in 0.5 mM external Ca^{2+} . This concentration, however, turned out to be too low when the myocytes were loaded with Fura-2 to acquire intracellular Ca^{2+} transients. Myocytes loaded with Fura-2 hardly contracted in 0.5 mM external Ca^{2+} .

Fura-2 belongs to the fluorescent, Ca^{2+} -sensitive dyes which were developed during the 1980s. It provides a powerful tool for monitoring intracellular Ca^{2+} transients (Grynkiewicz et al., 1985). Inside myocytes Fura-2 selectively binds Ca^{2+} and the association and dissociation of the Ca^{2+} -Fura-2 complex is quick enough to monitor the Ca^{2+} transient in beating myocytes. A further advantage of Fura-2 is that it is a ratiometric indicator and can be used without calibration. However, Fura-2 is a Ca^{2+} chelator and complexes part of the Ca^{2+} ions originally released for contraction and thus influences the contractile parameters. Indeed, measurements of shortening in the presence and absence of Fura-2 in different extracellular Ca^{2+} concentrations confirmed that in myocytes loaded with Fura-2 shortening amplitude was lower in each concentration of extracellular Ca^{2+} .

compared to myocytes not loaded with Fura-2. This indicates that in the conditions used Fura-2 is able to buffer part of the intracellular Ca^{2+} . This may be important especially in low concentrations of extracellular Ca^{2+} , where the effect on the shortening amplitudes was relatively strong. Here the buffering capacity of Fura-2 could mask possible differences.

4.2 The role of cMyBP-C in cardiac contractility

To assess the functional role of cMyBP-C, alterations in the contractility of a KO model were determined. The KO model used in this work exhibits already at a young age severe cardiac hypertrophy and dilation. The hypertrophy phenotype was confirmed in this work by comparison of the ventricular weight to body weight ratios of KO and WT mice. Furthermore, this study could also show hypertrophy in isolated ventricular myocytes. In general, functional impairment causes the development of hypertrophy and/or dilation, giving rise to the assumption that cMyBP-C plays an important role during contraction. However, it still remains possible that the absence of cMyBP-C causes the formation of unstable sarcomeres. Although sarcomere structure was unaltered in the KO, subtle changes in the ultrastructure of the sarcomeres may be possible as it has been reported for the two other KO models (McConnell et al., 1999; Harris et al., 2002).

4.2.1 Reduced diastolic sarcomere length in KO

The most striking finding in the sarcomere length measurements of the KO was the lower diastolic sarcomere length compared to WT. KO myocytes seemed to be pre-contracted even in diastole, and the fact that this effect was sensitive to two inhibitors of cross-bridge cycling (BDM and blebbistatin) argues for the involvement of force developing cross-bridges. A similar mechanism was proposed recently for the impact of a cardiac Troponin I (cTn-I) mutation leading to restrictive cardiomyopathy (Davis et al., 2007). cTn-I, is the so-called inhibitory unit of troponin that prevents myosin-actin interaction in diastole. The fact that with a mutated cTn-I similar observations with regard to sarcomere length were made than with the KO of cMyBP-C in this study support the view that cMyBP-C in the thick filament plays a similar role than cTn-I in the thin filament. Both seem to inhibit actin-myosin interaction, cTn-I by blocking the binding site for myosin heads, cMyBP-C by tethering the myosin heads close to the thick filament backbone.

Therefore both proteins can be regarded as sarcomeric regulators of cardiac contractility. This is in line with evidence from studies which also conclude that cMyBP-C acts as an internal load during contraction which impedes myosin-actin interaction (Hofmann et al., 1991a; Korte et al., 2003; Stelzer et al., 2006a; Stelzer et al., 2006b). Removal of cMyBP C, as in our KO, would facilitate myosin-actin interaction and therefore promote active cross-bridge cycling even in diastole.

Alternatively, the lower diastolic sarcomere length could be the result of a weak restoring force due to changed properties of titin. This, however, can be ruled out, since Cazorla et al. (2006) showed in the same KO model no alterations in passive force, implicating unchanged titin properties in KO. Yet, titin properties can account for other observations with regard to sarcomere length. Resting sarcomere length also decreased with age equally in both groups, WT and KO. Aging of myocytes is accompanied by loss of elasticity and this has been shown to be associated with the replacement of the compliant isoform of titin, N2BA, by the stiff N2B (Warren et al., 2004; Kruger et al., 2006). This could well explain the reduction of diastolic sarcomere length in older WT and KO. Furthermore, the KO group exhibited a greater variability of diastolic sarcomere length and a negative correlation between diastolic sarcomere length and fractional sarcomere shortening, meaning myocytes with the lowest diastolic sarcomere length exhibited the greatest amplitude of shortening. Resting or slack sarcomere length in a myocyte is determined by the equilibrium between passive force (which pulls the Z-discs towards each other when the sarcomeres are stretched, Figure 4.2 C-D) and restoring force (which pushes the Z-discs away from each other when sarcomeres shorten, Figure 4.2 A). The restoring force, against which myocytes contract, is mainly determined by the elastic recoil properties of titin and, in intact tissues, also by extracellular collagen (Helmes et al., 1996; Granzier et al., 1996). In KO, the balance is shifted to lower sarcomere lengths by active, force developing cross-bridges. Myocytes with the weakest elastic recoil properties, show lowest diastolic sarcomere length and consequently also greatest absolute and fractional shortening. The variability of elastic recoil properties in isolated cardiac myocytes may explain the great variability in diastolic sarcomere length.

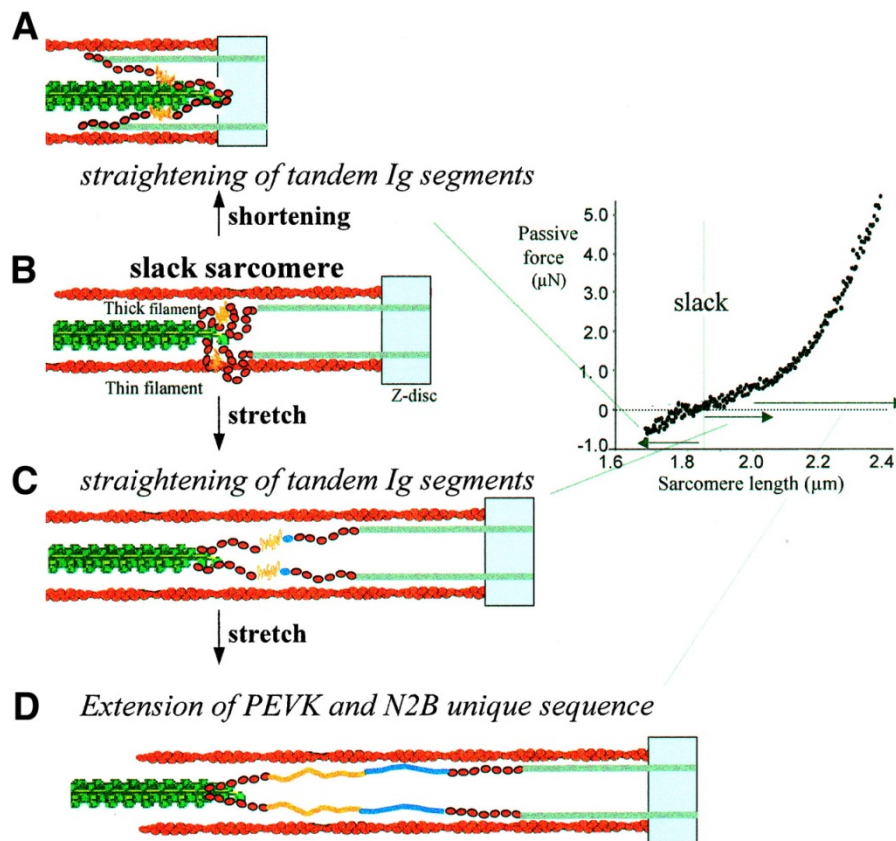


Figure 4.2 Mechanism of passive and restoring force generation. Titin's extensible region is in a shortened state in slack sarcomeres (B) and extends on sarcomere stretch (C and D) giving rise to passive force. When sarcomeres shorten to below slack length (A), the thick filament moves into titin's incompressible region and the extensible region now extends in a direction opposite to that during stretch, developing restoring force (From Granzier and Labeit, 2004).

4.2.2 Altered Ca^{2+} sensitivity in KO

Residual cross-bridge cycling during diastole in the absence of cMyBP-C could be mediated via a Ca^{2+} -independent mechanism, as proposed for the cTn-I mutation associated with restrictive cardiomyopathy (Davis et al., 2007), or could be the result of increased Ca^{2+} sensitivity of the myofilaments. Increased Ca^{2+} sensitivity has been frequently observed in experimental ablation of cMyBP-C (Hofmann et al., 1991b; Palmer et al., 2004a; Cazorla et al., 2006), and several observations in the present study favor this concept. First, the phase-plane diagrams of isolated myocytes, showing the relation of shortening amplitude versus Fura-2 fluorescence, revealed that KO myocytes started to shorten at a lower level of intracellular Ca^{2+} . Second, loaded left atria from KO still developed force in nominally 0.002 mM external Ca^{2+} , when WT atria did not. Furthermore, in the same experiment, the EC_{50} for external Ca^{2+} to activate force was

significantly lower in KO compared to WT. A decreased sarcomere length in myocytes has been observed as a result of pharmacological Ca^{2+} sensitizers and induced alkalosis, which is also known to sensitize myofilaments towards Ca^{2+} (Wolska et al., 1996; Spurgeon et al., 1992). Although increased Ca^{2+} sensitivity of force was frequently observed in experimental ablation of cMyBP-C (Hofmann et al., 1991b; Palmer et al., 2004a; Cazorla et al., 2006), also opposite or no effects have been described (Harris et al., 2002; Palmer et al., 2004b). These discrepancies are likely explained by the different experimental models (different KO mouse models of cMyBP-C, extraction of cMyBP-C from myofilaments) and experimental procedures (e.g. the imposed stretch sarcomere length of skinned fibers). Yet, the results of this present study are in agreement with two recent studies: Cazorla et al. (2006) found increased Ca^{2+} sensitivity at 1.9 μm stretch sarcomere length in our KO model, and (Stelzer et al., 2006b) found, in another cMyBP-C KO model, increased Ca^{2+} sensitivity at low concentrations of activating Ca^{2+} . However, the often observed increase in maximal shortening (or force, respectively) in classical Ca^{2+} sensitization was not seen in the experiments of this present work. This suggests that ablation of cMyBP-C affects Ca^{2+} sensitivity predominantly at low Ca^{2+} levels. Consistent with this interpretation is the finding that in KO myocytes sarcomere shortening was greater only in 0.5 mM extracellular Ca^{2+} . In contrast, the KI model recently created by our group, which is the only other cMyBP-C model characterized in an intact myocytes context so far, displays this increased sarcomere shortening also in higher Ca^{2+} concentrations. This model, which expresses only a low amount of mutant cMyBP-C and which develops a similar phenotype than the KO model, also showed a decreased diastolic sarcomere length, reversible by application of BDM, thus implicating similar mechanisms in the two models (a manuscript on the contractile properties of KI myocytes is currently in preparation).

These findings implicate a role for cMyBP-C to act as an internal load that tethers the myosin heads to the thick filament backbone and thus prevents force generation in diastole. cMyBP-C would therefore be necessary to allow full relaxation of the sarcomeres during diastole. Confirmation for this model was presented in a recent study with a different KO mouse model describing radial displacement of cross-bridges away from the thick filament in the absence of Ca^{2+} (Colson et al., 2007). The absence of cMyBP-C in the KO could therefore lead to cross-bridge cycling in the absence of stimulation due to increased Ca^{2+} sensitivity of the myofilaments and prevent complete relaxation.

4.2.3 Compensatory changes in KO

Significant alterations concerning the duration of the shortening and relengthening phase were observed in KO myocytes. Both phases were slower in KO myocytes compared to WT and the prolongation was greater in the 30 week-old myocytes compared to 6 week-old myocytes. In the 6 week-old myocytes the prolonged phases of shortening and relengthening were paralleled by prolongations in the durations of intracellular Ca^{2+} release and Ca^{2+} decline. These alterations could be directly related to the depletion in cMyBP-C, yet it cannot be excluded that compensatory changes influenced these results. Indeed, many observations suggest the concept that compensatory changes are at least partly involved: The KO mice exhibited cardiac hypertrophy already in the young age and a previous study reported upregulation of fetal genes like α -skeletal actin, brain natriuretic peptide and β -MHC (Carrier et al., 2004). Furthermore, the present study showed increased protein levels of β -MHC and phosphorylated phospholamban (PLB) and decreased protein amount of the sodium-calcium-exchanger (NCX).

β -MHC provides a slower ATPase activity and is more energy-saving than the α -isoform and its presence in the KO hearts might compensate for the high energy expenditure due to increased actin-myosin interaction. Likely the upregulation of β -MHC contributes to the slower sarcomere shortening (Fitzsimons et al., 1998; Herron et al., 2001; Stelzer et al., 2007a). However, while the deficit in shortening worsened with age the fraction of β -MHC decreased more than two-fold. So it can be concluded that the switch in the MHC-isoform expression is not the major reason for the impaired myocyte function. Since in the older hearts β -MHC even seems to decrease again, it can be assumed that the initial switch to the β -isoform, which is energetically more beneficial is later counteracted by re-expression of the α -isoform with the faster kinetics.

An increased ratio of PLB/SERCA would lead to slower Ca^{2+} reuptake and could have accounted for slower relaxation. However, the slower relengthening phase of KO myocytes cannot be explained with compensatory protein expression since the total amounts of SERCA and PLB were similar in KO and WT. In contrast, PLB was hyperphosphorylated in KO compared to WT, which would release inhibition of SERCA and hasten Ca^{2+} reuptake into the SR, implicating that this is a compensatory mechanism in KO which tries to hasten impaired relaxation.

The downregulation of NCX implicates a defect in the KO myocytes to extrude Ca^{2+} . This could explain why after removal of extracellular Ca^{2+} KO myocytes needed a longer time to arrest beating and intact left atria in extremely low extracellular Ca^{2+} still develop twitch force. The lower amount of NCX might also participate in the prolonged relengthening.

Taken together, it is difficult to evaluate to what extent the absence of cMyBP-C in KO affects velocities of shortening and relengthening. However, the significantly lower slopes in KO of the correlations between systolic sarcomere length and shortening or relengthening velocity provides a hint that the lack of cMyBP-C might influence the kinetics of contraction and relaxation, maybe via changes in the sarcomeric ultrastructure.

4.2.4 Contractile behavior in HET myocytes

The HET mice, in contrast to KO, develop a quite mild phenotype at 10 – 11 months of age (Carrier et al., 2004). At the age of 30 weeks, when hypertrophy is not yet present, myocytes from HET displayed already slower times of shortening and relengthening than WT myocytes. This shows that contractile dysfunction in HET myocytes precedes hypertrophy, suggesting that at this time point the amount of cMyBP-C might be already decreased and this partial depletion could cause the dysfunction.

Recently, 9 week-old KO and HET hearts were submitted to a microarray analysis yielding at discovering changes in gene expression (Eijssen et al., 2008). A large spectrum of differently expressed genes was discovered, most of which involved in energy conversion, protein turnover, apoptosis and proliferation. Whereas these changes could be expected for KO, they are quite surprising for the HET at this young age. The results emphasize that adaptations can occur very early, in the case of the HET already at a time when the single allele of the *MYBPC3* gene still seems capable of supplying enough new protein.

Myocyte function in HET was also determined in 60 week-old myocytes when hypertrophy in the HET was previously found (Carrier et al., 2004). Surprisingly, no differences to WT myocytes were detected at this age in Hamburg. Comparison with the 30-week old myocytes revealed that in both groups contractile performance worsened with age. This phenomenon, which may be explained by altered titin properties as

discussed above, might in this case obscure possible differences. A surprising observation, which may also be responsible for the lack of difference between 60 week-old WT and HET, were similar ventricular weight to body weight ratios in 60 week-old WT and HET mice. Since previous data were obtained in Paris and the shortening measurements in Hamburg, different housing conditions should be taken into account. Especially differences in the diet of the mice could have an immense impact, e.g. via the phytoestrogens occurring in soy. A recent study reported significant differences in disease status and cardiac function in a transgenic mouse model of hypertrophic cardiomyopathy by switching from a soy-based diet to a casein-based diet (Stauffer et al., 2006). Further analyses are needed to solve this problem.

4.3 The role of cMyBP-C phosphorylation: β -Adrenergic response in the KO

The contractile properties of the KO mouse model were also assessed under β -adrenergic stimulation. This should help to evaluate the role of cMyBP-C phosphorylation in the regulation of contraction. For stimulation the β -adrenergic receptor-agonist isoprenaline was used and the concentrations that were applied (100 nM – 1 μ M) were sufficient to achieve complete cMyBP-C phosphorylation (El-Armouche et al., 2006).

In KO myocytes the increase in fractional shortening amplitude induced by isoprenaline stimulation was more pronounced than in WT leading to greater fractional shortening in KO. Interestingly, in the isometric conditions (left atria and Langendorff perfused hearts) isoprenaline had a less strong effect on developed force in KO than in WT. One explanation could be the different experimental conditions. Isolated myocytes are freely suspended in their environmental solution with the entire extracellular matrix removed; they are not attached and stretched, meaning they are unloaded and contract isototically. Consequently, the parameter measured cannot be force but sarcomere length. In contrast, Langendorff-perfused hearts and isolated left atria are complete tissues that are stretched to a fixed length and the parameter measured is the developed force. The stretching of the muscles serves the purpose to exert the Frank-Starling mechanism to obtain maximal basal force. The Frank-Starling mechanism is normally attributed to the fact that by stretching the Ca^{2+} sensitivity of the myofilaments increases (Bers, 2008). Now, as was already mentioned before, the KO left atria in isometric conditions were sensitized to Ca^{2+} and were contracting already at more than half-maximal force in the Ca^{2+} concentration used (1.8 mM). This could explain why after isoprenaline stimulation the KO left atria and Langendorff perfused hearts were not

capable to increase force to such an extent as WT. However, in the KO myocytes an increased Ca^{2+} sensitivity was only detectable at a low level of activation (i.e. in low extracellular Ca^{2+}) or in the SL- $[\text{Ca}^{2+}]_i$ relationship (phase-plane diagram of shortening transient vs. intracellular Ca^{2+} transient), and it can be assumed that the differences in the experimental conditions are at least partly responsible for this. So, although the measurements in isolated myocytes do not well reproduce the *in vivo* conditions, they are able to reveal properties of the myocytes which could be obscured by the experimental conditions in loaded preparations.

Interestingly, the KI model, which carries a low amount of mutant cMyBP-C, also exhibited greater fractional sarcomere shortening after isoprenaline stimulation. However, since sarcomere shortening in KI was also greater than in WT under basal conditions, the relative increase was only 50% in KI compared to 120% in WT. This matched with the less strong effect of isoprenaline seen in isometrically contracting left atria or Langendorff perfused hearts from KI (Figure 4.3). Since our KI only contains ~10% of mutant cMyBP-C, it can be regarded as a partial knock-out of cMyBP-C, which can explain the similarities to the KO. For the occurring differences, however, it has to be

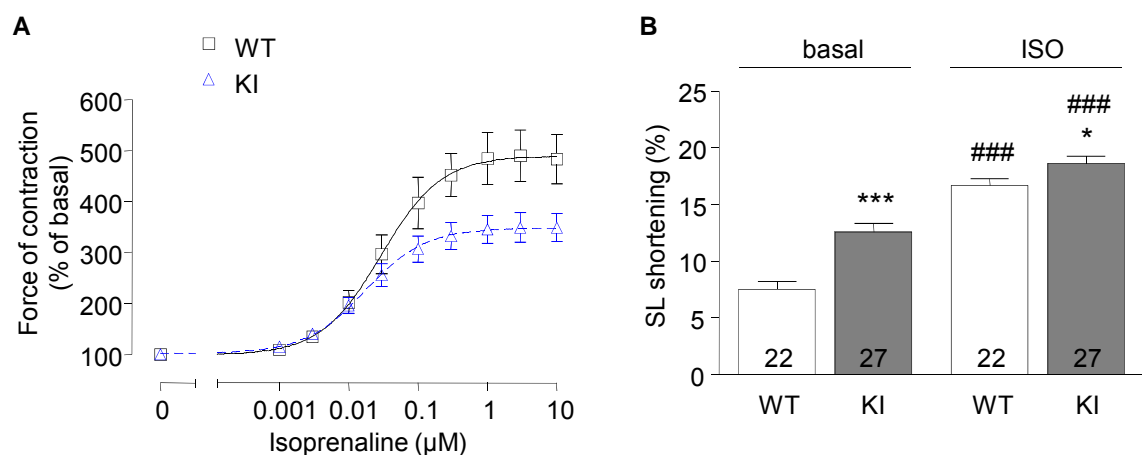


Figure 4.3 Isometric and isotonic contractions of 13 week-old cMyBP-C knock-in (KI) and wild-type (WT) mice. (A) Effect of isoprenaline stimulation on the isometric force of contraction of isolated left atria from KI and WT mice. Muscle length was adjusted to maximal twitch force in 1.8 mM external Ca^{2+} and the twitch forces obtained with different concentrations of isoprenaline were expressed as percentage of basal twitch force. Values are mean \pm SEM. $P < 0.001$, two-way ANOVA. $N = 6$ (WT), $N = 6$ (KI). The experiment was performed by Michael Grimm (Hamburg). (B) Effect of 100 nM isoprenaline (ISO) on the fractional sarcomere length (SL) shortening of isolated KI and WT myocytes. * $P < 0.05$, *** $P < 0.001$ vs. WT; ### $P < 0.001$ vs. basal, Student's *t*-test. The number of myocytes is indicated in the bars. The experiment was performed by Bodvaël Fraysse (Paris).

considered that the full-length protein expressed is a mutant, which might act as a poison peptide and exert a significantly altered function.

The greater increase in shortening in KO myocytes after isoprenaline stimulation was paralleled by a greater amount of binding sites for β -adrenergic receptor ligands in KO hearts, which argues for an increase in β -adrenergic receptor density in KO and might cause this increased β -adrenergic response. Upregulation of β -adrenergic receptor density is rarely observed in cardiac pathology, whereas downregulation is often reported and commonly accepted as a hallmark in heart failure (Brodde and Michel, 1999). When the heart is no longer able to answer increased demands, sympathetic tone is enhanced, which is reflected in increased concentrations of adrenaline and noradrenaline. This is believed to be the trigger for the downregulation of β -adrenergic receptors. So if downregulation of β -adrenergic receptors is related to increased catecholamines, upregulation of β -adrenergic receptors could possibly be due to a lower catecholamine concentration. The reason for this unusual finding remains unknown at present and further investigations have to be performed.

The diastolic intracellular Ca^{2+} concentration increased after isoprenaline stimulation in both KO and WT, but to a lesser extent in KO. The lower level of Ca^{2+} in KO, however, remains unexplained. The PLB/SERCA ratio was similar in KO and WT at this age, as was the Ca^{2+} influx via L-type Ca^{2+} channels. And the decreased amount of NCX would rather implicate a higher level of diastolic Ca^{2+} . Interestingly, although intracellular Ca^{2+} concentration increased less in KO, the decrease in diastolic sarcomere length was more pronounced than in WT. This is a hint towards increased Ca^{2+} sensitivity in KO myocytes. Also the greater shortening amplitude in KO despite similar Ca^{2+} peak amplitudes in WT and KO indicates a greater Ca^{2+} sensitivity. Thus, greater Ca^{2+} sensitivity in KO myocytes, which was quite concealed under basal conditions, became overtly visible after β -adrenergic receptor stimulation.

The kinetics of shortening and relengthening as well as the kinetics of Ca^{2+} rise and decline were slower in KO compared to WT before isoprenaline stimulation and in the presence of 100 nM isoprenaline. Shortening velocity in KO, however, increased with isoprenaline to a greater extent, so that it was only 12% lower than WT in the presence of isoprenaline compared to 33% lower than WT before isoprenaline stimulation. Relengthening velocity increased similarly in WT and KO, so that relengthening velocity in KO myocytes was ~30% lower both before and after isoprenaline stimulation,

suggesting that the absence of cMyBP-C did not alter the positive lusitropic effect by β -adrenergic receptor stimulation. On the one hand, this fits to the notion that the positive lusitropic effect after β -adrenergic receptor stimulation is mediated by phosphorylation of cTn-I and PLB, the first decreasing the Ca^{2+} sensitivity of the thin filament allowing Ca^{2+} to dissociate quicker from Tn-C, the latter releasing inhibition of PLB on SERCA and thus speeding Ca^{2+} reuptake into the SR. Yet, there is still argument about the relative contribution of cTn-I, PLB and cMyBP-C phosphorylation mainly because of the difficulties to selectively phosphorylating only one protein since they are all targets of PKA (Bers, 2002; de Tombe, 2003). In addition, myofilaments from the KO mice did not show Ca^{2+} -desensitization after addition of PKA, suggesting that cMyBP-C does play an important role in this process (Cazorla et al., 2006). It has been argued that, under isotonic conditions, the shortening kinetics are mainly determined by Ca^{2+} transient kinetics and therefore, unchanged lusitropic effects are likely due to unchanged PLB phosphorylation.

4.4 General conclusions

The aim of the present work was determining the role of cMyBP-C in contraction by using a targeted KO mouse model deficient of cMyBP-C and it was the first time that isolated intact ventricular myocytes were used as an approach. The initial experiments served to establish a stable method to measure contractile properties of isolated myocytes simultaneously with intracellular Ca^{2+} transients.

Myocytes from KO were then analysed in the absence and presence of isoprenaline to evaluate the role of cMyBP-C during contraction in its non-phosphorylated state or when it is fully phosphorylated by PKA. The major finding of a lower sarcomere length in diastole indicated incomplete relaxation and constant contractile activation in KO. This confirms the assumption that cMyBP-C acts as an internal load on contraction and tethers the myosin heads to the thick filament backbone. Furthermore, residual cross-bridge cycling in diastole is likely to cause diastolic dysfunction and energy expenditure, which are both hallmarks of FHC. Therefore the results propose a mechanism by which cMyBP-C mutations that lead to a reduced amount of cMyBP-C by haploinsufficiency can cause FHC.

After β -adrenergic stimulation KO myocytes displayed a dramatic increase in shortening and the previously observed greater Ca^{2+} sensitivity was then accentuated. These

results suggest that cMyBP-C is not only an internal load during contraction which is removed after phosphorylation, but that it also prevents hypercontracture during a highly activated state of the sarcomere, e.g. during β -adrenergic stimulation. Unfortunately, these results were not confirmed under isometric conditions, implicating that the different techniques might obscure results. Therefore, further examination of the β -adrenergic effect in KO seems advisable.

5 Summary

Cardiac myosin binding protein C (cMyBP-C, C-Protein) is a protein associated with the thick filaments in the sarcomeres of cardiac myocytes. It contributes to the thick filament structure through its various interactions with other sarcomeric proteins. After β -adrenergic stimulation cMyBP-C is phosphorylated via cAMP-dependent protein kinase (PKA) suggesting that it has also a regulatory function in cardiac contraction. However, this regulatory role is still not fully resolved. Interest in cMyBP-C has intensified since the discovery that mutations in the gene encoding for cMyBP-C are frequent causes of familial hypertrophic cardiomyopathy (FHC). The aim of the present work was to determine the role cMyBP-C plays in regulating contraction both in the absence of phosphorylation and after phosphorylation by PKA. Therefore, a targeted cMyBP-C knock-out (KO) mouse model was used, which does not express cMyBP-C and which develops cardiac hypertrophy. Contractile parameters were assessed mainly on the level of the intact myocytes where sarcomere shortening and intracellular Ca^{2+} transients were simultaneously measured. Further functional analysis was performed in intact left atrium and work-performing heart under loaded conditions. Protein analysis was performed to detect compensatory changes in the KO hearts.

The isolated myocytes from KO mice exhibited a markedly lower diastolic sarcomere length, which was sensitive to two inhibitors of cross-bridge cycling, indicating residual actin-myosin interaction and consequently incomplete relaxation during diastole. The relationship between cytosolic Ca^{2+} and sarcomere length showed that KO myocytes started to contract at a lower level of intracellular Ca^{2+} . Furthermore, a marked increase in sensitivity to external Ca^{2+} concentration was observed in isolated left atria from KO mice. The kinetics of both sarcomere shortening and the intracellular Ca^{2+} transient were slowed in KO, which was associated with changes in the amount of proteins involved in contraction and relaxation.

After β -adrenergic stimulation, isolated myocytes from KO displayed a more pronounced increase in fractional sarcomere shortening than myocytes from wild-type (WT) despite similar amplitudes of the Ca^{2+} transient. In loaded preparations, however, β -adrenergic stimulation resulted in a lower increase of force in KO than in WT. Moreover, ligand binding to β -adrenergic receptors was found to be increased in KO hearts. Taken together, ablation of cMyBP-C results in increased Ca^{2+} sensitivity under basal conditions and even more pronounced after β -adrenergic stimulation. This obviously

results in a relaxation deficit and constant contractile activation at low levels of Ca^{2+} during diastole. These results favor the concept that cMyBP-C acts as a constraint on myosin-actin interaction, thus allowing complete relaxation during diastole. This mechanism is of particular importance after β -adrenergic stimulation, when the sarcomeres are highly activated, and a pre-contracted state would dramatically reduce, rather than increase, the dynamic range of contraction.

5 Zusammenfassung

Das kardiale Myosin bindende Protein C (cMyBP-C, C-Protein) ist eine Komponente der dicken Filamente in den Sarkomeren der Herzmuskelzellen. Durch zahlreiche Interaktionen mit anderen Proteinen des Sarkomers trägt es zur Stabilität der dicken Filamente bei. Nach β -adrenerger Stimulation wird es durch die cAMP-abhängige Proteinkinase (PKA) phosphoryliert. Dies spricht dafür, dass cMyBP-C außerdem eine Rolle in der Regulation der Kontraktion spielt. Jedoch ist diese Rolle immer noch nicht hinreichend aufgeklärt. Das Interesse an Struktur und Funktion des cMyBP-C hat zugenommen, seit bekannt ist, dass Mutationen in diesem Protein zu den häufigsten Ursachen der familiären hypertrophen Kardiomyopathie (FHC) gehören. Ziel der vorliegenden Arbeit war es, die Rolle des cMyBP-C in der Regulation der Kontraktion, sowohl im nicht-phosphorylierten Zustand, als auch nach Phosphorylierung durch PKA, zu bestimmen. Dazu wurde ein cMyBP-C *knock-out* (KO) Maus-Modell benutzt, welches kein cMyBP-C exprimiert und Hypertrophie entwickelt. Die kontraktile Eigenschaften wurden hauptsächlich auf der Ebene isolierter intakter Kardiomyozyten bestimmt, wobei Sarkomerverkürzung und intrazelluläre Ca^{2+} -Transients gleichzeitig gemessen wurden. Weiterhin wurde die Kontraktilität von intakten linken Vorhöfen und isolierten Herzen unter isometrischen Bedingungen untersucht. Bestimmung herzspezifischer Proteine wurde durchgeführt, um kompensatorische Veränderungen in den KO-Hezen zu erfassen.

Isolierte Kardiomyozyten aus den KO-Mäusen wiesen eine deutlich verringerte diastolische Sarkomerlänge auf. Diese war durch Inhibitoren der Myosin-Aktin-Querbrückenbildung umkehrbar, was dafür spricht, dass die verringerte diastolische Sarkomerlänge Folge einer residualen Aktin-Myosin-Interaktion ist. Die Beziehung zwischen zytosolischem Ca^{2+} und Sarkomerlänge während der Kontraktion zeigte, dass sich die KO-Kardiomyozyten schon bei geringeren intrazellulären Ca^{2+} -Konzentrationen verkürzen als vergleichbare Wildtyp (WT)-Kardiomyozyten. Darüberhinaus wurde in den

linken Vorhöfen der KO-Mäuse eine deutlich gesteigerte Sensitivität gegenüber der extrazellulären Ca^{2+} -Konzentration beobachtet. Die Geschwindigkeiten sowohl der Sarkomerverkürzung als auch der Ca^{2+} -Transienten waren in KO-Kardiomyozyten verlangsamt, was mit Veränderungen in Proteinen, die an Kontraktion und Relaxation beteiligt sind, einherging.

Nach β -adrenerger Stimulation der Kardiomyozyten war die Zunahme der prozentualen Sarkomerverkürzung in KO stärker ausgeprägt als in WT, trotz gleichbleibender Amplitude des intrazellulär freigesetzten Ca^{2+} . Im Gegensatz dazu war der Anstieg in der Kraft, die an intakten Vorhöfen bzw. isolierten Herzen unter isometrischen Bedingungen gemessen wurde, in KO geringer ausgeprägt als in WT. Die Liganden-Bindung an β -adrenergen Rezeptoren war in KO-Herzen erhöht. Die Ergebnisse zeigen, dass das Fehlen des cMyBP-C im KO zu erhöhter Ca^{2+} -Sensitivität führt, sowohl basal als auch nach β -adrenerger Stimulation. Dies hat eine unvollständige Relaxierung der Sarkomere und somit dauerhafte Kontraktion bei den niedrigen Ca^{2+} -Konzentrationen, wie sie während der Diastole auftreten, zur Folge. Die Ergebnisse sprechen daher für ein Modell, in dem cMyBP-C als interne Last in den Sarkomeren wirkt, die die Myosin-Aktin-Interaktion behindert und deshalb vollständige Relaxation in der Diastole ermöglicht. Dies ist besonders nach β -adrenerger Stimulation von Bedeutung, wenn die Sarkomere stark aktiviert sind und ein vorkontrahierter Zustand nicht mehr in der Lage wäre, das Ausmaß der Kontraktion zu steigern.

6 References

Alcalai R, Seidman JG and Seidman CE (2007) Genetic Basis of Hypertrophic Cardiomyopathy: From Bench to the Clinics. *J Cardiovasc Electrophysiol*

Bennett P, Craig R, Starr R and Offer G (1986) The ultrastructural location of C-protein, X-protein and H-protein in rabbit muscle. *J Muscle Res Cell Motil* 7:550-67

Bers DM (2000) Calcium fluxes involved in control of cardiac myocyte contraction. *Circ Res* 87:275-81

Bers DM (2002) Cardiac excitation-contraction coupling. *Nature* 415:198-205

Bers DM (2008) Calcium Cycling and Signaling in Cardiac Myocytes. *Annu Rev Physiol* 70:23-49

Blough ER, Rennie ER, Zhang F and Reiser PJ (1996) Enhanced electrophoretic separation and resolution of myosin heavy chains in mammalian and avian skeletal muscles. *Anal Biochem* 233:31-5

Bonne G, Carrier L, Bercovici J, Cruaud C, Richard P, Hainque B, Gautel M, Labeit S, James M, Beckmann J, Weissenbach J, Vosberg HP, Fiszman M, Komajda M and Schwartz K (1995) Cardiac myosin binding protein-C gene splice acceptor site mutation is associated with familial hypertrophic cardiomyopathy. *Nat Genet* 11:438-40

Bradford MM (1976) A rapid and sensitive method for the quantitation of microgram quantities of protein utilizing the principle of protein-dye binding. *Anal Biochem* 72:248-54

Bristow MR (2000) beta-adrenergic receptor blockade in chronic heart failure. *Circulation* 101:558-69

Brodde OE and Michel MC (1999) Adrenergic and muscarinic receptors in the human heart. *Pharmacol Rev* 51:651-90

- Calaghan SC, Trinick J, Knight PJ and White E (2000) A role for C-protein in the regulation of contraction and intracellular Ca^{2+} in intact rat ventricular myocytes. *J Physiol* 528 Pt 1:151-6
- Carrier L, Knoll R, Vignier N, Keller DI, Bausero P, Prudhon B, Isnard R, Ambroisine ML, Fisman M, Ross J, Jr., Schwartz K and Chien KR (2004) Asymmetric septal hypertrophy in heterozygous cMyBP-C null mice. *Cardiovasc Res* 63:293-304
- Carrier L (2007) Cardiac myosin-binding protein C in the heart. *Arch Mal Coeur Vaiss* 100:238-43
- Cazorla O, Szilagyi S, Vignier N, Salazar G, Kramer E, Vassort G, Carrier L and Lacampagne A (2006) Length and protein kinase A modulations of myocytes in cardiac myosin binding protein C-deficient mice. *Cardiovasc Res* 69:370-80
- Colson BA, Bekyarova T, Fitzsimons DP, Irving TC and Moss RL (2007) Radial displacement of myosin cross-bridges in mouse myocardium due to ablation of myosin binding protein-C. *J Mol Biol* 367:36-41
- Craig R and Offer G (1976) The location of C-protein in rabbit skeletal muscle. *Proc R Soc Lond B Biol Sci* 192:451-61
- Crilley JG, Boehm EA, Blair E, Rajagopalan B, Blamire AM, Styles P, McKenna WJ, Ostman-Smith I, Clarke K and Watkins H (2003) Hypertrophic cardiomyopathy due to sarcomeric gene mutations is characterized by impaired energy metabolism irrespective of the degree of hypertrophy. *J Am Coll Cardiol* 41:1776-82
- Dalloz F, Osinska H and Robbins J (2001) Manipulating the contractile apparatus: genetically defined animal models of cardiovascular disease. *J Mol Cell Cardiol* 33:9-25
- Davis J, Wen H, Edwards T and Metzger JM (2007) Thin filament disinhibition by restrictive cardiomyopathy mutant R193H troponin I induces Ca^{2+} -independent mechanical tone and acute myocyte remodeling. *Circ Res* 100:1494-502
- Davis JS (1988) Interaction of C-protein with pH 8.0 synthetic thick filaments prepared from the myosin of vertebrate skeletal muscle. *J Muscle Res Cell Motil* 9:174-83

de Tombe PP (2003) Cardiac myofilaments: mechanics and regulation. *J Biomech* 36:721-30

de Tombe PP (2006) Myosin binding protein C in the heart. *Circ Res* 98:1234-6

Eijssen LM, van den Bosch BJ, Vignier N, Lindsey PJ, van den Burg CM, Carrier L, Doevendans PA, van der Vusse GJ and Smeets HJ (2008) Altered myocardial gene expression reveals possible maladaptive processes in heterozygous and homozygous cardiac myosin-binding protein C knockout mice. *Genomics* 91:52-60

El-Armouche A, Boknik P, Eschenhagen T, Carrier L, Knaut M, Ravens U and Dobrev D (2006) Molecular determinants of altered Ca²⁺ handling in human chronic atrial fibrillation. *Circulation* 114:670-80

El-Armouche A, Pohlmann L, Schlossarek S, Starbatty J, Yeh YH, Nattel S, Dobrev D, Eschenhagen T and Carrier L (2007) Decreased phosphorylation levels of cardiac myosin-binding protein-C in human and experimental heart failure. *J Mol Cell Cardiol* 43:223-9

Fitzsimons DP, Patel JR and Moss RL (1998) Role of myosin heavy chain composition in kinetics of force development and relaxation in rat myocardium. *J Physiol* 513 (Pt 1):171-83

Flashman E, Redwood C, Moolman-Smook J and Watkins H (2004) Cardiac myosin binding protein C: its role in physiology and disease. *Circ Res* 94:1279-89

Fougerousse F, Delezoide AL, Fiszman MY, Schwartz K, Beckmann JS and Carrier L (1998) Cardiac myosin binding protein C gene is specifically expressed in heart during murine and human development. *Circ Res* 82:130-3

Gautel M, Zuffardi O, Freiburg A and Labeit S (1995) Phosphorylation switches specific for the cardiac isoform of myosin binding protein-C: a modulator of cardiac contraction? *Embo J* 14:1952-60

Gautel M, Furst DO, Cocco A and Schiaffino S (1998) Isoform transitions of the myosin binding protein C family in developing human and mouse muscles: lack of isoform transcomplementation in cardiac muscle. *Circ Res* 82:124-9

Gauthier C, Langin D and Balligand JL (2000) Beta3-adrenoceptors in the cardiovascular system. *Trends Pharmacol Sci* 21:426-31

Geisterfer-Lowrance AA, Kass S, Tanigawa G, Vosberg HP, McKenna W, Seidman CE and Seidman JG (1990) A molecular basis for familial hypertrophic cardiomyopathy: a beta cardiac myosin heavy chain gene missense mutation. *Cell* 62:999-1006

Granzier H, Helmes M and Trombitas K (1996) Nonuniform elasticity of titin in cardiac myocytes: a study using immunoelectron microscopy and cellular mechanics. *Biophys J* 70:430-42

Granzier HL and Labeit S (2004) The giant protein titin: a major player in myocardial mechanics, signaling, and disease. *Circ Res* 94:284-95

Gruen M, Prinz H and Gautel M (1999) cAPK-phosphorylation controls the interaction of the regulatory domain of cardiac myosin binding protein C with myosin-S2 in an on-off fashion. *FEBS Lett* 453:254-9

Grynkiewicz G, Poenie M and Tsien RY (1985) A new generation of Ca²⁺ indicators with greatly improved fluorescence properties. *J Biol Chem* 260:3440-50

Harris SP, Bartley CR, Hacker TA, McDonald KS, Douglas PS, Greaser ML, Powers PA and Moss RL (2002) Hypertrophic cardiomyopathy in cardiac myosin binding protein-C knockout mice. *Circ Res* 90:594-601

Hartzell HC and Titus L (1982) Effects of cholinergic and adrenergic agonists on phosphorylation of a 165,000-dalton myofibrillar protein in intact cardiac muscle. *J Biol Chem* 257:2111-20

Hartzell HC and Glass DB (1984) Phosphorylation of purified cardiac muscle C-protein by purified cAMP-dependent and endogenous Ca²⁺-calmodulin-dependent protein kinases. *J Biol Chem* 259:15587-96

Helmes M, Trombitas K and Granzier H (1996) Titin develops restoring force in rat cardiac myocytes. *Circ Res* 79:619-26

Herron TJ, Korte FS and McDonald KS (2001) Loaded shortening and power output in cardiac myocytes are dependent on myosin heavy chain isoform expression. *Am J Physiol Heart Circ Physiol* 281:H1217-22

Heubach JF, Rau T, Eschenhagen T, Ravens U and Kaumann AJ (2002) Physiological antagonism between ventricular beta 1-adrenoceptors and alpha 1-adrenoceptors but no evidence for beta 2- and beta 3-adrenoceptor function in murine heart. *Br J Pharmacol* 136:217-29

Hofmann PA, Greaser ML and Moss RL (1991a) C-protein limits shortening velocity of rabbit skeletal muscle fibres at low levels of Ca²⁺ activation. *J Physiol* 439:701-15

Hofmann PA, Hartzell HC and Moss RL (1991b) Alterations in Ca²⁺ sensitive tension due to partial extraction of C-protein from rat skinned cardiac myocytes and rabbit skeletal muscle fibers. *J Gen Physiol* 97:1141-63

Keller DI, Coirault C, Rau T, Cheav T, Weyand M, Amann K, Lecarpentier Y, Richard P, Eschenhagen T and Carrier L (2004) Human homozygous R403W mutant cardiac myosin presents disproportionate enhancement of mechanical and enzymatic properties. *J Mol Cell Cardiol* 36:355-62

Kobayashi T and Solaro RJ (2005) Calcium, thin filaments, and the integrative biology of cardiac contractility. *Annu Rev Physiol* 67:39-67

Koretz JF (1979) Effects of C-protein on synthetic myosin filament structure. *Biophys J* 27:433-46

Korte FS, McDonald KS, Harris SP and Moss RL (2003) Loaded shortening, power output, and rate of force redevelopment are increased with knockout of cardiac myosin binding protein-C. *Circ Res* 93:752-8

Kruger M, Kohl T and Linke WA (2006) Developmental changes in passive stiffness and myofilament Ca²⁺ sensitivity due to titin and troponin-I isoform switching are not critically triggered by birth. *Am J Physiol Heart Circ Physiol* 291:H496-506

Kulikovskaya I, McClellan G, Flavigny J, Carrier L and Winegrad S (2003) Effect of MyBP-C binding to actin on contractility in heart muscle. *J Gen Physiol* 122:761-74

Kunst G, Kress KR, Gruen M, Uttenweiler D, Gautel M and Fink RH (2000) Myosin binding protein C, a phosphorylation-dependent force regulator in muscle that controls the attachment of myosin heads by its interaction with myosin S2. *Circ Res* 86:51-8

McClellan G, Kulikovskaya I and Winegrad S (2001) Changes in cardiac contractility related to calcium-mediated changes in phosphorylation of myosin-binding protein C. *Biophys J* 81:1083-92

McConnell BK, Jones KA, Fatkin D, Arroyo LH, Lee RT, Aristizabal O, Turnbull DH, Georgakopoulos D, Kass D, Bond M, Niimura H, Schoen FJ, Conner D, Fischman DA, Seidman CE and Seidman JG (1999) Dilated cardiomyopathy in homozygous myosin-binding protein-C mutant mice. *J Clin Invest* 104:1235-44

McConnell BK, Fatkin D, Semsarian C, Jones KA, Georgakopoulos D, Maguire CT, Healey MJ, Mudd JO, Moskowitz IP, Conner DA, Giewat M, Wakimoto H, Berul CI, Schoen FJ, Kass DA, Seidman CE and Seidman JG (2001) Comparison of two murine models of familial hypertrophic cardiomyopathy. *Circ Res* 88:383-9

Moolman-Smook J, Flashman E, de Lange W, Li Z, Corfield V, Redwood C and Watkins H (2002) Identification of novel interactions between domains of Myosin binding protein-C that are modulated by hypertrophic cardiomyopathy missense mutations. *Circ Res* 91:704-11

O'Connell TD, Ni YG, Lin K-M, Han H and Yan Z (2003) Isolation and culture of adult mouse cardiac myocytes for signaling studies. *AfCS Research Reports* 1: No. 5 CM [online]

Available from: <http://www.signaling-gateway.org/reports/v1/CM0005/CM0005.htm>

Offer G, Moos C and Starr R (1973) A new protein of the thick filaments of vertebrate skeletal myofibrils. Extractions, purification and characterization. *J Mol Biol* 74:653-76

Palmer BM, McConnell BK, Li GH, Seidman CE, Seidman JG, Irving TC, Alpert NR and Maughan DW (2004a) Reduced cross-bridge dependent stiffness of skinned myocardium from mice lacking cardiac myosin binding protein-C. *Mol Cell Biochem* 263:73-80

Palmer BM, Noguchi T, Wang Y, Heim JR, Alpert NR, Burgon PG, Seidman CE, Seidman JG, Maughan DW and LeWinter MM (2004b) Effect of cardiac myosin binding protein-C on mechanoenergetics in mouse myocardium. *Circ Res* 94:1615-22

Reiser PJ and Kline WO (1998) Electrophoretic separation and quantitation of cardiac myosin heavy chain isoforms in eight mammalian species. *Am J Physiol* 274:H1048-53

Richard P, Villard E, Charron P and Isnard R (2006) The Genetic Bases of Cardiomyopathies. *J Am Coll Cardiol* 48:A79-89

Rome E, Offer G and Pepe FA (1973) X-ray diffraction of muscle labelled with antibody to C-protein. *Nat New Biol* 244:152-4

Sadayappan S, Osinska H, Klevitsky R, Lorenz JN, Sargent M, Molkentin JD, Seidman CE, Seidman JG and Robbins J (2006) Cardiac myosin binding protein C phosphorylation is cardioprotective. *Proc Natl Acad Sci U S A* 103:16918-23

Spurgeon HA, duBell WH, Stern MD, Sollott SJ, Ziman BD, Silverman HS, Capogrossi MC, Talo A and Lakatta EG (1992) Cytosolic calcium and myofilaments in single rat cardiac myocytes achieve a dynamic equilibrium during twitch relaxation. *J Physiol* 447:83-102

Squire JM, Luther PK and Knupp C (2003) Structural evidence for the interaction of C-protein (MyBP-C) with actin and sequence identification of a possible actin-binding domain. *J Mol Biol* 331:713-24

Starr R and Offer G (1971) Polypeptide chains of intermediate molecular weight in myosin preparations. *FEBS Lett* 15:40-44

Starr R and Offer G (1978) The interaction of C-protein with heavy meromyosin and subfragment-2. *Biochem J* 171:813-6

Stauffer BL, Konhilas JP, Luczak ED and Leinwand LA (2006) Soy diet worsens heart disease in mice. *J Clin Invest* 116:209-16

Stelzer JE, Dunning SB and Moss RL (2006a) Ablation of cardiac myosin-binding protein-C accelerates stretch activation in murine skinned myocardium. *Circ Res* 98:1212-8

Stelzer JE, Fitzsimons DP and Moss RL (2006b) Ablation of myosin-binding protein-C accelerates force development in mouse myocardium. *Biophys J* 90:4119-27

Stelzer JE, Patel JR and Moss RL (2006c) Protein kinase A-mediated acceleration of the stretch activation response in murine skinned myocardium is eliminated by ablation of cMyBP-C. *Circ Res* 99:884-90

Stelzer JE, Brickson SL, Locher MR and Moss RL (2007a) Role of myosin heavy chain composition in the stretch activation response of rat myocardium. *J Physiol* 579:161-73

Stelzer JE, Patel JR, Walker JW and Moss RL (2007b) Differential roles of cardiac myosin-binding protein C and cardiac troponin I in the myofibrillar force responses to protein kinase A phosphorylation. *Circ Res* 101:503-11

Thierfelder L, Watkins H, MacRae C, Lamas R, McKenna W, Vosberg HP, Seidman JG and Seidman CE (1994) Alpha-tropomyosin and cardiac troponin T mutations cause familial hypertrophic cardiomyopathy: a disease of the sarcomere. *Cell* 77:701-12

Tiemann K, Weyer D, Djoufack PC, Ghanem A, Lewalter T, Dreiner U, Meyer R, Grohe C and Fink KB (2003) Increasing myocardial contraction and blood pressure in C57BL/6 mice during early postnatal development. *Am J Physiol Heart Circ Physiol* 284:H464-74

Warren CM, Krzesinski PR, Campbell KS, Moss RL and Greaser ML (2004) Titin isoform changes in rat myocardium during development. *Mech Dev* 121:1301-12

Watkins H, Conner D, Thierfelder L, Jarcho JA, MacRae C, McKenna WJ, Maron BJ, Seidman JG and Seidman CE (1995) Mutations in the cardiac myosin binding protein-C gene on chromosome 11 cause familial hypertrophic cardiomyopathy. *Nat Genet* 11:434-7

Weisberg A and Winegrad S (1996) Alteration of myosin cross bridges by phosphorylation of myosin-binding protein C in cardiac muscle. *Proc Natl Acad Sci U S A* 93:8999-9003

Whiting A, Wardale J and Trinick J (1989) Does titin regulate the length of muscle thick filaments? *J Mol Biol* 205:263-8

Winegrad S (1999) Cardiac myosin binding protein C. *Circ Res* 84:1117-26

Witt CC, Gerull B, Davies MJ, Centner T, Linke WA and Thierfelder L (2001) Hypercontractile properties of cardiac muscle fibers in a knock-in mouse model of cardiac myosin-binding protein-C. *J Biol Chem* 276:5353-9

Wolska BM, Kitada Y, Palmiter KA, Westfall MV, Johnson MD and Solaro RJ (1996) CGP-48506 increases contractility of ventricular myocytes and myofilaments by effects on actin-myosin reaction. *Am J Physiol* 270:H24-32

Yang Q, Sanbe A, Osinska H, Hewett TE, Klevitsky R and Robbins J (1998) A mouse model of myosin binding protein C human familial hypertrophic cardiomyopathy. *J Clin Invest* 102:1292-300

Yang Q, Sanbe A, Osinska H, Hewett TE, Klevitsky R and Robbins J (1999) In vivo modeling of myosin binding protein C familial hypertrophic cardiomyopathy. *Circ Res* 85:841-7

Yang Q, Hewett TE, Klevitsky R, Sanbe A, Wang X and Robbins J (2001) PKA-dependent phosphorylation of cardiac myosin binding protein C in transgenic mice. *Cardiovasc Res* 51:80-8

7 Appendix

7.1 List of abbreviations

°C	Degree Centigrade (Degree Celsius)
A	Ampere (unit of electrical current)
ADP	Adenosine 5'-diphosphate
APS	Ammonium persulfate
ATP	Adenosine 5'-triphosphate
A.U.	Arbitrary unit
BDM	2,3-Butanedione monoxime
CaMKII	Ca ²⁺ /calmodulin-dependant kinase II
CPM	Counts per minute
Cf.	Confer
cMyBP-C	Cardiac myosin binding protein C
CSQ	Calsequestrin
cAMP	3',5'-Cyclic adenosine monophosphate
cTn-I	Cardiac troponin I
Da	Dalton
DNA	Deoxyribonucleic acid
DHPR	Dihydropyridine receptor/L-type Ca ²⁺ channel
DPM	Disintegrations per minute
DTT	1,4-Dithiotreithol
EDTA	Ethylenediamintetraacetic acid
e.g.	Lat.: <i>exempli gratia</i> , for example
EGTA	Ethylene glycol-bis(2-aminoethylether)-N,N,N',N'-tetraacetic acid
F	Farad (unit of capacitance)
F340/380	Fluorescence ratio with 340 and 380 nm excitation wavelength
g	Acceleration of gravity (9.8 m/s ²)
g	Gram
h	Hour
HEPES	4-(2-Hydroxyethyl)-1-piperazineethanesulfonic acid
HET	Heterozygous knock-out
Hz	Hertz (1/s)
i.e.	Lat.: <i>id est</i> , that is

IU	International unit
Ig	Immunoglobulin
ISO	Isoprenaline
KI	Knock-in
KO	Knock-out
l	Litre
M	Molar (mol/L)
MHC	Myosin heavy chain
min	Minute
mRNA	Messenger ribonucleic acid
N	Newton (unit of force)
NCX	Na ⁺ /Ca ²⁺ -exchanger
PAGE	Polyacrylamide gel electrophoresis
PDE	Phosphodiesterase
PKA	cAMP-dependant protein kinase
PLB	Phospholamban
rpm	Rounds per minute
RyR	Ryanodine receptor
s	Second
SDS	Sodium-dodecylsulfate
SERCA	Sarco-endoplasmic reticulum ATPase
SL	Sarcomere length
SR	Sarco-endoplasmic reticulum
TEMED	N,N,N',N'-Tetramethylethylenediamine
UV	Ultra-violet
V	Volt
W	Watt (unit of power)
WT	Wild-type

SI prefixes

k	Kilo (10 ³)
m	Milli (10 ⁻³)
μ	Micro (10 ⁻⁶)
n	Nano (10 ⁻⁹)
p	Pico (10 ⁻¹²)
f	Femto (10 ⁻¹⁵)

7.2 List of chemicals

Acetic acid, Merck, Darmstadt

Acrylamide/Bis-acrylamide (37.5:1), 40% solution, Bio-Rad, München

Acrylamide, 40% solution, Bio-Rad, München

Albumin from bovine serum (BSA), Sigma-Aldrich, Steinheim

Ammonium persulfate (APS), Bio-Rad, München

Aqua ad injectabilia, Baxter, Unterschleißheim

L-Ascorbic acid, Merck, Darmstadt

(-)-Blebbistatin, Sigma-Aldrich, Steinheim

Bradford reagent, Bio-Rad, München

Bromophenol Blue, Merck, Darmstadt

2,3-Butanedione monoxime (BDM), Sigma-Aldrich, Steinheim

Calcium chloride dihydrate ($\text{CaCl}_2 \times 2 \text{H}_2\text{O}$), Sigma-Aldrich, Steinheim

(-)-[^3H]-CGP-12177 (37 MBq/ml (1 mCi/ml)), 27 μM , ethanol solution), Amersham/GE Healthcare, München

Coomassie Brilliant Blue, Merck, Darmstadt

Dimethyl sulfoxide (DMSO), Merck, Darmstadt

1,4-Dithiothreitol (DTT), Sigma-Aldrich, Steinheim

ECL plus detection kit, Amersham/GE Healthcare, München

Ethylene glycol-bis(2-aminoethylether)-N,N,N',N'-tetraacetic acid (EGTA), Merck, Darmstadt

Ethanol (96%), denatured, Merck, Darmstadt

Fetal calf serum (FCS), Invitrogen/Gibco®, Karlsruhe

Fura-2 AM, Invitrogen/Molecular Probes™, Karlsruhe

Fura-2 Calcium Imaging Calibration Kit, Invitrogen/Molecular Probes™, Karlsruhe

D-(+)-Glucose, anhydrous, Sigma-Aldrich, Steinheim

D-(+)-Glucose monohydrate, Merck, Darmstadt

Glycerol, Merck, Darmstadt

Glycine, Carl Roth, Karlsruhe

4-(2-hydroxyethyl)-1-piperazineethanesulfonic acid (HEPES), Carl Roth, Karlsruhe

Hydrochloric acid, 37% solution, Merck, Darmstadt

(\pm)-Isoprenaline hydrochloride, Sigma-Aldrich, Steinheim

Liberase Blendzyme 3, Roche Diagnostics, Mannheim

Liquemin® N 10 000 (heparin sodium salt 10,000 I.U./mL), Roche Pharma, Grenzach-Wyhlen

Liquid scintillation cocktail (Quicksafe A), Zinsser Analytic, Frankfurt/Main

Liquid nitrogen (LN₂), Linde, Hannover
Magnesium chloride hexahydrate (MgCl₂ × 6 H₂O), Merck, Darmstadt
Magnesium sulfate heptahydrate (MgSO₄ × 7 H₂O), Merck, Darmstadt
2-Mercaptoethanol, Sigma-Aldrich, Steinheim
Methanol, Merck, Darmstadt
N,N'-Methylene-bis-acrylamide, 2% solution, Bio-Rad, München
Milk powder, Carl Roth, Karlsruhe
Nadolol, Sigma-Aldrich, Steinheim
Ponceau S, Sigma-Aldrich, Steinheim
Potassium chloride (KCl), Merck, Darmstadt
Potassium phosphate monobasic (KH₂PO₄), Merck, Darmstadt
Potassium bicarbonate (KHCO₃), Merck, Darmstadt
Precision Plus Protein Standard, Bio-Rad, München
2-Propanol (Isopropanol), Merck, Darmstadt
Pyruvic acid, Sigma-Aldrich, Steinheim
Sodium bicarbonate (NaHCO₃), Merck, Darmstadt
Sodium chloride (NaCl), Mallinckrodt Baker, Deventer, NL
Sodium chloride, 0.9% solution, Baxter, Unterschleißheim
Sodium dodecyl sulfate (SDS), Merck, Darmstadt
Sodium ethylenediaminetetraacetate dihydrate (Na₂EDTA), Merck, Darmstadt
Sodium phosphate dibasic dihydrate (Na₂HPO₄ × 2 H₂O), Merck, Darmstadt
Sodium phosphate monobasic (NaH₂PO₄), Merck, Darmstadt
Sodium hydroxide (NaOH), Merck, Darmstadt
Sucrose, Merck, Darmstadt
Taurine, Merck, Darmstadt
N,N,N',N'-Tetramethylethylenediamine (TEMED), Bio-Rad, München
Tris(hydroxymethyl)aminomethane hydrochloride (Tris-HCl), Merck, Darmstadt
Trizma® base (Tris(hydroxymethyl)aminomethane), Sigma-Aldrich, Steinheim
Thiourea, Merck, Darmstadt
Tween® 20 (Polyethylene glycol sorbitan monolaurate), Sigma-Aldrich, Steinheim
Urea, Sigma-Aldrich, Steinheim

7.3 List of antibodies

Anti rabbit IgG, peroxidase conjugate, Sigma-Aldrich, Steinheim

Anti mouse IgG, peroxidase conjugate, Sigma-Aldrich, Steinheim

Anti goat IgG, peroxidase conjugate, Santa Cruz Biotechnology, Santa Cruz, CA, USA

Anti-myosin (skeletal, slow) (β -MHC), Sigma-Aldrich, Steinheim

Calsequestrin, Affinity BioReagents, Golden, CO, USA

NCX1 [300-127], Abcam, Cambridge, UK

PLB A1, Badrilla, Leeds, UK

Phospho PLB PS-16, Badrilla, Leeds, UK

Phospho PLB PT17, Badrilla, Leeds, UK

SERCA2 (N-19), Santa Cruz Biotechnology, Santa Cruz, CA, USA

7.4 List of laboratory consumables

96-well microtest plate, Sarstedt, Nümbrecht

Centrifugation tubes, 15 ml, 50 ml, Sarstedt, Nümbrecht

Sterican® disposable cannulas, B. Braun, Melsungen

Disposable syringes, B. Braun, Melsungen

Hybond™-P (hydrophobic PVDF membrane), Amersham/GE Healthcare, München

Insulin syringes, Becton Dickinson, Heidelberg

MultiScreen disposable punch tips, Millipore, Schwalbach

MultiScreen FB 96-well filtration plate, Millipore, Schwalbach

Nitrocellulose blotting membrane (Protran®), Whatman, Dassel

Petri dishes, 10 mm, Sarstedt, Nümbrecht

Pipette tips, 10 µl, 100 µl, 1000 µl, Sarstedt, Nümbrecht

Polystyrene cuvettes, Sarstedt, Nümbrecht

Reaction tubes, 1.5 ml, 2 ml, Sarstedt, Nümbrecht

Serological pipettes, 2 ml, 5 ml, 10 ml, 10 ml wide tip, 25 ml, Sarstedt, Nümbrecht

Scintillation vials, Rudolf Franke Labortechnik, Hamburg

Syringe filter, Sarstedt, Nümbrecht

Vacuum filtration units, 500 ml, Sarstedt, Nümbrecht

Whatman® 3 MM blotting paper, Whatman, Dassel

7.5 List of laboratory equipment

Accu jet® pipette controller, Brand, Wertheim
Analytical balance (Genius), Sartorius, Göttingen
Arc lamp power supply, Cairn Research, Faversham
Axiovert 25 inverse microscope, Zeiss, Jena
cFlow 8 channel flow controller, CellMicroControls, Norfolk, VA, USA
ChemieGenius² Bio Imaging System, Syngene, Cambridge, UK
Cooling centrifuge 5415 R, Eppendorf, Hamburg
Cooling centrifuge Universal 30 RF, Hettich, Tuttlingen
Counting chamber Fuchs-Rosenthal, VWR, Darmstadt
Fluorescence System Interface, IonOptix Corporation, Milton, MA, USA
Force transducers, G. Jäckel, Hanau
HyperSwitch high intensity arc lamp, IonOptix Corporation, Milton, MA, USA
Magnetic stirrer, Heidolph, Schwabach
Metal crucible, in-house production
Milli-Q Plus water purification system, Millipore, Schwalbach
Mini protean electrophoresis and Western blotting system, Bio-Rad, München
Minipuls 3 peristaltic pump, Gilson, Middleton, WI, USA
MultiScreen punch, Millipore, Schwalbach
MyoCam, IonOptix Corporation, Milton, MA, USA
MyoPacer field simulator, IonOptix Corporation, Milton, MA, USA
Nikon Eclipse TS 100 inverse microscope, Nikon, Düsseldorf
Organ baths, in-house production
Peristaltic pump, Pharmacia
Laboratory pH meter, Knick, Berlin
SmartSpec spectrophotometer, Bio-Rad, München
Pipettes, 0.5-10 µL, 10-100 µL, 100-1000 µL, Eppendorf, Hamburg
Polytron® homogenizer, Kinematica, Littau-Luzern, CH
Power Pac 300, Bio-Rad, München
Precision balance (Precision Advanced), Ohaus, Pine Brook, NJ, USA
Safire² microplate reader, Tecan, Männedorf, CH
Stimulation/Thermistor assay, CellMicroControls, Norfolk, VA, USA
Stimulation chamber for myocytes, CellMicroControls, Norfolk, VA, USA
Stimulation chamber holder with aspirator, CellMicroControls, Norfolk, VA, USA
Temperature controller, CellMicroControls, Norfolk, VA, USA

Thermomixer comfort, Eppendorf, Hamburg

Videopower, IonOptix Corporation, Milton, MA, USA

Vortex-Genie 2, Scientific Industries, Bohemia, NY, USA

Wallac 1409 Liquid Scintillation Counter, PerkinElmer, Waltham, MA, USA

Water bath, GFL, Burgwedel

Water bath Thermostat, Eppendorf, Hamburg

7.6 Chemicals with indication of risk phrases and security advices

Acetic acid	R: 10-35 S: 23.2-26-45
Acrylamide, 40% solution	R: 45-46-20/21-23/24/25-43-48 S: 36/37/39-45-60
Acrylamide/Bis, 40% solution	R: 45-46-20/21-23/24/25-43-48 S: 36/37/39-45-60
Ammonium persulfate	R: 8-22-36/37/38-42/43 S: 22-24-26-37
(-)-Blebbistatin	R: 20/21/22-36/37/38 S: 26-36/37
Bradford reagent	R: 20/21/22-36 S: 26-36/37-45-60
Bromophenol Blue	S: 22-24/25
2,3-Butanedione monoxime	S: 22-24/25
Calcium chloride dihydrate	R: 36 S: 22-24
Coomassie Brilliant Blue	S: 22-24/25
1,4-Dithiothreitol	R: 22-36/37/38 S: 26-36
Ethanol (96%)	R: 11 S: 7-16
Hydrochloric acid, 37% solution	R: 34-37 S: 26-36/37/39-45
(±)-Isoprenaline hydrochloride	R: 36/37/38 S: 26-36
Liberase Blendzyme 3	R: 36/37/38-42/43 S: 22-S24/25
2-Mercaptoethanol	R: 23/24/25 S: 45
Methanol	R: 11-23/24/25-39/23/24/25 S: 7-16-36/37-45
Ponceau S	R: 36/37/38 S: 26-36
2-Propanol	R: 11-36-37 S: 7-16-24/25-26
Pyruvic acid	R: 34 S: 26-36/37/39-45
Sodium dodecyl sulphate	R: 11-21/22-36/37/38 S: 26-36/37
Sodium hydroxide	R: 35 S: 26-37/39-45
TEMED	R: 11-20/22-34 S: 16-26-36/37/39-45-60
Tris base	R: 36/37/38 S: 26-36
Tris hydrochloride	R: 36/37/38 S: 26-36
Thiourea	R: 22-40-51/53-63 S: 36/37-61

7.6.1 Indication of particular risks

- 1: Explosive when dry
- 2: Risk of explosion by shock, friction, fire or other sources of ignition
- 3: Extreme risk of explosion by shock, friction, fire or other sources of ignition
- 4: Forms very sensitive explosive metallic compounds
- 5: Heating may cause an explosion

- 6: Explosive with or without contact with air
- 7: May cause fire
- 8: Contact with combustible material may cause fire
- 9: Explosive when mixed with combustible material
- 10: Flammable
- 11: Highly Flammable
- 12: Extremely Flammable
- 14: Reacts violently with water
- 15: Contact with water liberates extremely flammable gases
- 16: Explosive when mixed with oxidizing substances
- 17: Spontaneously flammable in air
- 18: In use may form flammable/explosive vapor-air mixture
- 19: May form explosive peroxides
- 20: Harmful by inhalation
- 21: Harmful in contact with skin
- 22: Harmful if swallowed
- 23: Toxic by inhalation
- 24: Toxic in contact with skin
- 25: Toxic if swallowed
- 26: Very Toxic by inhalation
- 27: Very Toxic in contact with skin
- 28: Very Toxic if swallowed
- 29: Contact with water liberates toxic gas
- 30: Can become highly flammable in use
- 31: Contact with acids liberates toxic gas
- 32: Contact with acids liberates very toxic gas
- 33: Danger of cumulative effects
- 34: Causes burns
- 35: Causes severe burns
- 36: Irritating to the eyes
- 37: Irritating to the respiratory system
- 38: Irritating to the skin
- 39: Danger of very serious irreversible effects
- 40: Limited evidence of a carcinogenic effect
- 41: Risk of serious damage to eyes
- 42: May cause sensitization by inhalation
- 43: May cause sensitization by skin contact

- 44: Risk of explosion if heated under confinement
- 45: May cause cancer
- 46: May cause heritable genetic damage
- 48: Danger of serious damage to health by prolonged exposure
- 49: May cause cancer by inhalation
- 50: Very Toxic to aquatic organisms
- 51: Toxic to aquatic organisms
- 52: Harmful to aquatic organisms
- 53: May cause long-term adverse effects in the aquatic environment
- 54: Toxic to flora
- 55: Toxic to fauna
- 56: Toxic to soil organisms
- 57: Toxic to bees
- 58: May cause long-term adverse effects in the environment
- 59: Dangerous for the ozone layer
- 60: May impair fertility
- 61: May cause harm to the unborn child
- 62: Possible risk of impaired fertility
- 63: Possible risk of harm to the unborn child
- 64: May cause harm to breast-fed babies
- 65: Harmful: May cause lung damage if swallowed
- 66: Repeated exposure may cause skin dryness or cracking
- 67: Vapors may cause drowsiness and dizziness
- 68: Possible risk of irreversible effects

7.6.2 Indication of safety precautions

- 1: Keep locked up
 - 2: Keep out of the reach of children
 - 3: Keep in a cool place
 - 4: Keep away from living quarters
 - 5: Keep contents under ... (appropriate liquid to be specified by the manufacturer)
 - 6: Keep under ... (inert gas to be specified by the manufacturer)
 - 7: Keep container tightly closed
 - 8: Keep container dry
 - 9: Keep container in a well-ventilated place
-

- 12: Do not keep the container sealed
- 13: Keep away from food, drink and animal feeding stuffs
- 14: Keep away from ... (incompatible materials to be indicated by the manufacturer)
- 15: Keep away from heat
- 16: Keep away from sources of ignition - No smoking
- 17: Keep away from combustible material
- 18: Handle and open container with care
- 20: When using, do not eat or drink
- 21: When using, do not smoke
- 22: Do not breathe dust
- 23: Do not breathe gas/fumes/vapor/spray (appropriate wording to be specified by the manufacturer)
- 24: Avoid contact with skin
- 25: Avoid contact with eyes
- 26: In case of contact with eyes, rinse immediately with plenty of water and seek medical advice
- 27: Take off immediately all contaminated clothing
- 28: After contact with skin, wash immediately with plenty of ... (to be specified by the manufacturer)
- 29: Do not empty into drains
- 30: Never add water to this product
- 33: Take precautionary measures against static discharges
- 35: This material and its container must be disposed of in a safe way
- 36: Wear suitable protective clothing
- 37: Wear suitable gloves
- 38: In case of insufficient ventilation, wear suitable respiratory equipment
- 39: Wear eye/face protection
- 40: To clean the floor and all objects contaminated by this material use ... (to be specified by the manufacturer)
- 41: In case of fire and/or explosion do not breathe fumes
- 42: During fumigation/spraying wear suitable respiratory equipment (appropriate wording to be specified)
- 43: In case of fire, use ... (indicate in the space the precise type of fire-fighting equipment. If water increases the risk add - Never use water)
- 45: In case of accident or if you feel unwell, seek medical advice immediately (show label where possible)
- 46: If swallowed, seek medical advice immediately and show this container or label

- 47: Keep at temperature not exceeding ... E C (to be specified by the manufacturer)
- 48: Keep wetted with ... (appropriate material to be specified by the manufacturer)
- 49: Keep only in the original container
- 50: Do not mix with ... (to be specified by the manufacturer)
- 51: Use only in well-ventilated areas
- 52: Not recommended for interior use on large surface areas
- 53: Avoid exposure - obtain special instruction before use
- 56: Dispose of this material and its container to hazardous or special waste collection point
- 57: Use appropriate container to avoid environmental contamination
- 59: Refer to manufacturer/supplier for information on recovery/recycling
- 60: This material and/or its container must be disposed of as hazardous waste
- 61: Avoid release to the environment. Refer to special instructions safety data sheet
- 62: If swallowed, do not induce vomiting: seek medical advice immediately and show this container or label
- 63: In case of accident by inhalation, remove casualty to fresh air and keep at rest
- 64: If swallowed, rinse mouth with water (only if the person is conscious)

7.7 Publications and congress participations

Original publications

El-Armouche A, **Pohlmann L**, Schlossarek S, Starbatty J, Yeh YH, Nattel S, Dobrev D, Eschenhagen T and Carrier L (2007) Decreased phosphorylation levels of cardiac myosin-binding protein-C in human and experimental heart failure. *J Mol Cell Cardiol* 43:223-9

Pohlmann L, Kröger I, Vignier N, Schlossarek S, Krämer E, Coirault C, Sultan KR, El-Armouche A, Winegrad S, Eschenhagen T and Carrier L (2007) Cardiac myosin-binding protein C is required for complete relaxation in intact myocytes. *Circ Res* 101:928-38

Congress posters and presentations

Pohlmann L, Krämer E, Vignier N, Kröger I, Eschenhagen T, Carrier L (2005a) Impairment of cardiac myocyte function in homozygous cardiac myosin-binding protein C null mice. *Working Group on Myocardial Function - Winter meeting "Molecular mechanisms of heart failure"*, Isola 2000, France, January 13-15, poster presented by Lucie Carrier.

Pohlmann L, Krämer E, Vignier N, Kröger I, Eschenhagen T, Carrier L (2005b) Impairment of cardiac myocyte function in cardiac myosin-binding protein C null mice. *71. Jahrestagung der Deutschen Gesellschaft für Kardiologie - Herz - und Kreislaufforschung e.V.*, Mannheim, Germany, March 31- April 2, oral communication.

Schlossarek S, Vignier N, Mearini G, Krämer E, **Pohlmann L**, Herrgesell N, Eschenhagen T, Carrier L (2005) Cardiac myosin-binding protein C and familial hypertrophic cardiomyopathy. *First International CCR Symposium. Cardiovascular Disease: From Basic Mechanisms to Therapeutic Targets*. Berlin, Germany, October 21-22, conference presented by Lucie Carrier.

Schlossarek S, Vignier N, Mearini G, **Pohlmann L**, Krämer E, Eschenhagen T, Carrier L (2006) Instability of cardiac myosin-binding protein C mutant in mouse models of familial hypertrophic cardiomyopathy: involvement of the ubiquitin-proteasome system? *5th International Ascona Workshop on Cardiomyocyte Cell Biology: Differentiation, Stability of Cytoarchitecture and Therapeutic Potential of Heart Muscle Cells*. Monte Verità, Ascona, Switzerland, April 2-6, oral communication by Lucie Carrier.

Pohlmann L, Kröger I, Vignier N, Schlossarek S, Krämer E, Coirault C, El-Armouche A, Winegrad S, Eschenhagen T, Carrier L (2007a) Effects of cardiac myosin-binding protein C knockout (KO) on intact isolated cardiac myocytes. *51st Annual Meeting of the Biophysical Society*, Baltimore, MD, March 3-7, poster presented by Saul Winegrad.

El-Armouche A, **Pohlmann L**, Nattel S, Dobrev D, Eschenhagen T, Carrier L (2007) Decreased phosphorylation levels of cardiac myosin-binding protein C in human and experimental heart failure. *73. Jahrestagung der deutschen Gesellschaft für Kardiologie – Herz- und Kreislaufforschung e.V.*, Mannheim, Germany, April 12-14, oral communication by Ali El-Armouche.

Pohlmann L, Kröger I, Vignier N, Schlossarek S, Krämer E, Coirault C, El-Armouche A, Winegrad S, Eschenhagen T, Carrier L (2007b) Cardiac myosin-binding protein C is required for complete sarcomere relaxation in intact myocytes: Evidence from a knock-out mouse model. *73. Jahrestagung der deutschen Gesellschaft für Kardiologie – Herz- und Kreislaufforschung e.V.*, Mannheim, Germany, April 12-14, oral communication.

Sultan KR, **Pohlmann L**, Juhr D, Eschenhagen T, Carrier L (2007) Liquid-phase isoelectric focusing of cardiac proteins: differential separation of cMyBP-C phosphorylation states. *XIX World Congress of the International Society for Heart Research*, Bologna, Italy, June 22-26, poster presented by Lucie Carrier.

7.8 Curriculum vitae

Name: Lutz Pohlmann
Date of birth: August 22, 1977
Place of birth: Papenburg
Nationality: German

School Education:

1984 – 1990: Kirchschole Papenburg
1990 – 1997: Gymnasium Papenburg
06/1997: Abitur

Alternative Civilian Service:

10/1997 – 10/1998: Landesbildungszentrum für Hörgeschädigte, Braunschweig

University Studies:

10/1998 – 11/2002: Studies of pharmacy, Kiel University
08/2000: 1st part of the Pharmaceutical Examination
11/2002: 2nd part of the Pharmaceutical Examination
12/2002 – 11/2003: One-year practical training: Mönckeberg-Apotheke, Hamburg
12/2003: 3rd part of the Pharmaceutical Examination and Licensing to practice as Dispensing Chemist

Ph.D. Thesis:

04/2004 – 02/2008: Institute of Experimental and Clinical Pharmacology and Toxicology, University Medical Center Hamburg-Eppendorf (Director: Prof. Dr. Thomas Eschenhagen), research group of Dr. Lucie Carrier

7.9 Affirmation

I herewith confirm that I prepared the doctoral thesis at hand myself and that I have cited correctly all publications consulted. All results obtained in collaboration with other researchers are indicated.

I furthermore declare that neither this present nor another doctoral thesis was submitted to any board of examiners for a degree at any other university.

Hamburg, February 2008

8 Acknowledgement

I would like to thank Prof. Dr. Thomas Eschenhagen who gave me the opportunity to perform my Ph.D. research in the Institute of Experimental and Clinical Pharmacology and Toxicology of the University Medical Center Hamburg-Eppendorf. I gratefully acknowledge his mentorship which ranged from help in evaluating results and preparing congress presentations up to practical support in performing experiments.

I thank Prof. Dr. Michael Korth for accepting the supervision of my Ph.D. thesis vis-à-vis the Department of Chemistry of the University of Hamburg.

Further I would like to thank Dr. Lucie Carrier for providing a subject of research which was both fascinating and challenging. I am thankful for her scientific guidance, for always taking time to discuss my results, and for her constant encouragement and inspiring motivation during the course of my work.

I am particularly grateful to all the collaborators both in Hamburg and abroad who obtained some of the results I presented in this work.

Thank you to the present and former colleagues in the Institute of Experimental and Clinical Pharmacology and Toxicology of the University Medical Center Hamburg-Eppendorf, and especially to the members of the research group of Lucie Carrier for all the helpful discussions, technical support, the good cooperation and motivating atmosphere.

Finally, I would like to thank my family for their confidence and patience. Their constant support enabled me to successfully complete this work.

This work was supported by grants to Lucie Carrier from the sixth Framework Program of the European Union (Marie Curie EXT-014051), the Deutsche Forschungsgemeinschaft (DFG-FOR-604), the Institut National de la Santé et de la Recherche Médicale (PNRMC-A04048DS) and the Association Française contre les Myopathies (AFM-9471).